Paper ID: TE-02

Finite Difference Solution of the Transient Free Convection in Micropolar Fluid with Heat Generation and Constant Heat Flux

GM Rashid[1], MM Alam[2], MA Hossain[1]
[1]Department of Mathematics, Khulna University of Engineering & Technology, Khulna, Bangladesh
[2]Mathematics Discipline, Khulna University, Khulna, Bangladesh
E-mail:arifhkhan63@hotmail.com

Abstract

In this paper the numerical solution of the transient free convection in micropolar fluid with heat generation and constant heat flux is discussed. The corresponding governing equations are a set of coupled nonlinear partial differential equations. Here the system of the governing equations is solved numerically using the finite difference method. Before use of the finite difference method the governing equations are transferred to their non-dimensional form by introducing suitable substitutions. As a result, some physically interesting non-dimensional numbers, viz. Prandtl number and Grasshof number, as well as some non-dimensional material parameters are aroused. The non-dimensional equations are then discretized and solved. The stability criterion of the solutions is considered, though is included due to space constraint. The numerical solutions thus obtained at different grid points at different time is plotted and discussed. The values proportional to the coefficient of skin friction and Nusselt number are also tabulated and discussed.

Keywords: *Finite difference method, Transient flow, Free Convection, Micropolar Fluid.*

1. Introduction

The concept of micropolar fluids introduced by Eringen [1] deals with a class of fluids which exhibit certain microscopic effects arising from the local structure and micromotions of the fluid elements. These fluids contain dilute suspensions of rigid macromolecules with individual motions which support stress and body moments and are influenced by spin-inertia. Physically micropolar fluids represent fluids consisting of randomly oriented particles suspended in a viscous medium, where the deformation of fluid particles is ignored It has found its applications specially, in lubrication theory. Zakaria [2] pointed that the theory of micropolar fluid and its extension to thermo-micropolar fluids may form suitable non-Newtonian fluid models which can be used to analyze the behavior of exotic lubricants, colloidal suspensions or polymeric fluids, liquid crystals and animal blood. Some theoretical studies have been compared and favorably agree with experimental measurement.

Natural convection with internal heat generation finds application in fire and combustion modeling. Gorla and Tornabene [3] investigated the effects of thermal radiation on mixed convection flow over a vertical plate with non-uniform heat flux boundary condition. Raptis [4] studied numerically the case of a steady two dimensional flow of a micropolar fluid past a continuously moving plate with a constant velocity in the presence of thermal radiation. Kim [5] studied the unsteady free convection flow of a micropolar fluid through a porous medium bounded by an infinite vertical plate. Kim and Fedorov [6] studied the transient mixed radiative convection flow of a micropolar fluid past a moving, semi-infinite vertical porous plate. El-Amin [7] studied the combined effect of internal heat generation and magnetic field on free convection and mass transfer flow in a micropolar fluid with constant suction. El-Hakiem [8] studied the natural convection in a micropolar fluid with thermal dispersion and internal heat generation.

2. Governing Equations and their manipulation

Let us consider the free convection of a micropolar fluid along the vertical plate. The temperature of the plate is held at constant value of T_s and the heat flux is considered as constant, the thermal dispersion effect is also included. Let the *x*-axis is along the plate in the vertical direction and *y*-axis is perpendicular to the plate. The governing equations with the Boussinesq approximation can be put in the following form

1) Mass equation: $\frac{\partial u}{\partial x}+\frac{\partial v}{\partial y}=0$

2) Momentum equation: $\frac{\partial u}{\partial t}+u\frac{\partial u}{\partial x}+v\frac{\partial u}{\partial y}=(\nu+\frac{k}{\rho})\frac{\partial^2 u}{\partial y^2}+g^*\beta(T-T_\infty)+\frac{k}{\rho}\frac{\partial N}{\partial y}$

3) Angular momentum equation: $\frac{\partial N}{\partial t}+u\frac{\partial N}{\partial x}+v\frac{\partial N}{\partial y}=\frac{\gamma}{\rho j}\frac{\partial^2 N}{\partial y^2}-\frac{k}{\rho j}(2N+\frac{\partial u}{\partial y})$

4) Energy equation: $\frac{\partial T}{\partial t}+u\frac{\partial T}{\partial x}+v\frac{\partial T}{\partial y}=\frac{k'}{\rho c_p}\frac{\partial^2 T}{\partial y^2}+Q(T-T_\infty)$

With the boundary conditions: $u(x,0,t)=0,\ N(x,0,t)=0,\ T(x,0,t)=T_s$

$$u(x,\infty,t)=0,\ N(x,\infty,t)=0,\ T(x,\infty,t)=T_\alpha,$$

Here *u* and *v* are velocity components associated with *x* and *y* directions measured along and normal to the vertical plate respectively, ν the kinematic coefficient of viscosity, k the vortex viscosity, ρ the density of the fluid, *g** the acceleration due to gravity, β the coefficient of thermal expansion, *T* the temperature of the fluid in the boundary layer, T_α the free steam temperature, *N* the angular velocity, γ the spin gradient viscosity, *j* the microinertia per unit mass, k' the thermal conductivity, c_p specific heat at constant pressure and *Q* the heat generation.

The variables are made dimensionless with the following substitutions.

$$u^*=\frac{u}{U_0},\ v^*=\frac{v}{U_0},\ x^*=\frac{U_0}{\nu}x,\ y^*=\frac{U_0}{\nu}y,\ t^*=\frac{U_0^2}{\nu}t,\ N^*=\frac{\nu}{U_0^2}N,\ j^*=\frac{U_0^2}{\nu^2}j,\theta=\frac{(T-T_\infty)}{(T_s-T_\infty)}$$

Along with them the following dimensionless quantities are introduced.

Prandtl Number, $P_r=\frac{\upsilon}{k/\rho C_p}=\frac{\upsilon\rho c_p}{k}$, Grashof number, $Gr=\frac{\nu g^*\beta(T_s-T_\infty)}{U_0^3}$

Dimensionless material parameters $\lambda=\frac{\gamma}{\rho\nu j}$, and $\Delta=\frac{k}{\rho\nu}$

On substitution of the dimensionless variables the Momentum equation becomes

$$\frac{\partial u^*}{\partial t^*}+u^*\frac{\partial u^*}{\partial x^*}+v^*\frac{\partial u^*}{\partial y^*}=(1+\Delta)\frac{\partial^2 u^*}{\partial y^{*2}}+G_r\theta+\Delta\frac{\partial N^*}{\partial y^*}$$

After dropping the asterisks, we have

$$\frac{\partial u}{\partial t}+u\frac{\partial u}{\partial x}+v\frac{\partial u}{\partial y}=(1+\Delta)\frac{\partial^2 u}{\partial y^2}+\Delta\frac{\partial N}{\partial y}+G_r\theta \quad (1)$$

Similarly the Angular momentum equation takes the following form

$$\frac{\partial N^*}{\partial t^*}+u^*\frac{\partial N^*}{\partial x^*}+v^*\frac{\partial N^*}{\partial y^*}=\lambda\frac{\partial^2 N^*}{\partial y^{*2}}-\frac{\Delta}{j^*}(2N^*+\frac{\partial u^*}{\partial y^*})$$

After dropping the asterisks, we have

$$\frac{\partial N}{\partial t}+u\frac{\partial N}{\partial x}+v\frac{\delta N}{\partial y}=\lambda\frac{\partial^2 N}{\partial y^2}-\frac{\Delta}{j}(2N+\frac{\partial u}{\partial y}) \quad (2)$$

And the Energy equation become

$$\frac{\partial\theta}{\partial t^*}+u^*\frac{\partial\theta}{\partial x^*}+v^*\frac{\partial\theta}{\partial y^*}=\frac{1}{P_r}\frac{\partial^2\theta}{\partial y^{*2}}+\alpha\theta$$

where, $\alpha=\frac{\nu}{U_0^2}Q$

After dropping the asterisks, we have

$$\frac{\partial \theta}{\partial t}+u\frac{\partial \theta}{\partial x}+v\frac{\partial \theta}{\partial y}=\frac{1}{P_r}\frac{\partial^2 \theta}{\partial y^2}+\alpha\theta \tag{3}$$

The transferred boundary conditions are:

$$u(x,0,t)=0,\ \ N(x,0,t)=0,\ \ \theta(x,0,t)=1$$
$$u(x,\infty,t)=0,\ \ N(x,\infty,t)=0,\ \ \theta(x,\infty,t)=0,$$

It is shown in [9] that the skin-friction coefficient c_f is proportional to $\frac{1}{U_0^2}[1+\Delta]\nu\left(\frac{\partial u}{\partial y}\right)_{y=0}$

For simplicity an explicit method is used to solve the obtained non-dimensional governing equations. Let *u′, N′, θ′* denote the values of *u*, *N* and *θ* at the end of a time step. Then the appropriate finite difference equations corresponding to equations (1), (2), and (3) are

$$\frac{u'_{ij}-u_{ij}}{\delta\tau}+u_{ij}\frac{u_{ij}-u_{i-1j}}{\delta X}+v_{ij}\frac{u_{ij+1}-u_{ij}}{\delta Y}=(1+\Delta)\frac{u_{ij+1}-2u_{ij}+u_{ij-1}}{(\delta Y)^2}+\Delta\frac{N_{ij+1}-N_{ij}}{\delta Y}+G_r\theta \tag{4}$$

$$\frac{N'_{ij}-N_{ij}}{\delta\tau}+u_{ij}\frac{N_{ij}-N_{i-1j}}{\delta X}+v_{ij}\frac{N_{ij+1}-N_{ij}}{\delta Y}=\lambda\frac{N_{ij+1}-2N_{ij}+N_{ij-1}}{(\delta Y)^2}-\frac{\Delta}{j}(2N_{ij}+\frac{u_{ij+1}-u_{ij}}{\delta Y}) \tag{5}$$

$$\frac{\theta'_{ij}-\theta_{ij}}{\delta\tau}+u_{ij}\frac{\theta_{ij}-\theta_{i-1j}}{\delta X}+v_{ij}\frac{\theta_{ij+1}-\theta_{ij}}{\delta Y}=\frac{1}{P_r}\frac{\theta_{ij+1}-2\theta_{ij}+\theta_{ij-1}}{(\delta Y)^2}+\alpha\theta_{ij} \tag{6}$$

during any time step. The coefficients u_{ij}, v_{ij} appearing in (4), (5) and (6) are generally considered as constant. Then at the end of any time step $\delta\tau$, the new temperature θ, the new angular momentum N' and the new velocity components u′ at all interior grid points may be obtained by successive applications of (6), (5) and (4) respectively. This process is repeated in time provided the time step is sufficiently small and *u*, *N*, θ should eventually converge to values which approximate the steady state solution of equations (1), (2) and (3).

3. Results and Discussion

In this paper, the effect of transient free convection on micropolar fluid with heat generation and constant heat flux has been investigated using the finite difference method. To study the physical situation of this problem, the numerical values of the velocity, temperature and angular momentum within the boundary layer has been computed and also the coefficients proportional to the skin friction coefficient and Nusselt number are calculated. It is seen that the solution has dependency on heat source parameter α, micro inertia per unit mass j, dimensionless material parameter Δ, the Grashof number Gr, dimensionless material parameter λ and the Prandtl number Pr. Due to space constraint effect of all the parameters is not presented here. The values 0.2, 0.5, 0.71, 0.73, 1, 2, 5, 7.01 are considered for Pr and the values of other parameters are however chosen arbitrarily.
Figures 1(a)-1(c) show the velocity, temperature and angular momentum profiles for different values of heat source parameter α respectively. From Fig. 1(a) and 1(b) it is observed that the effect of α on velocity and temperature is similar. They increase with the increase in α rapidly but within short distance become zero. In Fig. 1(c), with the increase in α, both the negative and positive values of angular momentum increases. When α is large the negative zone of the angular momentum is small in comparison to the small α. For large value of α the angular momentum oscillates more from negative to positive.

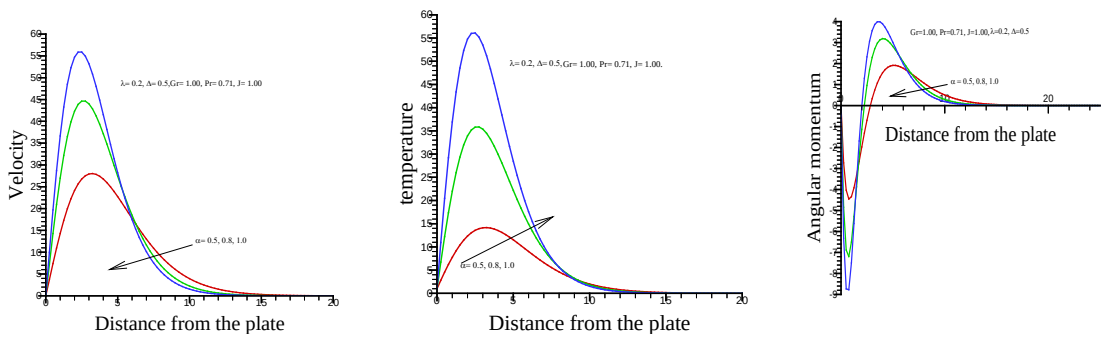

Fig. 1. Velocity, Temperature and Angular Momentum profiles for different values of heat source parameter, α

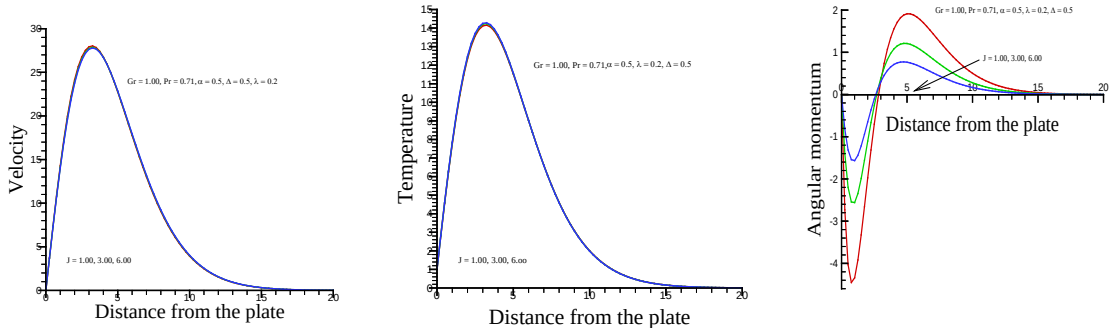

Fig. 2. Velocity, Temperature and Angular Momentum profiles for different values of micro inertia per unit mass, j

Figures 2(a)-2(c) are showing the velocity, temperature and angular momentum profiles for different values of micro inertia per unit mass, j respectively. From figure 2(a) and 2(b), there is a very small change in velocity and temperature due to increase the value of j. They spread a little with the increase of j and within a short distance becoming zero. The magnitude of the angular momentum, both negative and positive, decreases with the increase in j. Clearly j has dominant effect over angular momentum, but has less impact on velocity and temperature.

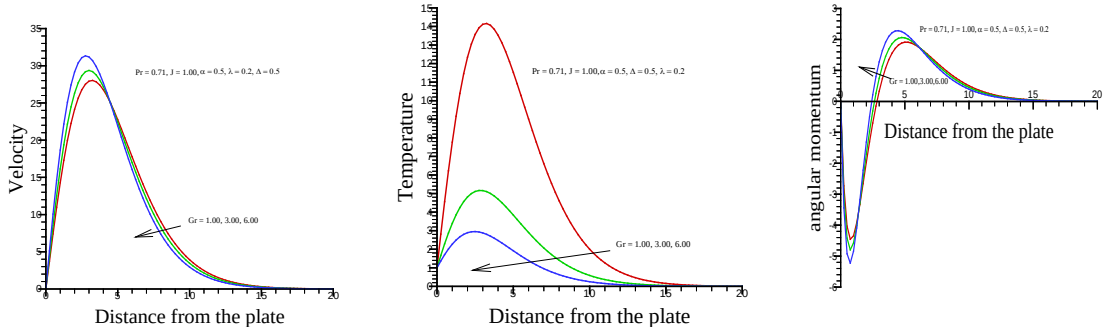

Fig. 3. Velocity, Temperature and Angular Momentum profiles for different values of the Grashof number, Gr

For different values of Grashof Number Gr, the profiles for velocity, temperature and angular momentum are presented in Fig 3(a)-3(c). In Fig. 3(a), we observed that with the increase in Gr value of the maximum velocity increases whereas the spreading of velocity decreases. From Fig. 3(b), it is found that the temperature decreases with the increase in Gr. Also the temperature is becoming zero far away from the plate for lower values of Gr. The angular momentum fluctuation from negative to positive increases with the increase in Gr and for lower values of Gr though the magnitude of angular momentum are less but its spreading is more.

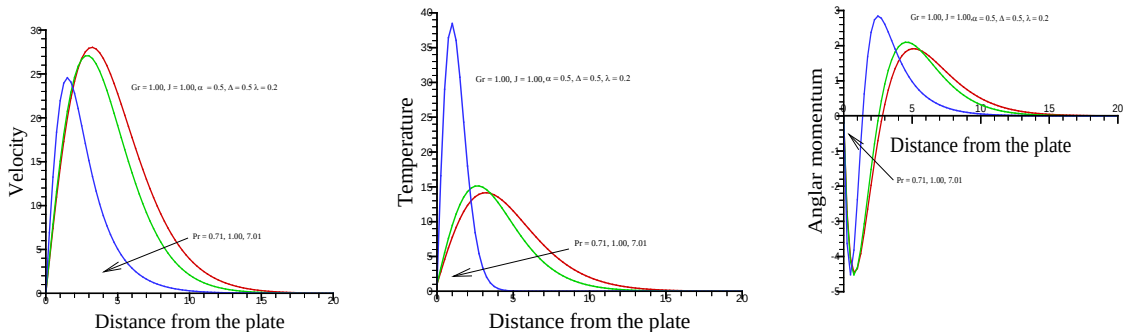

Fig. 4. Velocity, Temperature and Angular Momentum profiles for different values of the Prandtl number, Pr

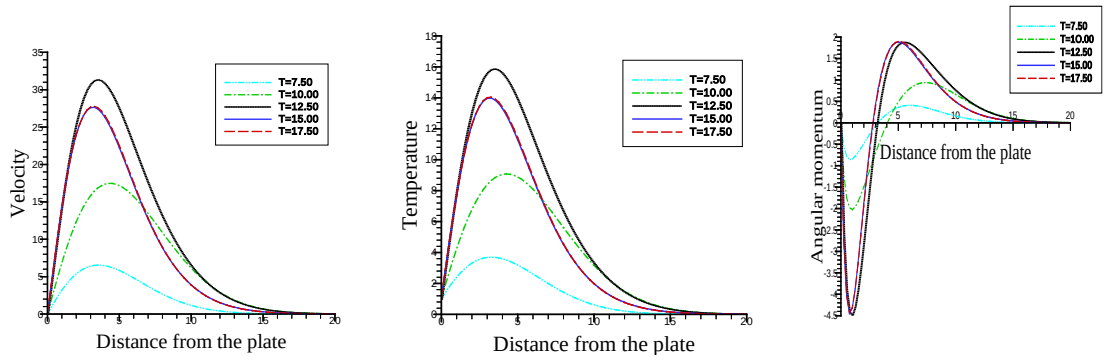

Fig. 5. Velocity, Temperature and Angular momentum profiles for different values of time, T

The profiles for velocity, temperature and angular momentum for different values of Prandtl number Pr are shown respectively in Figures 4(a)-4(c). The velocity is not only decreasing with the increase in Pr but also it is becoming zero within a short distance from the wall. The temperature profile squeezes with the increase in Pr but the pick value of the temperature rises sharply. The negative value of angular momentum near the wall has no appreciable change with the increase in Pr. But positive values of angular momentum increases with Pr and its effective zone decreases.

In Table 1, the values proportional to the coefficient of skin friction and Nusselt numbers for different values of α are tabulated with fixed values of the other parameters. From the table it is observed that with the increase in α the value proportional to the skin friction increases, whereas in the case of Nusselt number the situation is reversed. Also the rate of decrease in Nusselt number is far more than the rate of increase.

In Table 2, the same is tabulated as table (4.1), but different values of microinertia j with the other parameters are kept unchanged. It is seen that the microinertia has a very little impact on the coefficient of skin friction and Nusselt numbers.

In Table 3, the values proportional to the skin-friction coefficient and the Nusselt number are tabulated against the Grashhof number Gr. It is seen that both of them increases with the increase in Gr. For skin friction the rate of increase is almost same, but in the case of Nusselt number the rate slows down for higher values of Gr.

Finally the effect of Prandtl number, Pr on the coefficient of skin friction and Nusselt numbers are presented in Table 4. Here again, as usual, the other parameters are kept as constant. It is seen that with the increase in Pr the value proportional to skin friction increases, whereas the Nusselt number decreases.

Table 1, Numerical values proportional to skin friction coefficient C_f and Nusselt number Nu for different values of α , taking $Gr = 1.00, \Pr = 0.71, j = 1.00, \lambda = 0.2, \Delta = 0.5$ as fixed

α	Values proportional to C_f	Values proportional to Nu
0.5	9.822492	-4.726112
0.8	18.620130	-14.733240
1.0	25.665870	-25.549920
1.5	46.543100	-69.980420
2.0	71.292650	-143.382300
2.5	99.310490	-250.198700

Table 2, Numerical values proportional to skin friction coefficient C_f and Nusselt number Nu for different values of j, taking $Gr = 1.00, \Pr = 0.71, \alpha = 0.5, \lambda = 0.2, \Delta = 0.5$ as fixed.

j	Values proportional to C_f	Values proportional to Nu
1.00	9.822492	-4.726112
2.00	9.792691	-4.752003
3.00	9.788363	-4.766579
4.00	9.788019	-4.775903
5.00	9.788466	-4.782364
6.00	9.789032	-4.787105

Table 3, Numerical values proportional to skin friction coefficient C_f and Nusselt number Nu for different values of Gr , taking $\Pr = 0.71, j = 1.00, \alpha = 0.5, \lambda = 0.2, \Delta = 0.5$ as fixed.

Gr	Values proportional to C_f	Values proportional to Nu
1.00	9.822492	-4.726112
2.00	11.018580	-2.537850
3.00	12.156370	-1.796058
4.00	13.238690	-1.416348
5.00	14.273790	-1.182411
6.00	15.268690	-1.022038

Table 4, Numerical values proportional to skin friction coefficient C_f and Nusselt number Nu for different values of Pr, taking $Gr = 1.00, j = 1.00, \alpha = 0.5, \lambda = 0.2 \Delta = 0.5$ as fixed.

Pr	Values proportional to C_f	Values proportional to Nu
0.20	7.927539	-2.109994
0.71	9.822492	-4.726112
0.73	9.869625	-4.819553
1.00	10.446450	-6.076511
5.00	16.005450	-27.739200
7.01	18.124500	-40.557210

4. Conclusion

In this paper finite difference technique has been used to solve the governing partial coupled nonlinear differential equations of the transient free convection flow of a micropolar fluid. It is found that if the stability criterion of the time integration is satisfied then the obtained result reflects the behaviour of the flow with respect to the different flow parameters. In these type system when there are heat generation and constant heat flux then

i) With the increase in the heat source parameter velocity, temperature and angular momentum increases.

ii) With the increase in the Prandtl number the effective zone of change of velocity, temperature and angular momentum reduces.

iii) Temperature profile shows greater sensitivity of Grashof number and the Nusselt number increases with the increase in the Grashof number.

5. References

[1] A.C. Eringen, "Theory of micropolar fluids", *J. Math. Mech.* Vol. 16, pp. 1-18, 1966

[2] M. Zakaria, "Problem in electromagnetic free convection flow of micropolar fluid with relaxation time through a porous medium", *Appl. Math. Comp.* Vol. 151, No. 3, pp. 601-613, 2004.

[3] R.S.R Gorla, and R. Tornabane, "Free convection from a vertical plate with nonuniform surface heat flux and embedded in a porous medium", *Transport in Porous Media*, Vol-3, No. 1, pp. 95-106, 1988.

[4] A. Raptis, '"Flow of a micropolar fluid past a continuously moving plate by the presence of radiation", *Int. J. Heat and Mass Trans*, Vol. 41, No. 18, pp. 2865-2866, 1998.

[5] Y.J. Kim, "Unsteady convection flow of micropolar fluids past a vertical porous plate embedded in a porous medium", *Acta Mech.*,.Vol. 148, No. 1-4, pp. 105-116, 2001

[6] Y.J. Kim and A.G. Fedorov, "Transient mixed radiative convection flow of a micropolar fluid past a moving, semi-infinite vertical porous plate", *Int. J. Heat and Mass Trans*, Vol. 46, No. 10, pp. 1751-1758, 2003

[7] M.F. El-Amin, "Combined effect of internal heat generation and magnetic field on free convection and mass transfer flow in a micropolar fluid with constant suction", *J. Mag and Mag Mat*, Vol. 270, No. 1-2. pp. 130-135, 2004.

[8] M.A. El-Hakiem, "Natural Convection in a Micropolar Fliud with Thermal Dispersion and Internal Heat Generation", *Int. Comm. Heat Mass Transfer*, Vol- 31, No. 8, pp. 1177-1186, 2004.

[9] G.M. Rashid, "Transient Free Convection in Micropolar Fluid with Heat Generation and Constant Heat Flux", M. Phil thesis (Unpublished), Khulna University of Engineering & Technology, 2012

Paper ID: TE-03

Enhancement of Higher Evaporating Temperature of Household Refrigerator Using Phase Change Material

Md. Imran Hossen Khan*, Hasan M.M. Afroz, Md. Mostafizur Rahman
Department of Mechanical Engineering, Dhaka University of Engineering and Technology, Gazipur, Gazipur-1700, Bangladesh
E-mail: imran.duet56@gmail.com

Abstract

Experimental investigation of the performance improvement of a household refrigerator using phase change material (PCM) has been carried out. The PCM is located behind the five sides of the evaporator cabinet in which the evaporator coil is immersed. The refrigeration system has been tested with three different PCMs (Water, Eutectic solution-1, and Eutectic solution-2 of melting point 0℃, - 5℃, and -10℃, respectively) at different thermal loads. Experimental results show that the evaporating temperature of the refrigeration cycle with PCM is considerably higher than that of without PCM. Depending on the types of PCM and thermal load, around 2 - 5^0C higher evaporating temperature of the refrigeration cycle has been observed with PCM in respect to without PCM. This higher evaporating temperature ultimately increases the COP of the system. The enhancement of higher evaporating temperature of the system with PCM in comparison without PCM follows the sequence as Eutectic-2 is higher than Eutectic-1and Eutectic-1is higher than water.

Keywords: *Phase change material (PCM), House hold refrigerator, Evaporation Temperature, Heat transfer, Energy consumption,*

1. Introduction

A refrigerator is one of the most popular household appliances and its ownership is already high in developed economies and increasing rapidly in the developing countries. Today, 80 million refrigerators are produced each year worldwide, among which the Asia-Pacific Economic Cooperation (APEC) produces about 45 million [1]. In terms of energy consumption, a refrigerator is almost the largest single end user of electricity in the residential sector due to its widespread use and continuous operation and therefore, improving the energy efficiency of house hold refrigerator is thus an important issue in terms of energy savings and global warming reduction. A number of countries have introduced energy labeling programs [2] and minimum energy efficiency standards [3] [4] of different appliances and equipments to minimize the energy consumption. Scientists, engineers and researchers in the field of refrigeration and air conditioning are now involving themselves to develop different technical options for improving the energy efficiency of household refrigerators. Followings are the well known technical options in this regard-

- Developing high-efficiency compressors
- Improving the efficiency of heat exchangers by enhancing the heat transfer
- Improving the cabinet and door insulation to reduce heat losses

Heat transfer enhancement is an important factor in obtaining energy efficiency improvements of refrigeration and air conditioning applications. During last two decades, huge effort have been paid to enhance the heat transfer performance of heat exchanger like evaporator of air conditioning and refrigeration system. Improving the efficiency of heat exchangers, and particularly of the evaporator, which is a key component of a household refrigerator, is the most emphasized topic in the performance improvement of household refrigerator. Heat transfer through the evaporator requires a temperature difference between the air and the refrigerant: the higher the air side convective coefficient, the lower the temperature difference between the evaporation temperature and the air. For a given cabinet air temperature this results in a higher evaporation temperature consequently an enhanced performance of the system. Many researchers are involved in improving the heat transfer performance of this heat exchanger in many different ways like- using loop heat pipe based evaporator, using micro fin tubes for both condenser and evaporator, etc. Using **phase change material (PCM)** as a latent heat thermal energy storage system could be a new option of performance improvement of a household refrigerator by enhancing heat transfer of the evaporator and reducing efficiency losses of conventional compressor. Very few

experimental and theoretical studies have been carried out on the thermal performance of latent heat thermal energy storage systems and their behavior on the evaporator in a household refrigerator. Marques et al. [5] developed a model to investigate the performance improvement provided by a phase change material associated with the evaporator in a domestic refrigerator. The PCM heat release and storage model showed that the melting and freezing time increases proportionally with PCM thickness. Employing thin PCM slabs (5 mm) ensures that the net volume of the compartment is not reduced substantially, while reasonable length compressor run times (i.e. on-cycle times) can be obtained. The refrigerator autonomy was strongly affected by the refrigerator heat load and compressor cooling capacity. An increase in ambient temperature from 20 to 43 °C resulted in a 47 % reduction in autonomy. Cerri [6] has simulated a domestic refrigerator including cold storage. This model, based on differential equations, was used to determine appropriate operating conditions in order to achieve a minimum electrical power. In this study, the coefficient of performance is improved by 12% using PCM. Nevertheless, it must be observed that Cerri used a low quantity of PCM in his study. Maltini et al. [7] performed an experimental study of a household refrigerator using a sodium chloride–water mixture as cooling storage system. It was observed that the PCM behaved as a temperature damper and minimized the temperature fluctuations, leading to a better preservation of food. Wang et al. [8] have developed a dynamic mathematical model for coupling a refrigeration system and a PCM heat exchanger, Positioned between the condenser and the thermal expansion valve (TEV). This model is able to predict the refrigerant states and dynamic coefficient of performance. However, none of the investigation was carried out to examine the effects of the PCM heat exchanger on the refrigeration system performance. K. Azzouz et al. [9] developed a dynamic model of the vapor compression cycle including the presence of the phase change material and showed its experimental validation. The simulation results of the system with PCM show that the addition of thermal inertia globally enhances heat transfer from the evaporator and allows a higher evaporating temperature, which increases the energy efficiency of the system. The energy stored in the PCM is yielded to the refrigerator cell during the off cycle and allows for several hours of continuous operation without power supply. K Azzouz et al. [10] design and developed a model of an improved refrigerator using phase change material as a cold storage. A simplified dynamic model on differential equation is developed for predicting the energy impact due to the addition of the PCM. The numerical result yields a 72% increase in the COP and a 25% decrease in the global working time of the compressor. K. Azzouz et al. [11] experimentally investigated the performance of a household refrigerator by using phase change material. The experimental results indicate that the response of the refrigerator to the addition of PCM and its efficiency are strongly dependent on the thermal load. The integration of latent heat storage allows 5-9h of continuous operation without electrical supply (to be compared to 1-3h without PCM) and a 10–30% increase of the coefficient of performance, depending on the thermal load.

2. Experimental Methodology

A conventional household refrigerator is used in the modified form with PCM box located behind the evaporator cabinet to carry out the necessary experiments. The experimental set up comprised with a refrigerator, pressure transducer, pressure gauge, thermocouple, phase change material box, and data acquisition system. Fig.1 shows the details of the location of the PCM box with the evaporator cabinet. The PCM box is made up by galvanized iron (GI) sheet have 1mm thickness, which is 0.56m width, 0.44m height and 0.47m depth. The evaporator cabinet box of outer volume $0.04m^3$ with cooling coil [Fig. 1(a)] is inserted into the empty PCM box of internal volume $0.11m^3$ [Fig. 1(b)]. The thickness of the annular space between PCM box and evaporator cabinet box is 0.006m. The open face of the annular space is sealed by a third sheet metal. Two copper tubes are attached with the top of the annular space for PCM supply in the box and to maintain the overflow. Another tube is attached in the bottom of the annular space to discharge the PCM if necessary. This modified PCM based refrigerator has a single evaporator cabinet with a single door. The followings are the major technical specifications of the refrigerator.

1. Cabinet : Internal volume, $0.03\ m^3$
2. Evaporator : Mode of heat transfer - Free convection, Linear length of the coil /tube: 12.2 m, Internal and external diameter of the tube: 0.0762 m and 0.0772 m respectively, Material of the coil/tube: Copper tube
3. Condenser : Mode of heat transfer - Free convection, Linear length of the coil /Tube: 5.8 m, Internal and external diameter of the tube: 0.003 and 0.004 m respectively, Material of the coil/tube: Steel and wire tube
4. Hermetic reciprocating compressor, HITACHI FL 1052-SK, 13 FL 220-240V, 50Hz
5. Expansion device: Capillary tube (Internal diameter 1.00 mm)
6. On/off control and self defrost

7. Refrigerant: 1,1,1,2-Tetrafluoroethane (R-134a)

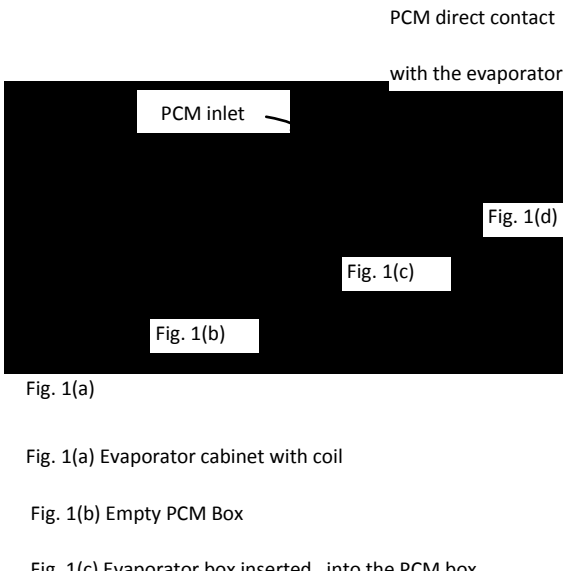

Fig. 1. The arrangement of the PCM based evaporator

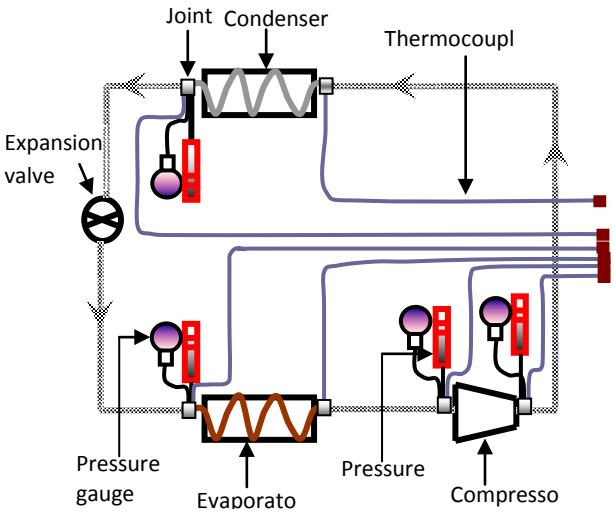

Fig. 2. Location of pressure transducer, pressure gauge and thermocouples

Temperatures at various locations (compressor, condenser, evaporator and cabinet) are measured with K-type (copper–constantan) thermocouples having 0.0005 m diameter as shown in Fig. 2. Three thermocouples are also positioned at the bottom, middle and the top of the PCM in the left face of the cabinet to measure the temperatures of PCM. The uncertainty of the temperature measurements by the thermocouples is estimated to be ±2.78% with respect to a high precision (0.002^0C) thermometer (begman thermometer), which can be found in the table-1. Two pressure transducers are used to measure the evaporation and condensation pressures at the inlet and outlet of the compressor. Another pressure transducer is placed at the inlet of the evaporator to measure the pressure drop in the evaporator section. Four pressure gauges are used to cross check the pressure measurements of the pressure transducer and the deviations have been found within ± 0.03 kg /cm^2. The location of all of the pressure transducers and pressure gauges are shown in Fig. 2. A heater is used in the cabinet to do experiments at different thermal loads. The heater is located at the bottom of the cabinet box, which is linked with a variable voltage transformer (variac) to control the supply voltage for required thermal load variation into the cabinet. A K-type thermocouple is used for the measurement of the air temperature within the cabinet, which is located at the center of the cabinet space. A thermostat is used to drive the compressor cycling; the thermocouple of the thermostat is located at the centre of the cabinet. The experimental set-up is equipped with a data acquisition system linked to a personal computer, which allows a high sampling rate and the monitoring of all the measurements made by means of the thermocouples. The experiments have been carried out in a room where the temperature and humidity are maintained constant with the aid of air conditioner. All the data have been collected from the data acquisition system after ensuring the steady state condition of the refrigerator. To obtain the steady state condition the system is allowed to run for several minutes (about 70 minutes).

Table 1. Estimated uncertainties of measurement

Measured Parameter	Measuring Device	Uncertainty
Temperature	Thermocouples	± 2.78 %
Pressure	Pressure Transducer	± 0.01bar
Pressure	Pressure Gauge	±0.03kg/cm^2

3. Experimental Condition

Experiment was carried out under three different thermal loads with three different PCMs of different quantities.

Table 2. Experimental conditions

Types of PCM	Test time (min)	Thermal load (watt)	Ambient Temp. (°C)	Cabinet setting Temp. (°C)
Without PCM	121	0, 5, 10	22.8 - 23.8	-5
Water	121	0, 5, 10	22.8 - 23.8	-5
Eutectic solution-1	121	0, 5, 10	22.8 - 23.8	-5
Eutectic solution-2	121	0, 5, 10	22.8 - 23.8	-5

4. Experimental results and discussions

Experiments were carried out under three different thermal loads with three different PCMs. In this section the effects of different PCMs at different thermal loads on the Evaporation temperature of house hold refrigerator are discussed.

Figs. 3 - 5 Show the effect of PCM on evaporating temperature of the system at different thermal load condition. From this figure followings are the significant findings

- Average evaporating temperature per cycle is significantly increased for the system with PCM in respect to without PCM, which ultimately enhanced higher heat transfer rate for the system with PCM.
- Depending on the PCM and thermal load around 2 – 5 ^{0}C higher evaporating temperature has been achieved by the PCM in respect to without PCM.
- Among the three PCM , the increase of evaporating temperature with PCM in comparison with no PCM maintain the sequence as Eutectic-2 is higher than Eutectic-1 than Water
- This higher evaporating temperature ultimately increases the heat transfer of heat exchanger (evaporator).

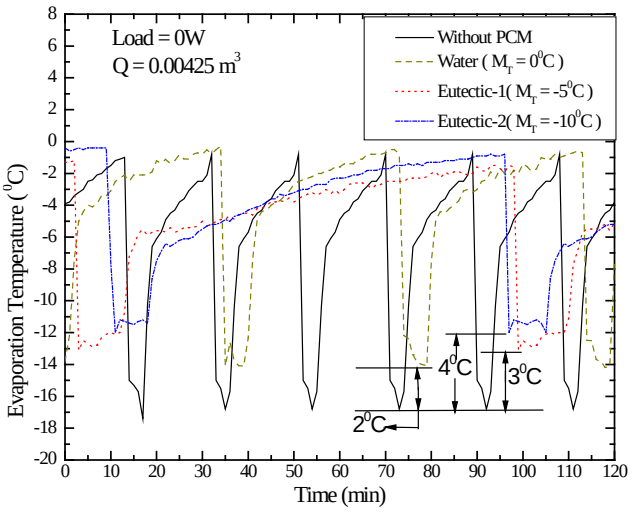

Fig. 3. The effect of PCM on evaporating temperature of the system (Load = 0 W)

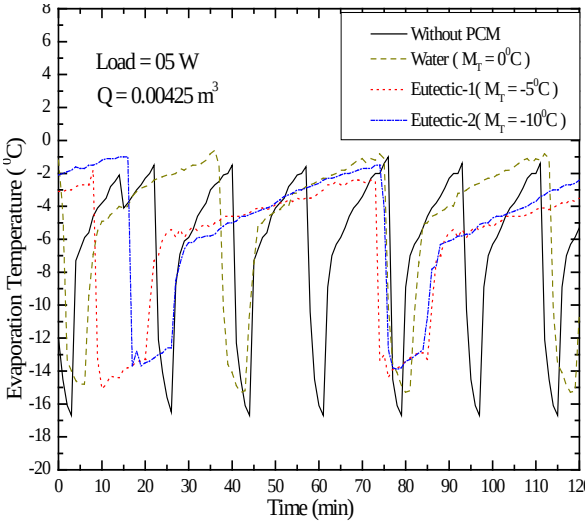

Fig. 4. The effect of PCM on evaporating temperature of the system (Load = 05 W)

During the compressor running time the refrigerant takes the chamber heat by free convection in case of without PCM, which is slower heat transfer process in respect to conduction process. For that reason the operating

temperature of the cooling coil drops very low to maintain the desired cabinet temperature. But with PCM most of the heat in the cabinet is stored in the PCM during compressor off time and this heat is extracted by the refrigerant through conduction during compressor running time. Since conduction heat transfer process is faster than the free convection process the cooling coil temperature does not require dropping very low to maintain desired cabinet temperature. As a result the evaporator works at high temperature and pressure with PCM which shown in Fig. 6. Fig. 6 shows a refrigeration cycle with and without PCM on pressure enthalpy diagram which shows how the evaporating temperature increases the COP of the refrigeration process. Moreover, due to high operating temperature of the evaporator the density of the refrigerant vapor increases, as a result the mass flow extracted from the evaporator by the fixed volumetric rate compressor is higher than without PCM.

Among the three PCMs, Eutectic-2 shows higher evaporating temperature because of its lower phase change temperature. Eutectic-2 starts to change its phase at -10^0C while Eutectic-1 is at -5^0C and water at 0^0C. As a result Eutectic-2 stores more latent heat by phase change than other two during the off mode of the compressor and transfer this heat to the refrigerant by faster conduction method during on period of compressor which ultimately increases the evaporation temperature of the evaporator and enhanced higher heat transfer.

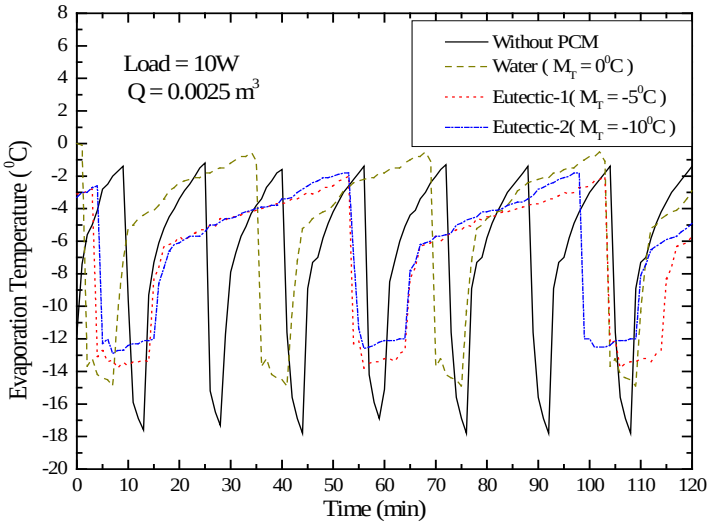

Fig. 5. The effect of PCM on evaporating temperature of the system (Load = 10 W)

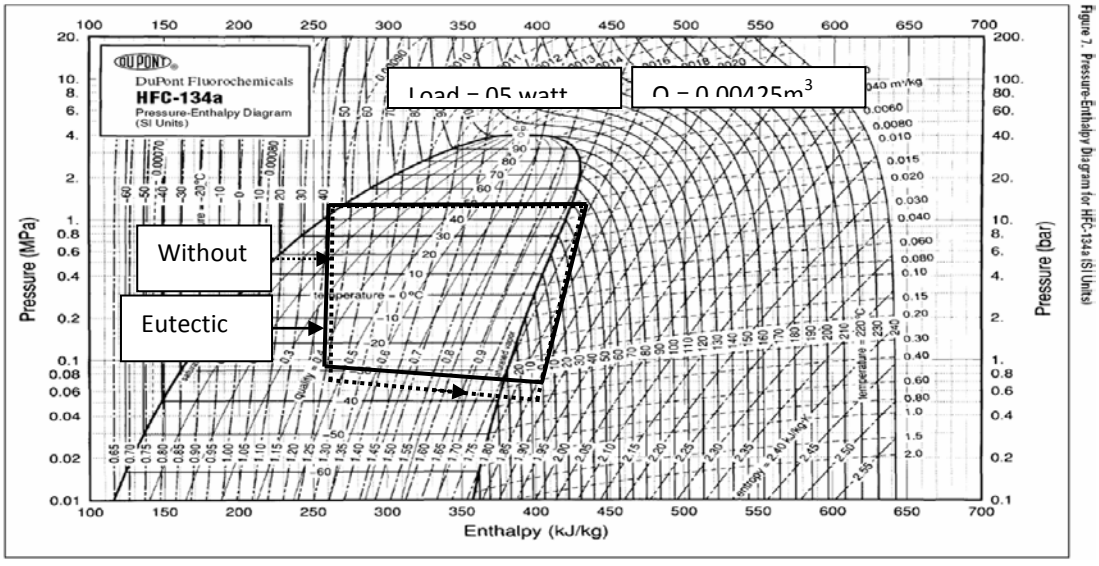

Fig. 6 Refrigeration Cycle with and without PCM on P-h diagram

5. Conclusions

Experimental tests have been carried out to investigate the performance improvement of a household refrigerator using three different phase change materials at different thermal loads. Depending on the PCM and thermal load around 2-5 ^{0}C higher evaporating temperature has been achieved by the PCM in respect to without PCM. The evaporating temperature increase with PCM in comparison with no PCM maintains the sequence as Eutectic-2 is higher than Eutectic-1than Water.

The higher evaporating temperature ultimately reduces the compressor work done as well as increase the heat transfer of heat transfer of heat exchanger (evaporator) which improves the coefficient of performance of a household refrigerator.

6. References

[1] D.Cogan, L. Harrington, "Proceedings of the APEC Symposium on Domestic Refrigeration Appliances" International Institute for Energy Conservation, Asia Regional office (IIECAsia) for the APECS ecretariat. www.clasponline.org/download/. Energy_Testing/2000/17/Proceedings_Final.pdf, 09/11/2002.

[2] E. Vine, P. du Pont, P. Waide, "Evaluating the impact of appliance efficiency labeling programs and standards: process, impact, and market transformation evaluations" Energy, 26, 1041–1059, 200.

[3] P. Waide, B. Lebot, M. Hinnells, "Appliance energy standards in Europe" Energy and Building, 26, 45 67, 1997.

[4] I. Turiel, "Present status of residential appliance energy efficiency standards -an international review" Energy and Buildings, 26, 5–15,1997.

[5] C. Marques, G. Davies, G. Maidment, J.A. Evans, and I. Wood, "Application of phase change materials to domestic refrigerators" *IIR Proceedings Series 'Refrigeration Science and Technology'*, 5: 167-175, 2010. Copyright © 2010 International Institute of Refrigeration, 9th International Conference on Phase-Change Materials and Slurries for Refrigeration and Air Conditioning 29 September – 1 October, Sofia, Bulgaria.

[6] G. Cerri, "Identification of domestic refrigerator models including cool storage" In: Proceedings of 20th Int Cong. of Refrigeration 2003, Washington.

[7] E. Maltini, G. Cortella, M. Stecchini, M. Deltorre, P. Pittia, M. Spaziani, G. Mansutti, "Design and Performances of a Constant Temperature Compartment for Domestic Refrigerator" International Congress on Engineering and Food 2004, Montpellier.

[8] F. Wang, G. Maidment, J. Missenden, R. Tozer, "The novel use of phase change materials in refrigeration Plant" Part 2: dynamic simulation model for the combined system. Appl.Therm. Eng., 27, 2902–2910, 2007.

[9] K. Azzouz, D. Leducq, J. Guilpart, D. Gobin, "Improving the energy efficiency of a vapor compression system using a phase change material" In: Proceedings 2ndConference on Phase Change Material & Slurry 2005, Yverdon les Bains, Switzerland.

[10] K. Azzouz, D. Leducq and D. Gobin, "Performance enhancement of a household refrigerator by addition of latent heat storage" Int. J. of Ref., 31(5), 892–901, 2008.

[11] K. Azzouz, D. Leducq and D. Gobin, "Enhancing the performance of household refrigerators with latent heat Storage: an experimental investigation" Int. J. of Ref., 32, 1634-1644, 2009.

Nomenclature

Symbol	Meaning	Unit
COP	Coefficient of Performance	
M_T	Melting temperature	(^{0}C)
PCM	Phase change material	
Q	Quantity of PCM	(m^3)

Paper ID: TE-04

Aspen-Hysys Simulation of a Condensate Fractionation Plant

Sukanta Kumar Mondal[1*], M. Rakib Uddin[1], A. K. Azad[2]
[1*,1]Department of Chemical Engineering and Polymer Science, Shah Jalal University of Science and Technology (SUST), Sylhet-3114, Bangladesh.
[2]Department of Mechanical Engineering, School of Engineering and Technology, Central Queensland University, Rockhampton, Queensland-4701, Australia.
E-mail: sukanta_sust@yahoo.com, mruddincep@gmail.com, azad_sgfl@yahoo.com

Abstract

The steady state simulation of condensate fractionation plant was carried out using Hysys 3.2 Process Simulator. The condensate is the byproduct, produced by processing of natural gas which contains mostly C_2 to C_{16} complex carbon chain. In this simulation, using atmospheric distillation (fractionation) has the volumetric flow rates of three products like Petrol (Motor Sprit or MS), Kerosene and Diesel are 50%, 25% and 25% respectively on basis of the condensate feed to the plant. This unit models a condensate processing facility consisting of a pre-heating train used to heat up the liquid condensates, an atmospheric distillation column to fractionate the condensates into its straight run products, stripper, heat exchangers, buffer tanks and oil transferring systems. Preheated condensate (from a preheat train) is fed to the fractionator, where vapor-liquid separation done and specialized products are produced from different zone. A furnace was used to heat the oils at desired level. A comprehensive study has done between the simulated data and the plant's operating data.

Keywords: *Simulation, Design data, Hysys, Condensate fractionation, Heat exchanger.*

1. Introduction

Petroleum refineries have advanced periodically with the passage of time. Refinery operations for the creation of products such as Naphtha, Diesel, Kerosene and Gasoline have grown complex affecting the refinery profit. Limitations such as safety and environmental regulations, for maintaining plants to run at cleaner processes, are some constraints to achieve such profits [1]. Crude oil trapped in different reservoirs of the world of a specific field hold unique characteristics from one another on a physical and chemical basis [2]. Refineries fractionate these barrels of crude by their boiling points in order to obtain high value products such as gasoline, diesel, jet fuel, heating oil, fuel oil, lubricants, asphalt, coke, wax, and chemical feed stocks [3].

Many studies have been published related to crude distillation unit (CDU) study with reference to refinery planning and scheduling [4, 5], estimation of product properties [6, 7] and process control, modeling, simulation and optimization [8, 9]. Optimization of a crude distillation unit using a binary feed was carried out on the basis of the gross profit instead of the costs inferred by energy and raw materials [8]. An atmospheric distillation unit subjected to transient behavior due to changes in the operating conditions can be improved by a suitable control strategy to obtain better operations [10]. An expert system was designed for a CDU to predict the product flow and temperature values by minimizing the model output error by genetic algorithm frame work and maximizing the oil production subjected to control parameters [9].

The crude oil distillation unit (CDU) is the first processing unit in virtually all petroleum refineries. The CDU distills the incoming crude oil into various fractions of different boiling ranges, each of them are then processed further in the other refinery processing units. The CDU is often referred to as the atmospheric distillation unit because it operates at slightly above atmospheric pressure [11].

Varieties of products are obtained from fractionation of natural gas condensate. Heavy parts of it are used as diesel whereas the lighter parts are divided into different fractions for different uses. Distillation column is used for the separation of different fraction of condensate. One distillation column is sufficient for producing three products – two solvents and diesel. If any design change for the column is to be suggested, a new column cannot be built because it will require a lot of money. To evaluate different designs, simulators have become very handy. Several soft-wares have been developed for the petroleum industries. ASPEN™ HYSYS is one of the software which is widely accepted and used for refinery simulation. ASPEN™ HYSYS performs the oil distillation calculation through detail plate by plate calculation. This calculation includes generating pseudo-

components from the ASTM D86 data and generating properties from them. ASPEN HYSYS contains an oil manager which organizes the data for the pseudo-components separately [12, 13].
The purpose of this paper is to present the work developed at a typical condensate fractionation plant in Bangladesh. The work was done by HYSYS as a simulation tool. The challenge here was to model a complete process unit in order to allow the optimization of the operation.

2. Design basis

True Boiling Point (TBP) analysis was done for the raw condensate in laboratory which is one of the base inputs for this simulation study. The condensate feed rate was 1250 Barrel/day (BPD) as a basis. A fractionation column was used to produce two solvents as top and side product and diesel as the bottom product. The industrial data was regenerated in the simulation environment. The package and method used for this work is listed below:

Table 1. Design basis for simulation by HYSYS

Fluid Package	Peng-Robinson
Method of Simulation	Pseudo-component generation and plate by plate calculation
Properties generation	HYSYS properties

Fluid package was selected to be Peng-Robinson (Table 1). The main reason behind this, it is widely used for refinery simulation as it can handle the hypothetical pseudo-components. The method of simulation for HYSYS is pseudo-component generation and plate by plate calculation from the 'True Boiling Point' or 'ASTM D86' input data. For this simulation, ASTM D86 input data were available from the refinery laboratory. The HYSYS solver uses different numerical methods for simulation and the selected method for the simulation was HYSIM Inside-Out which is suitable for most cases. From properties generation, two databases can be used for ASPEN HYSYS 3.2 – HYSYS properties and ASPEN properties. But as they are exclusive, HYSYS properties were used for property generation of the streams. The ASTM D86 data obtained from the refinery for condensate that were used as input for the oil manager in HYSYS are shown in Fig. 1.

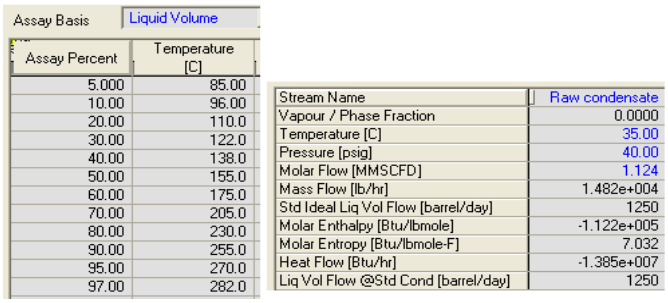

Fig. 1. Input data for oil manager and basis for simulation

3. Simulation of condensate fractionation plant

The condensate fractionation unit is first processed in the refinery and is composed by the following equipment:
Three pre-heater (heat exchangers), one main distillation column and one kerosene stripper. The objective of the present works was to validate the model, checking all the settings and calibrations, to verify the answer of the model to real operating conditions.
The actual distillation column was a traditional distillation column which has a reboiler at the bottom and a condenser at the top. The column was simulated in HYSYS 3.2 to regenerate the data. The simulation model can be seen in Fig. 2. Among the three products, MS was the top product and it was the lightest of all. It would be used as thinner for paints. Kerosene was the side draw from the column. It was composed of mostly medium heavy oil components. Diesel was the bottom product of the column and heaviest of all.
Condensate comes from gas fields and stored in condensate storage tanks (Fig. 2). Then it (stream: raw condensate) fed to feed pre-heaters in fractionation area. At first feed pre-heater condensate pre-heated by kerosene products and then it (stream: condensate1) goes to another feed-preheater E-101 and heated up by diesel products. Then finally it pre-heated by heat transfer oil (thermal oil) coming from thermal oil heater to enrich with sufficient temperature before fed into fractionation column (stream: condensate).

In fractionation column due to relative volatility of different components of condensate it's divided mainly in three portions. Heat transfer and mass transfer are played at different stages and try to get equilibrium conditions. At top get MS vapor at 130 ^{o}C to 135 ^{o}C with 10 to 11 psig, kerosene as a side product (stream- kerosene) produced at 190 ^{o}C to 200 ^{o}C with 11 psig, the rest portion diesel as a bottom product (stream- Diesel) produced at 275 ^{o}C to280 ^{o}C with 12 psig. MS vapors then goes to condenser, then (stream- petrol) more cooled by exchanging heat with cooling water at E-104. Then liquid MS goes to buffer tank V-100 and then the MS pumped by P-100 to product storage tank.

As a side product kerosene goes to kerosene stripper, and then from the bottom of the stripper it's pumped to the first pre-heater and E-103 to be cooled by exchanging heat with fed condensate and with cooling water accordingly. Then it goes to buffer tank (V-101) and finally pumped to kerosene storage tank.

The bottom product diesel is pumped to the heat exchangers E-101 and E-100 to be cooled by exchanging heat with condensate and with cooling water accordingly. Then it goes to buffer tank (V-102) and finally pumped to diesel storage tank.

A high boiling point heat transfer oil (Therminol VP-1) heated up in a heater and supplied to feed pre-heater (E-102), fractionator reboiler and kerosene reboiler to heat up condensate, diesel and kerosene accordingly. For better quality of the products by more fractions, in the fractionation column, reflux of certain amount of MS, kerosene and diesel was done.

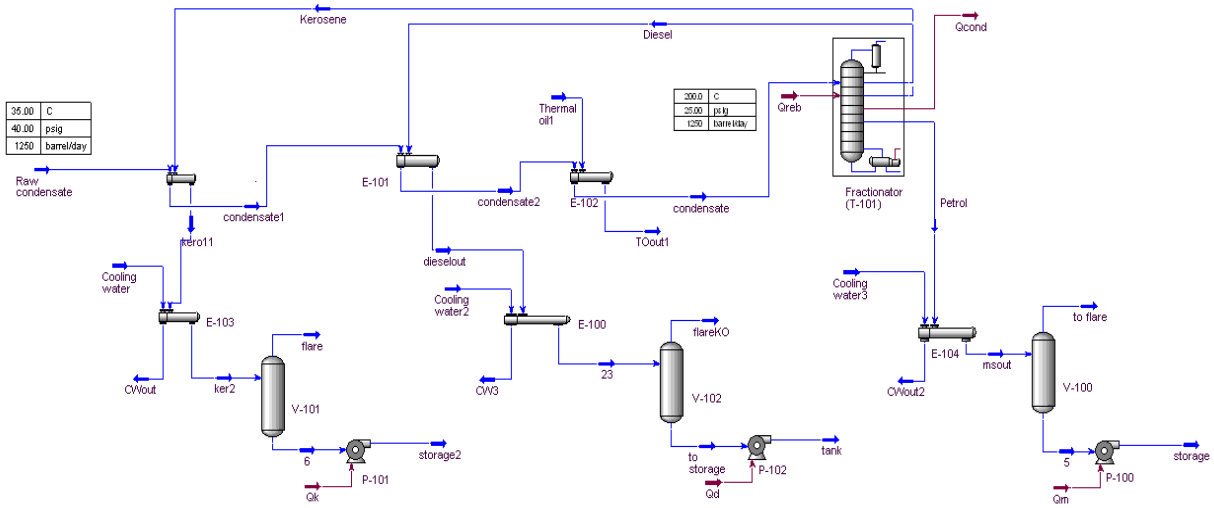

Fig. 2. Process simulation model for condensate fractionation plant.

The Heat and Material Balance (HMB) of the whole streams in the plant is shown in Fig. 3 as a result of the simulation.

Streams											
		condensate	Petrol	Diesel	Kerosene	Raw condensate	condensate1	kero11	condensate2	dieselout	Thermal oil1
Vapour Fraction		0.6845	0.0000	0.0000	0.0000	0.0000	0.0000	0.0000	0.0000	0.0000	0.0000
Temperature	C	200.0	35.00	280.9	200.8	35.00	60.00	123.2	125.0	64.30	316.0
Pressure	psig	25.00	10.00	12.00	10.74	40.00	35.00	5.741	30.00	7.000	100.0
Molar Flow	MMSCFD	1.124	0.6925	0.1870	0.2443	1.124	1.124	0.2443	1.124	0.1870	10.80
Mass Flow	lb/hr	1.482e+004	7055	3983	3785	1.482e+004	1.482e+004	3785	1.482e+004	3983	1.968e+005
Std Ideal Liq Vol Flow	barrel/day	1250	625.0	312.5	312.5	1250	1250	312.5	1250	312.5	1.271e+004
Heat Flow	Btu/hr	-1.041e+007	-6.629e+006	-2.713e+006	-2.928e+006	-1.385e+007	-1.354e+007	-3.235e+006	-1.265e+007	-3.601e+006	3.231e+007
Molar Enthalpy	Btu/lbmole	-8.437e+004	-8.718e+004	-1.321e+005	-1.091e+005	-1.122e+005	-1.097e+005	-1.206e+005	-1.025e+005	-1.754e+005	2.725e+004
		TOout1	CWout	Cooling water	ker2	23	Cooling water2	CW3	msout	Cooling water3	CWout2
Vapour Fraction		0.0000	0.0000	0.0000	0.0000	0.0000	0.0000	0.0000	0.0000	0.0000	0.0000
Temperature	C	304.0	35.00	30.00	35.00	35.00	30.00	35.00	35.00	30.00	35.00
Pressure	psig	95.00	55.00	60.00	0.7407	2.000	60.00	55.00	5.000	60.00	55.00
Molar Flow	MMSCFD	10.80	16.06	16.06	0.2443	0.1870	5.148	5.148	0.6925	5.117e-003	5.117e-003
Mass Flow	lb/hr	1.968e+005	3.176e+004	3.176e+004	3785	3983	1.018e+004	1.018e+004	7055	10.12	10.12
Std Ideal Liq Vol Flow	barrel/day	1.271e+004	2179	2179	312.5	312.5	698.8	698.8	625.0	0.6945	0.6945
Heat Flow	Btu/hr	3.007e+007	-2.157e+008	-2.160e+008	-3.529e+006	-3.695e+006	-6.927e+007	-6.918e+007	-6.630e+006	-6.885e+004	-6.875e+004
Molar Enthalpy	Btu/lbmole	2.536e+004	-1.224e+005	-1.225e+005	-1.315e+005	-1.800e+005	-1.225e+005	-1.224e+005	-8.718e+004	-1.225e+005	-1.224e+005
		to flare	5	storage	flare	6	storage2	flareKO	to storage	tank	Qcond
Vapour Fraction		1.0000	0.0000	0.0000	1.0000	0.0000	0.0000	1.0000	0.0000	0.0000	<empty>
Temperature	C	35.00	35.00	35.11	35.00	35.00	35.09	35.00	35.00	35.07	<empty>
Pressure	psig	5.000	5.000	40.00	0.7407	0.7407	35.74	2.000	2.000	37.00	<empty>
Molar Flow	MMSCFD	0.0000	0.6925	0.6925	0.0000	0.2443	0.2443	0.0000	0.1870	0.1870	<empty>
Mass Flow	lb/hr	0.0000	7055	7055	0.0000	3785	3785	0.0000	3983	3983	<empty>
Std Ideal Liq Vol Flow	barrel/day	0.0000	625.0	625.0	0.0000	312.5	312.5	0.0000	312.5	312.5	<empty>
Heat Flow	Btu/hr	0.0000	-6.630e+006	-6.628e+006	0.0000	-3.529e+006	-3.528e+006	0.0000	-3.695e+006	-3.695e+006	4.618e+006
Molar Enthalpy	Btu/lbmole	-5.718e+004	-8.718e+004	-8.717e+004	-9.906e+004	-1.315e+005	-1.315e+005	-1.370e+005	-1.800e+005	-1.800e+005	<empty>

Fig. 3(a). Heat and Material balances for process streams

		Qreb	Qm	Qk	Qd	Reflux	To Condenser	Boilup	To Reboiler	MS	Diesel
Vapour Fraction		<empty>	<empty>	<empty>	<empty>	0.0000	1.0000	1.0000	0.0000	0.0000	0.0000
Temperature	C	<empty>	<empty>	<empty>	<empty>	35.00	119.3	280.9	272.4	35.00	280.9
Pressure	psig	<empty>	<empty>	<empty>	<empty>	10.00	10.00	12.00	12.00	10.00	12.00
Molar Flow	MMSCFD	<empty>	<empty>	<empty>	<empty>	1.385	2.078	1.004	1.191	0.6925	0.1870
Mass Flow	lb/hr	<empty>	<empty>	<empty>	<empty>	1.411e+004	2.117e+004	2.030e+004	2.428e+004	7055	3983
Std Ideal Liq Vol Flow	barrel/day	<empty>	<empty>	<empty>	<empty>	1250	1875	1606	1918	625.0	312.5
Heat Flow	Btu/hr	2.392e+006	1309	651.4	650.9	-1.326e+007	-1.527e+007	-1.167e+007	-1.678e+007	-6.629e+006	-2.713e+006
Molar Enthalpy	Btu/lbmole	<empty>	<empty>	<empty>	<empty>	-8.718e+004	-6.694e+004	-1.059e+005	-1.283e+005	-8.718e+004	-1.321e+005
		condensate	kerosene stripper_Draw	kerosene stripper_Return	Kerosene	kerosene stripper_BoilUp	kerosene stripper_ToReb	Qcond	Qreb	kerosene stripper_Energy	
Vapour Fraction		0.6845	0.0000	1.0000	0.0000	1.0000	0.0000	<empty>	<empty>	<empty>	
Temperature	C	200.0	180.7	184.6	200.8	200.8	195.3	<empty>	<empty>	<empty>	
Pressure	psig	25.00	10.74	10.74	10.74	10.74	10.74	<empty>	<empty>	<empty>	
Molar Flow	MMSCFD	1.124	0.4066	0.1623	0.2443	0.1833	0.4276	<empty>	<empty>	<empty>	
Mass Flow	lb/hr	1.482e+004	5975	2190	3785	2690	6475	<empty>	<empty>	<empty>	
Std Ideal Liq Vol Flow	barrel/day	1250	497.4	184.9	312.5	224.1	536.6	<empty>	<empty>	<empty>	
Heat Flow	Btu/hr	-1.041e+007	-4.754e+006	-1.460e+006	-2.928e+006	-1.754e+006	-5.049e+006	4.618e+006	2.392e+006	3.666e+005	
Molar Enthalpy	Btu/lbmole	-8.437e+004	-1.065e+005	-8.195e+004	-1.091e+005	-8.718e+004	-1.075e+005	<empty>	<empty>	<empty>	

Fig. 3(b). Heat and Material balances for process streams

The fractionation column environment (Fig. 4) is to install and define the streams and operations contained in a column sub-flowsheet. There contains tray section, condensers, reboilers, side strippers, heat exchangers, pumps. HYSYS contains a number of pre-built column sub-flowsheet template that quickly install a column of a typical type and then customize it's as required within its column environment [14]. In the column the condensate feed tray number was 21, kerosene withdrawn from 11 and kerosene reflux to column was 10. Diesel and MS were withdrawn from bottom and top of the column respectively and both were refluxed again to the column. Column (T-101) environment is given below with it's process flow diagram containing heat and mass balances.

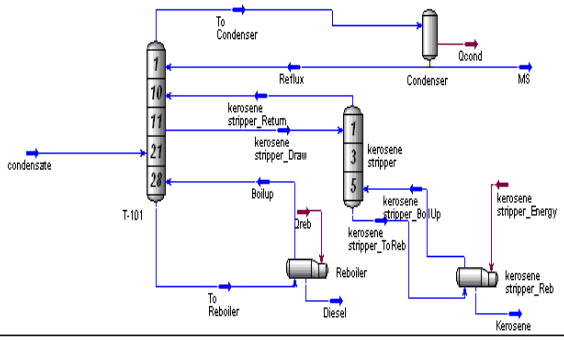

Material Streams													
		Reflux	To Condenser	Boilup	To Reboiler	MS	Diesel	condensate	kerosene stripper_Draw	kerosene stripper_Return	Kerosene	kerosene stripper_BoilUp	kerosene stripper_ToReb
Vapour Fraction		0.0000	1.0000	1.0000	0.0000	0.0000	0.0000	0.6845	0.0000	1.0000	0.0000	1.0000	0.0000
Temperature	C	35.00	119.3	280.9	272.4	35.00	280.9	200.0	180.7	184.6	200.8	200.8	195.3
Pressure	psig	10.00	10.00	12.00	12.00	10.00	12.00	25.00	10.74	10.74	10.74	10.74	10.74
Molar Flow	MMSCFD	1.385	2.078	1.004	1.191	0.6925	0.1870	1.124	0.4066	0.1623	0.2443	0.1833	0.4276
Mass Flow	lb/hr	1.411e+004	2.117e+004	2.030e+004	2.428e+004	7055	3983	1.482e+004	5975	2190	3785	2690	6475
Liquid Volume Flow	barrel/day	1250	1875	1606	1918	625.0	312.5	1250	497.4	184.9	312.5	224.1	536.6
Heat Flow	Btu/hr	-1.326e+007	-1.527e+007	-1.167e+007	-1.678e+007	-6.629e+006	-2.713e+006	-1.041e+007	-4.754e+006	-1.460e+006	-2.928e+006	-1.754e+006	-5.049e+006

Fig. 4. Process Flow Diagram (PFD) of the Fractionator

The column converges quickly with the good estimate provided from the shortcut model (Fig. 5). The column profiles can be checked by selecting the ''Performance'' tab in the column environment and then selecting ''Plots'' from the menu on the left and ''Composition'' from the list of possible plots. To size the trays in Hysys, must activate the tray sizing utility (from the Tools menu via Tools/Utilities/Tray Sizing). When bubble cap trays are selected withthe default spacing of 24 in (2 ft.) and the other default parameters. The column diameter is found to be 4.921 ft. The data on column size, number of trays, reboiler, and condenser duty can then be extracted from the simulation and put into a cost model or spreadsheet to carry out optimization of the total annual cost of production.

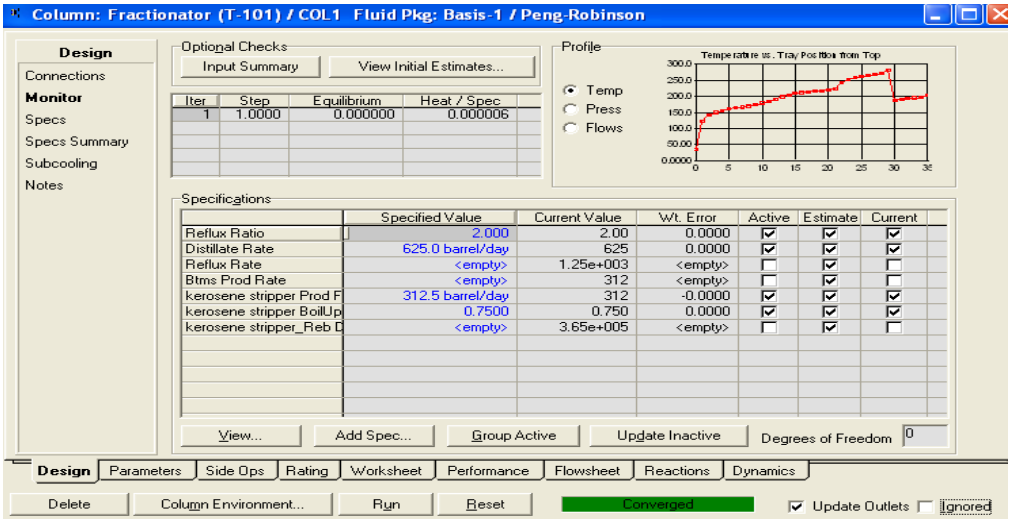

Fig. 5. Column specifications.

In this simulation 28 bubble cap trays were used in the main column for vapor-liquid equilibrium (Fig. 6). Bubble cap calculations are based on the method described in design of equilibrium stage processes by Bufford D. Smith [14]. Tray efficiency was used as 75%. Conditions on the trays like pressure, temperature, liquid and vapor flowrate are calculated for every tray which is given in the Fig.6

	Stage	Pressure [psig]	Temp [C]	Net Liquid [barrel/day]	Net Vapour [barrel/day]
1___T-100	1	10.00	123.2	1712	1875
2___T-100	2	10.07	141.4	1798	2337
3___T-100	3	10.15	150.8	1832	2423
4___T-100	4	10.22	156.6	1846	2457
5___T-100	5	10.30	160.7	1850	2471
6___T-100	6	10.37	163.9	1847	2475
7___T-100	7	10.44	166.9	1837	2472
8___T-100	8	10.52	170.0	1818	2462
9___T-100	9	10.59	173.7	1778	2443
10___T-100	10	10.67	179.2	1770	2403
11___T-100	11	10.74	184.0	1210	2210
12___T-100	12	10.81	192.2	1174	2148
13___T-100	13	10.89	199.6	1157	2112
14___T-100	14	10.96	205.4	1149	2094
15___T-100	15	11.04	209.6	1143	2086
16___T-100	16	11.11	212.5	1137	2081
17___T-100	17	11.19	214.7	1130	2075
18___T-100	18	11.26	216.5	1120	2067
19___T-100	19	11.33	218.3	1104	2057
20___T-100	20	11.41	220.4	1062	2041
21___T-100	21	11.48	224.2	1638	2000
22___T-100	22	11.56	243.3	1816	1325
23___T-100	23	11.63	253.2	1929	1503
24___T-100	24	11.70	258.2	1980	1617
25___T-100	25	11.78	261.6	2002	1667
26___T-100	26	11.85	264.6	2012	1690

Fig. 6. Process conditions at different trays

4. Results and discussion

Table 2. Comparison between the real operation and the simulation.

Parameters	Units	Simulation	Real
Column top temperature	^{o}C	123	130
Column top pressure	psig	10	11
Column bottom temperature	^{o}C	270	275
Column bottom pressure	psig	12	12
Column temperature at tray 11	^{o}C	184	170
Kerosene stripper temp.	^{o}C	200.8	195
Kerosene stripper press.	psig	10.74	11
Column feed temp.	^{o}C	200	200
Column feed press.	psig	25	25
MS product flowrate	BPD	625	675
Kerosene product flowrate	BPD	312.5	275
Diesel product flowrate	BPD	312.5	300
Products storage temp.	^{o}C	35	35

Fig. 3, Fig. 4 and Fig. 6 are the process simulation results. Table 2 is for the comparison between real plant's data and simulated data. Some major plant's operating data are compared with simulation results. The simulated volumetric flow rates with their corresponding temperatures for MS product, kerosene product and diesel product were 625 BPD, 312.5 BPD and 312.5 BPD but in real they are 675 BPD, 275 BPD and 300 BPD respectively. There was an increase in the real temperature for column top and column bottom whereas a decrease in the real temperature for kerosene stripper. The operating pressure remains almost same in both simulation result and plant data. Column feed condition was same for both cases.

5. Conclusion

Simulation software is a very good tool for the process industry, not only at the level of conceptual design but also during the entire lifecycle of the equipment, were it can be very useful for performance, debottlenecking and process studies. The study presents the simulation of a condensate fractionation plant. A Process Flow Diagram (PFD) was presented with heat and mass balances. The simulated results were compared with the real plant's data. Almost all the parameters matched with each other. This showed that the Column needed to be optimized in order to convert more of the atmospheric residue into other premium products like diesel, kerosene and petrol. The presented results have been obtained using the steady state version of the software, but all the simulations done in steady state can have an evolution to a dynamic simulation (for example to build process simulators for operator training or to study the behavior of the process units in transient conditions), or to a real time optimization system where, together with the advanced process control tools, can be very profitable in the optimization of the operation in real time.

6. References

[1] Fahim, T . A. Al-Sahhaf and A. S. Elkilani, "Fundamentals of Petroleum Processing" , 1st ed., *Elsevier*, Oxford , 2010.

[2] Boulet," Composition of Crude Oil and Petroleum Products", in Crude Oil Petroleum Products Process Flow sheets, Ch. 1,*T ECHNIP*, France, 2001.

[3] Young,"Petroleum refining process control and real-time optimization", Control Systems, *IEEE*, 26 (6), pp. 73-83,Dec. 2006.

[4] B. A. I. Liang, Y. Jiang, D. Huang and X. Liu, "A Novel Scheduling Strategy for Crude Oil Blending", *Chinese Journal of Chemical Engineering*, 18(5), pp. 777-86, Oct. 2010.

[5] G. K. D. Saharidis,M. Minoux and Y. Dallery, "Scheduling of loading and unloading of crude oil in a refinery using event-based discrete time formulation", *Chemical Engineering*, 33(8), pp. 1413-26, Aug. 2009.

[6] P. Behrenbruch and T. Dedigama, "Classification and characterization of crude oils based on distillation properties", *Journal of Petroleum Science and Engineering*, 57(1-2), pp. 166-80, May 2007.

[7] T. Chatterjee and D. N. Saraf, "On-line estimation of product properties for crude distillation units", *Journal of Process Control*, 1st Ed., vol. 14, pp. 61-77, Feb. 2004.

[8] R. K. More, V. K. Bulasara, R. Uppaluri and V. R. Banjara,"Optimization of crude distillation system using aspen plus: Effect of binary feed selection on grass-root design", *Chemical Engineering Research and Design*, 88(2), pp. 121-34, Feb. 2010.

[9] S. Motlaghi, F. Jalali and M. Nili Ahmadabadi, "An expert system design for a crude oil distillation column with the neural networks model and the process optimization using genetic algorithm framework", *Expert Systems with Applications*, 35(4), pp. 1540-45, Nov. 2008.

[10] D. D. Gonçalves and F. G. Martins,"Dynamic Simulation and Control: Application to Atmospheric Distillation Unit of Crude Oil Refinery", *Computer Aided Chemical Engineering*, vol. 28, 2010.

[11] Process simulation tutorial, Available at *http://process-simulations.net/hysys/oil-refining/fractional-distillation-of-crude-oil-hysys*]

[12] A. Rahman, K. Kirtania," simulation study of a fractionation column with varying parameters**",** *Engineering e-Transaction (ISSN 1823-6379)Vol. 6, No. 1, pp 43-4,9 June 2011,*

[13] José Egídio Fernandes Inverno[1,] Eurico Correia[2], Pablo Jiménez-Asenjo[3], Josep A. Feliu[3], 'Two examples of steady state simulation with HYSYS at GALPenergia sines refinery", *Elsevier*, Volume 18, Pages 211–216, 2004

[14] Hysys 3.2 User Guide, Available at *http://www.ece.jcu.edu.au/subjects/cl4070/HySyS%20documentation/Doc/HYSYS/UserGuide.pdf*

Paper ID: TE-05

Conjugate Effect of Convection and Conduction in a Nanofluid–Filled Complicated Cavity

Salma parvin*, Rehena Nasrin and M. A. Alim
Department of Mathematics,
Bangladesh University of Engineering and Technology, Dhaka-1000, Bangladesh
**E-mail: salpar@math.buet.ac.bd*

Abstract

Convective and conductive flow and thermal behaviors of nanofluid inside a complicated square enclosure is investigated numerically. The cavity consists of a centered heated diamond shaped solid obstacle. The vertical walls are uniformly heated at constant temperature while the base surface of the cavity is insulated. The upper horizontal part of the enclosure is surrounded by solid material with constant thermal conductivity. The upper boundary of this solid region is considered as adiabatic. The working fluid is water based nanofluid having alumina nanoparticle. The integral forms of the governing equations are solved numerically using Galerkin's Weighted Residual Finite Element method. Computational domains are divided into finite numbers of body fitted control volumes with collocated variable arrangement. Results are presented in the form of average Nusselt number, average temperature, mean velocity of the nanofluid, mid height horizontal and vertical velocities for a selected range of convective parameter Rayleigh number (10^3 - 10^6). Streamlines and isothermal lines are also displayed for the above mentioned parameter. The results indicate that the highest heat transfer rate is found for the greatest Rayleigh number.

Keywords: *Free convection, conduction, complicated enclosure, nanofluid, finite element method.*

1. Introduction

The fluids with solid-sized nanoparticles suspended in fluids are called "nanofluids". Due to small sizes and very large specific surface areas of the nanoparticles, nanofluids have superior properties like high thermal conductivity, minimal clogging in flow passages, long-term stability, and homogeneity. Thus, nanofluids have a wide range of potential applications like electronics, automotive, and nuclear applications where improved heat transfer or efficient heat dissipation is required.

House et al. [1] considered natural convection in a vertical square cavity with heat conducting body, placed on center in order to understand the effect of the heat conducting body on the heat transfer process in the cavity. They found that the heat transfer across the enclosure enhanced by a body with thermal conductivity ratio less than unity. Nasrin [2] analyzed numerically flow and heat transfer characteristics for wavy enclosure with a centered heat conducting cylinder. The author showed that the considered parameters strongly affect the flow phenomenon and temperature field inside the chamber. Conducting largest obstacle was preferable for effective heat transfer mechanism. Conjugate natural convection in a square porous cavity was studied by Baytas et al. [3]. A numerical study of convection heat transfer for air from two vertically separated horizontal heated cylinders confined to a rectangular enclosure had been conducted by Lacroix and Joyeux [4], where the vertical walls have finite conductivity and the heat conduction has been taken into consideration. Dong and Li [5] studied conjugate of natural convection and conduction in a complicated enclosure. They concluded that the flow and heat transfer increased with the increase of the thermal conductivity in solid region as well as both geometric shape and Rayleigh number affected the overall flow and heat transfer greatly.

Saleh et al. [6] investigated effect of conduction in bottom wall on Darcy–Bénard convection in a porous enclosure where increasing either the Rayleigh number or the thermal conductivity ratio or both, and decreasing the thickness of the bounded wall could increase the average Nusselt number for the porous enclosure. Conjugate natural convection around a finned pipe in a square enclosure with internal heat generation was studied by Ben-Nakhi and Chamkha [7]. Result illustrated that the effects of the finned pipe inclination angle and fins length on the streamlines and temperature contours within the enclosure were significant. Kuznetsov and Sheremet [8] analyzed conjugate natural convection in an enclosure with local heat sources where the

governing unsteady, three-dimensional heat transfer equations, written in dimensionless terms of the vorticity vector, vector potential functions and temperature, had been solved using an implicit finite-difference method. Conduction with natural convection heat transfer across multi-layer building blocks was studied by Baig and Antar [9]. The effect of both techniques could compensate for removing the insulation layer in the cavity used to increase the wall thermal resistance. Parvin et al. [10] analyzed heat transfer by nanofluid with different geometries. From their study it was observed that nanofluid enhanced rate of heat transfer than base fluid (clear water). Conjugate natural convection in an inclined nanofluid - filled enclosure was performed by Aminossadati and Ghasemi [11]. The result showed that the utilization of the nanofluid enhanced the thermal performance of the enclosure and that the length of the centered block affected the heat transfer rate.

The present study introduces heat transfer phenomena by water based nanofluid having Al_2O_3 nanoparticles. The numerical computation covers a wide range of Rayleigh number ($10^3 \leq Ra \leq 10^6$).

2. Model Specification

As shown in Fig. 1, a horizontal high temperature (T_h) diamond shaped hollow cylinder of diameter d is enclosed by an enclosure of square cross-section. Both vertical side walls in Fig. 1 of this cross-section are isothermal, the temperature is T_c. The upper horizontal boundary part of the rectangular is surrounded by solid material with constant thermal conductivity k_s. The upper of this solid region horizontal boundary is considered as adiabatic. The lower horizontal boundary of the cavity is supposed as ideal adiabatic boundary with infinite small wall thickness and zero thermal conductivity. It is assumed that the nanoparticles are spherical shaped and diameters are less than 10nm. All dimensions and boundaries of this geometrical model are noted in Fig. 1. The operational fluid is water based nanofluid having alumina nanoparticles. The thermophysical properties of the nanofluid are taken from Ogut [12] and given in Table 1.

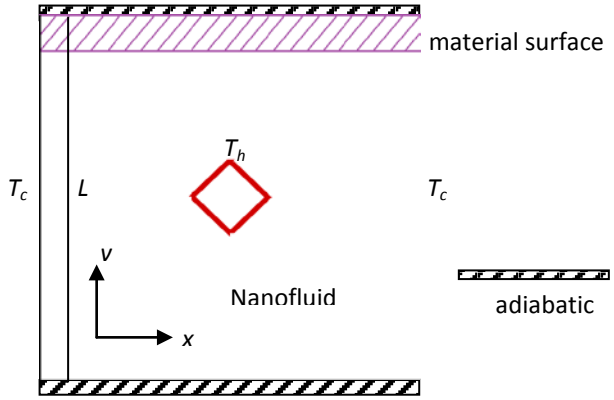

Fig. 1. Physical model of the complicated cavity

Table 1: Thermo physical properties of base fluid and alumina nanoparticles

Physical Properties	Fluid phase (Water)	Al_2O_3
C_p(J/kgK)	4179	765
ρ (kg/m^3)	997.1	3970
k (W/mK)	0.613	40
$\alpha\times10^7$ (m^2/s)	1.47	131.7
$\beta\times10^5$ (1/K)	21	2.4

3. Mathematical Formulation

A two-dimensional, steady, laminar, incompressible, free convection flow is considered within the enclosure and the fluid properties are assumed to be constant. The gravitational force acts in the vertically downward direction. The nanofluid containing two nanoparticles is assumed incompressible and the flow is considered to be laminar. It is taken that water and both nanoparticles are in thermal equilibrium and no slip occurs between them. The density of the nanofluid is approximated by the Boussinesq model. Only steady state case is considered. The radiation effects are taken as negligible. The dimensional equations describing the flow under Boussinesq approximation are as follows:

$$\frac{\partial u}{\partial x}+\frac{\partial v}{\partial y}=0 \tag{1}$$

$$\rho_{nf}\left(u\frac{\partial u}{\partial x}+v\frac{\partial u}{\partial y}\right)=-\frac{\partial p}{\partial x}+\mu_{nf}\left(\frac{\partial^2 u}{\partial x^2}+\frac{\partial^2 u}{\partial y^2}\right) \tag{2}$$

$$\rho_{nf}\left(u\frac{\partial v}{\partial x}+v\frac{\partial v}{\partial y}\right)=-\frac{\partial p}{\partial y}+\mu_{nf}\left(\frac{\partial^2 v}{\partial x^2}+\frac{\partial^2 v}{\partial y^2}\right)+g\left(\rho\beta\right)_{nf}(T-T_c) \tag{3}$$

$$u\frac{\partial T}{\partial x}+v\frac{\partial T}{\partial y}=\alpha_{nf}\left(\frac{\partial^2 T}{\partial x^2}+\frac{\partial^2 T}{\partial y^2}\right) \tag{4}$$

For solid material region the energy equation is

$$\frac{k_m}{\left(\rho C_p\right)_{nf}}\left(\frac{\partial^2 T_m}{\partial x^2}+\frac{\partial^2 T_m}{\partial y^2}\right)=0 \tag{5}$$

Here the effective density $\rho_{nf}=(1-\phi)\rho_f+\phi\rho_s$ (6)

the effective heat capacitance $\left(\rho C_p\right)_{nf}=(1-\phi)\left(\rho C_p\right)_f+\phi\left(\rho C_p\right)_s$ (7)

the effective thermal expansion coefficient $\left(\rho\beta\right)_{nf}=(1-\phi)\left(\rho\beta\right)_f+\phi\left(\rho\beta\right)_s$ (8)

the effective thermal diffusivity $\alpha_{nf}=k_{nf}\Big/\left(\rho C_p\right)_{nf}$ (9)

the effective dynamic viscosity (modified form) of Brinkman model [12]

$$\mu_{nf}=\mu_f(1-\phi)^{-2.5} \tag{10}$$

and the effective thermal conductivity (modified form) of Maxwell Garnett (MG) model [14]

$$k_{nf}=k_f\frac{k_s+2k_f-2\phi\left(k_f-k_s\right)}{k_s+2k_f+\phi\left(k_f-k_s\right)} \tag{11}$$

The boundary conditions for the present problem can be written as follows:
at all solid boundaries: $u = 0$, $v = 0$
at the bottom of the cavity: $\frac{\partial T}{\partial y}=0$
at the top of the material surface: $\frac{\partial T_m}{\partial y}=0$
at the vertical walls: $T = T_c$
at the diamond shaped boundaries: $T = T_h$
at the fluid-solid interface: $\left(\frac{\partial T}{\partial y}\right)_{nanofluid}=\frac{k_m}{k_{nf}}\left(\frac{\partial T_m}{\partial y}\right)_{material}$

The above equations are non-dimensionalized by using the following dimensionless quantities

$$X=\frac{x}{L},\ Y=\frac{y}{L},\ D=\frac{d}{L},\ U=\frac{uL}{\nu_f},\ V=\frac{vL}{\nu_f},\ P=\frac{pL^2}{\rho_f\nu_f^2},\ \theta=\frac{(T-T_c)}{(T_h-T_c)},\ \theta_m=\frac{(T_m-T_c)}{(T_h-T_c)}$$

Then the governing equations take the non-dimensional form given below

$$\frac{\partial U}{\partial X}+\frac{\partial V}{\partial Y}=0 \tag{12}$$

$$U\frac{\partial V}{\partial X}+V\frac{\partial V}{\partial Y}=-\frac{\rho_f}{\rho_{nf}}\frac{\partial P}{\partial Y}+\frac{\nu_{nf}}{\nu_f}\left(\frac{\partial^2 V}{\partial X^2}+\frac{\partial^2 V}{\partial Y^2}\right) \tag{13}$$

$$U\frac{\partial V}{\partial X}+V\frac{\partial V}{\partial Y}=-\frac{\rho_f}{\rho_{nf}}\frac{\partial P}{\partial Y}+\frac{\nu_{nf}}{\nu_f}\left(\frac{\partial^2 V}{\partial X^2}+\frac{\partial^2 V}{\partial Y^2}\right)+\frac{Ra}{Pr}\frac{(1-\phi)\left(\rho\beta\right)_f+\phi\left(\rho\beta\right)_s}{\rho_{nf}\beta_f}\theta \tag{14}$$

$$U\frac{\partial \theta}{\partial X}+V\frac{\partial \theta}{\partial Y}=\frac{1}{Pr}\frac{\alpha_{nf}}{\alpha_f}\left(\frac{\partial^2 \theta}{\partial X^2}+\frac{\partial^2 \theta}{\partial Y^2}\right) \tag{15}$$

For heat generating obstacle the energy equation is

$$\frac{K}{Pr}\left(\frac{\partial^2\theta_m}{\partial X^2}+\frac{\partial^2\theta_m}{\partial Y^2}\right)=0 \tag{16}$$

where $Pr=\frac{\nu_f}{\alpha_f}$ is the Prandtl number, $Ra=\frac{g\beta_f L^3\left(T_h-T_c\right)}{\nu_f\,\alpha_f}$ is the Rayleigh number and $K=\frac{k_m}{k_{nf}}$ is the dimensionless ratio of the thermal conductivities of solid and nanofluid.

The boundary conditions for the present problem are specified as follows:

at all solid boundaries: $U = 0$, $V = 0$

at the bottom of the cavity: $\frac{\partial\theta}{\partial Y}=0$

at the top of the material surface: $\frac{\partial\theta_m}{\partial Y}=0$

at the vertical walls: $\theta = 0$

at the diamond shaped boundaries: $\theta = 1$

at the fluid-solid interface: $\left(\frac{\partial\theta}{\partial Y}\right)_{nanofluid}=K\left(\frac{\partial\theta_m}{\partial Y}\right)_{material}$

The normal temperature gradient can be written as $\frac{\partial\theta}{\partial N}=\sqrt{\left(\frac{\partial\theta}{\partial X}\right)^2+\left(\frac{\partial\theta}{\partial Y}\right)^2}$

The average Nusselt number at the diamond shaped heated boundaries may be expressed as $Nu=\frac{1}{S}\int_0^S\overline{Nu}dS$

where N, S and dS are the non-dimensional distances either X or Y direction acting normal to the surface, arc length and coordinate along the cylinder surface respectively.

4. Computational Procedure

The penalty finite element method [15] is used to solve the Eqs. (2) - (4), where the pressure P is eliminated by a penalty constraint. The continuity equation is automatically fulfilled for large values of this penalty constraint. Then the velocity components (U, V), temperature (θ) and concentration (C) are expanded using a basis set. The Galerkin finite element technique yields the subsequent nonlinear residual equations. Three points Gaussian quadrature is used to evaluate the integrals in these equations. The non-linear residual equations are solved using Newton–Raphson method to determine the coefficients of the expansions. The convergence of solutions is assumed when the relative error for each variable between consecutive iterations is recorded below the convergence criterion ε such that $\left|\psi^{n+1}-\psi^{n}\right|\le 10^{-4}$, where n is the number of iteration and Ψ is a function of U, V, θ and C.

5. Results and Discussion

The natural convection and conduction phenomenon inside a complicated cavity filled with water alumina nanofluid is influenced by different Rayleigh number Ra. Analysis of the results is made through obtained streamlines, isotherms, average Nusselt number, mean temperature and velocity of the nanofluid, mid height horizontal and vertical velocities of nanofluid for various Ra. The ranges are varied as $10^3 \le Ra \le 10^6$, while the other parameters Pr, K and ϕ, are kept fixed at 6.2, 1 and 5% respectively.

Thermal current and flow activities are offered in Fig. 2 (a)-(b) with different Raleigh number (Ra). The strength of the flow circulation and the thermal current activities is much more activated with increasing Ra. For higher Ra, the isothermal lines take an onion shape from the diamond shaped body to the solid material surface. This is due to releasing the thermal boundary layer for the effect of higher buoyancy force. The lines become more concentrated near the heated obstacle which indicates steep temperature gradients and hence, an increase in the overall heat transfers from the heated surface to the surroundings of the complicated cavity. On the other hand, two main circulating vortices cover the whole region of the cavity without the upper material surface at $Ra = 10^3$. The right and left vortices near the diamond shaped cylinder rotate in clockwise and counterclockwise direction respectively. Size of spinning cells in the velocity field becomes larger and they become more strengthen due to buoyancy force for increasing Ra from 10^3 to 10^6. In addition more perturbation is observed in the streamlines at $Ra = 10^6$ because of rising buoyancy force.

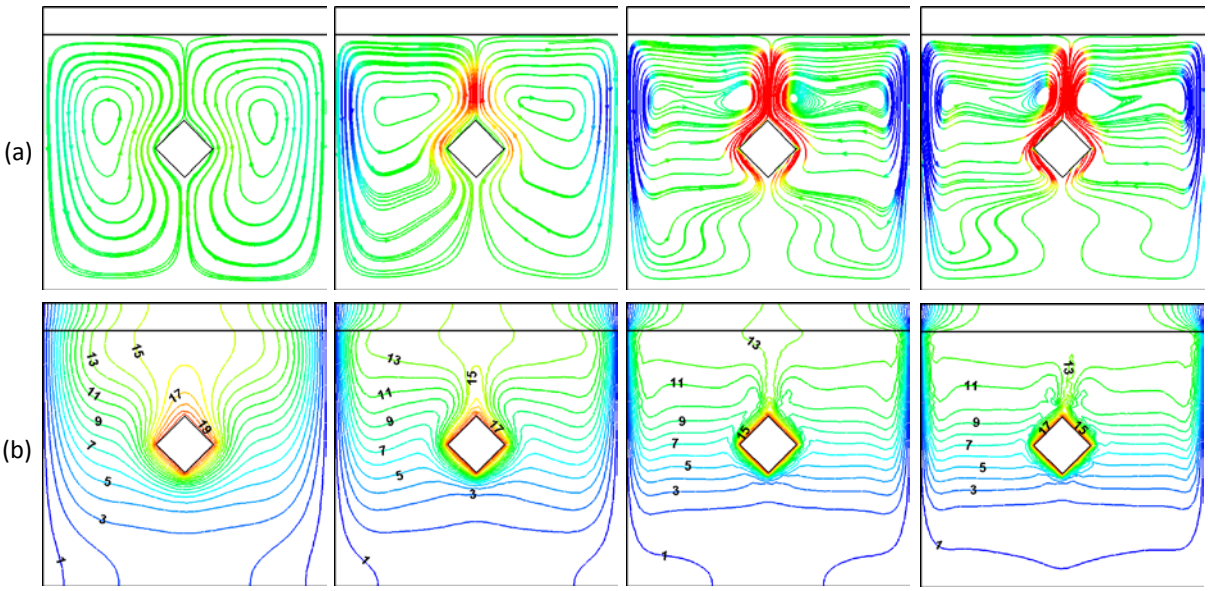

Fig. 2. Effect of Raleigh number on (a) Isotherms and (b) Streamlines

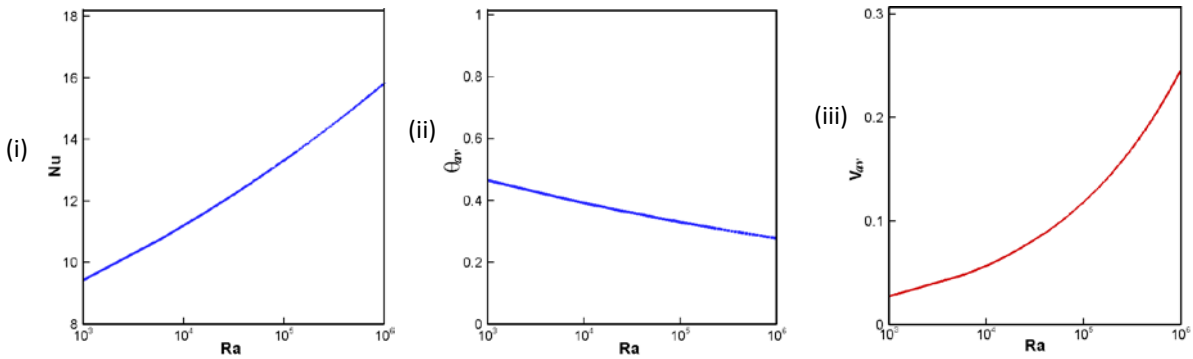

Fig. 3. (i) Average Nusselt number (ii) mean temperature and (iii) mean velocity of nanofluid for various *Ra*

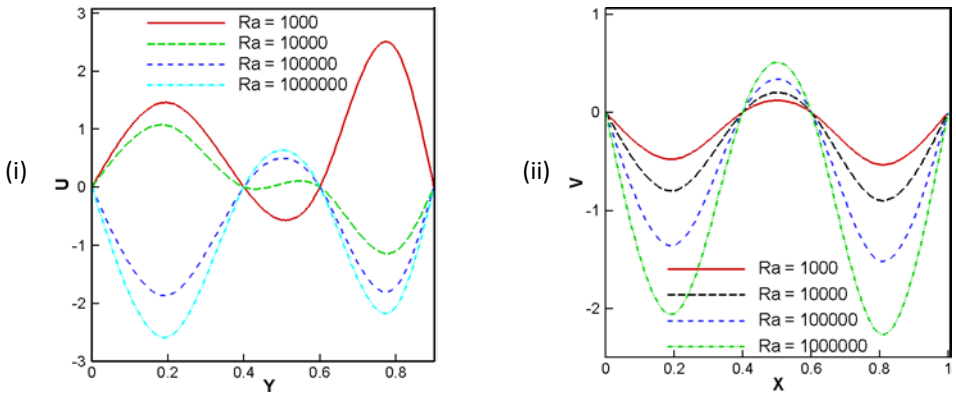

Fig. 4. Plot of mid height (i) *U* velocity and (ii) *V* velocity for various *Ra*

The variation of the average Nusselt number (*Nu*) at the centered heated cylinder, mean temperature of the nanofluid (θ_{av}) and average velocity of the nanofluid (V_{av}) for different Rayleigh numbers have been presented in Fig. 3(i)-(iii). It is clearly seen from the figure that the average Nusselt number is highest for the largest *Ra* = 10^6. This is because, the fluid with the highest Rayleigh number is capable to carry more heat away from the heated surface and dissipated through the whole domain. On the other hand, the rate of heat transfer for water based nanofluid having alumina nanoparticles is found to be more effective than the base fluid (clear water) due to higher thermal conductivity of solid nanoparticles. For this reason, rate of convective heat transfer enhances by 38% for the effect of *Ra*.

The mid height horizontal (U) velocity at $X = 0.5$ and the vertical (V) velocity at the middle ($Y = 0.05$) of the complicated geometry for various *Ra* is displayed in Fig. 4 (i)-(ii). Significant variation in velocity is found due to changing the *Ra*. It is observed that for the lowest *Ra* ($= 10^3$) the horizontal velocity line graphs are less varied than others. The waviness in the *V-X* profile devalues for lower values of *Ra*.

6. Conclusion

The following conclusions may be drawn from the present investigation:

The effect of buoyancy parameter *Ra* on isotherms and streamlines are remarkable.
Escalating *Ra* enhances the average Nusselt number at the heated diamond shaped cylinder.
The mean temperature of the nanofluid devalues for rising *Ra*.
Higher average velocity of the working fluid is found for higher *Ra*.

7. Acknowledgement

The work is supported by the department of mathematics, Bangladesh University of Engineering and Technology.

8. References

[1] J.M., House, C., Beckermann, T.F., Smith, "Effect of a centered conducting body on natural convection heat transfer in an enclosure", *Num. Heat Transfer, Part A*, 18, 213–225, 1990.

[2] R., Nasrin, "Influence of centered conducting obstacle on MHD combined convection in a wavy chamber", *J. of Naval Archit. and Marine Engg.*, 8, 2, 93-104, 2011.

[3] A.C., Baytas, A., Liaqat, I., Pop, "Conjugate natural convection in a square porous cavity", *Heat Mass Trans.* 37, 467, 2001.

[4] M., Lacroix, A., Joyeux, "Coupling of wall conduction with natural convection from heated cylinders in a rectangular enclosure", *Int. Commun. Heat Mass Trans.* 23, 1, 143–151, 1996.

[5] S., Dong, Y., Li, "Conjugate of natural convection and conduction in a complicated enclosure", *Int. J. of Heat and Mass Trans.*, 47, 2233–2239, 2004.

[6] H., Saleh, NH., Saeid, I., Hashim, Z., Mustafa, "Effect of Conduction in Bottom Wall on Darcy–Bénard Convection in a Porous Enclosure", *Transport in Porous Media*, 88, 3, 357-368, 2011.

[7] A., Ben-Nakhi, A.J., Chamkha, "Conjugate natural convection around a finned pipe in a square enclosure with internal heat generation", *Int. J. of Heat and Mass Trans.*, 50, 2260–2271, 2007.

[8] G.V., Kuznetsov, MA., Sheremet, "Conjugate natural convection in an enclosure with local heat sources", *Comp. Thermal Sci.*, 1, 341–360, 2009.

[9] H., Baig, M.A., Antar, "Conduction / natural convection analysis of heat transfer across multi-layer building blocks", *5th Europ. Thermal-Sci. Conf.*, The Netherlands, 2008.

[10] S., Parvin, R., Nasrin, MA., Alim, N.F., Hossain, A.J., Chamkha, "Thermal conductivity variation on natural convection flow of water-alumina nanofluid in an annulus", *Int. J. of Heat and Mass Trans.*, 55, 19-20, 5268-5274, 2012.

[11] S.M., Aminossadati, B., Ghasemi, "Conjugate natural convection in an inclined nanofluid - filled enclosure", *Int. J. of Num. Methods for Heat & Fluid Flow* , 22, 4, 21, 2012.

[12] E.B., Ogut, "Natural convection of water-based nanofluids in an inclined enclosure with a heat source", *Int. J. of Thermal Sci.*, 48, 1–11, 2009.

[13] H.C., Brinkman, "The viscosity of concentrated suspensions and solution", *J. Chem. Phys.*, 20, 571–581, 1952.

[14] J.C., Maxwell-Garnett, "Colours in metal glasses and in metallic films", *Philos. Trans. Roy. Soc. A*, 203, 385–420, 1904.

[15] T. Basak, S. Roy, I. Pop, "Heat flow analysis for natural convection within trapezoidal enclosures based on heatline concept", *Int. J. Heat Mass Transfer* 52, 2471–2483, 2009.

Paper ID: TE-07

Experimental Investigation and Prediction of Heat Transfer in Turbulent Flow through Tube with Conical Ring Inserts

Saddam Hossain Khan, M. A. Rashid Sarkar[1]
[1]Professor, Department of Mechanical Engineering, Bangladesh University of Engineering & Technology, Dhaka-1000
E-mail: shkhan.buet0710131@gmail.com

Abstract

An experimental investigation has been carried out to study the effect of conical-ring inserts on heat transfer and turbulent flow friction in a horizontal circular tube. The conical-rings were of three different pitch ratios (PR = 0.0, 7.5 and 9.0) corresponding to three different number of conical-rings (N = 1, 2 and 3), respectively. The diameter ratio of the conical-rings was 0.5. The experiments were conducted for air as the working fluid with Reynolds number ranging from about $2x10^4$ to $6x10^4$ under uniform wall heat flux condition. The results revealed that as much as three-fold improvement in heat transfer coefficient might be achieved at the cost of increased pumping power. Over the range investigated, the maximum thermal performance factor of around 1.7 has been found at PR =7.5. Finally, a correlation has been developed for the prediction of Nusselt number in turbulent flow for tubes with conical-ring inserts.

Keywords: conical-ring insert, heat transfer, friction factor, pumping power, thermal performance factor.

1. Introduction

The efficiency and economic competitiveness of industrial processes depend, to a great extent, on the performance of heat exchangers. This performance can be improved by using various enhancement techniques [1]. The uses of turbulence promoters or turbulator devices are heat transfer enhancement techniques that have been widely employed for improving the heat transfer rate in heat exchangers. Typically, the turbulators increase fluid mixing, by increasing turbulence or by limiting the growth of fluid boundary layers close to the heat transfer surfaces [2]. The effects of reverse flow and boundary layer disruption by the turbulators are to enhance the heat transfer coefficient and momentum transfers. Various designs of turbulator devices are being used to improve the heat transfer rate such as V-nozzles, truncated hollow cones, conical nozzles, conical-rings (CR), conical wires, circular cross-sectional rings, etc.

A.A. Jadoaa [3] experimented with drilled conical-ring inserts for enhancing heat transfer rate in a constant heat flux circular tube. He showed that the average Nusselt number increases as the space length between the conical-rings decrease and as the Reynolds number increases. But the friction factor for drilled conical-ring is higher than the plain tube. Kongkaitpaiboon, V. et al [8] experimentally investigated the influences of the perforated conical rings (PCR). The perforated conical rings arranged in the diverging pattern were of three different pitch ratios and three different numbers of perforated holes. It was found that the PCR considerably diminishes the development of thermal boundary layer, leading to the heat transfer rate up to about 137% over that of the plain tube. P. Promvonge and S. Eiamsa-ard [9] experimentally investigated heat transfer and friction characteristics with combined conical-ring and twisted-tape insert in a uniform heat flux tube. The average Nusselt numbers for employing the conical-ring together with the twisted-tape for Y=3.75 and 7.5 respectively, are found to be 10% and 4% over that for using the conical-ring alone or to be about 367% and 350% over the plain tube.

As declared in the literature review, the survey shows that very limited data has been published on the heat transfer performance of tubes with conical-ring inserts in converging arrangement. However, any numerical investigation on conical-rings inserts has hardly been carried out for understanding its action on enhancing thermo-hydraulic performance.

The present work was, therefore, undertaken for fulfilling the following objectives:

1) To study the influence of conical ring inserts on heat transfer located at different pitch ratios inside a tube with properly fabricated experimental facility.
2) To determine experimentally different heat transfer parameters such as heat transfer coefficient, friction factor and pumping power at different Reynolds numbers for tubes with conical ring inserts and compare these parameters with that of the smooth tube.
3) To analyze the heat transfer performance by determining the thermal performance factors.
4) To develop a correlation as a recommendation for prediction of heat transfer in tubes with conical-ring inserts.

2. Experimental apparatus and procedure

Experimental apparatus

All Fig. 1 depicts the schematic view of an experimental setup. It mainly consists of a heat transfer test section with proper insulation, data acquisition system for displaying temperature values, a pitot tube and a high pressure induced draft fan. For the test section, the test tube was heated by continually winding flexible nichrome wire to provide a uniform wall heat flux boundary condition. The test tube is made of brass with a dimension of L = 1500 mm for length, D = 70 mm for inner diameter, D_o = 80 mm for outer diameter, and t = 5 mm for tube thickness. For keeping a uniform wall heat flux conditions along the entire length of the test section, the electrical power was controlled by a variable voltage transformer. The temperature distribution at the inner tube wall was measured using type K thermocouples which were tapped on the local wall of the tube. The outer surface of the test tube was well insulated to minimize convective heat loss to surroundings, and necessary precautions were taken to prevent leakages from the system. A traversing pitot tube was used to measure the air flow. The pressure drop was measured using a U-tube manometer.
In the experiments, all of the conical-ring inserts were located in converging conical-ring arrangements (CR array). The arrangement of these enhancement devices in the tube and their geometrical details are shown in Fig. 2. The conical-ring inserts were made of aluminum with 65 mm in length and its throat diameter was 32.5 mm (0.5D), with 2 mm thickness. Single conical-ring located at 30 mm from the test tube inlet, two conical-rings (N = 2) with pitch length, p = 630 mm (PR = 9.0) and three conical-rings (N =3) with pitch length, p = 525 mm (PR = 7.5) were used in the present work for comparison. It should be noted that to fix the conical-rings in the tube, they were fastened with two very smooth wire rods.

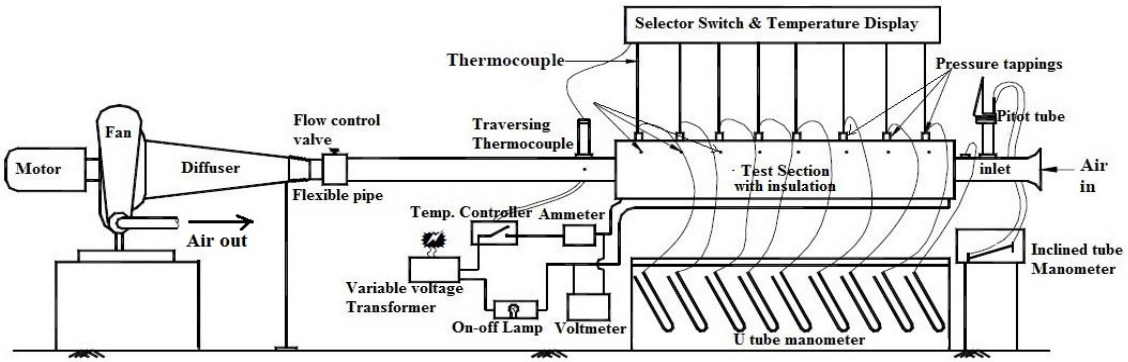

Fig. 1. Schematic diagram of the experimental setup

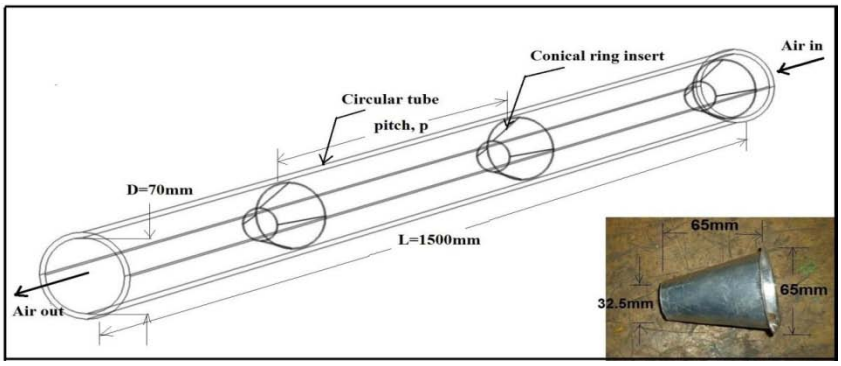

Fig. 2. Converging arrangement of three conical rings inside the test section

Experimental procedure

The fan was first switched on and allowed to run for about ten minutes to neutralize the transient characteristics. The flow of air through the test section was set to a desired value and was kept constant with the help of a butterfly valve. The electric heater was then switched on, adjusting the output level with the help of a regulating transformer, if necessary. At the steady-state condition thermocouple readings were recorded manually with the help of selector switch and at the same time, manometric readings were taken by the inclined manometer.

3. Data reduction

The convective heat flux is assumed to be uniform distribution over the heated wall tube and evaluated as:

$$Q = hA(T_w - T_b) = h(\pi D_i L)(T_w - T_b) \tag{1}$$

Where, h is the local heat transfer coefficient, Di is the inside diameter of the tube, L is the tube length, T_w is the local temperature of the inner wall surface, T_b is the bulk air temperature in the test section that is assumed to be linearly rising along the test section, whereas,

$$T_b = \frac{T_o + T_i}{2} \tag{2}$$

Thus the heat transfer coefficient can be written as follows,

$$h_x \frac{MC_{p,a}(T_o - T_i)}{\pi D_i L(T_w - T_b)}; h = \frac{\sum h_{1-8}}{8} \tag{3}$$

Where h is the average heat transfer coefficient, which is mean value of the 8 local points lined between the inlet and the exit of the test section and evaluated at the outer wall surface of the inner tube. The mass flow rate is calculated as follows,

$$M = \rho_a A_x v_m = \rho \frac{\pi D_i^{\,2}}{4} v_m \tag{4}$$

Where ρ_a is the density of air at room temperature, v_m is the mean velocity of air inside the tube and Ax is the cross-sectional area at the inlet of the tube. The average heat transfer coefficient is reported in term of Nusselt number, Nu which is defined as follows,

$$Nu = \frac{hD_i}{k} \tag{5}$$

Reynolds number is defined as,

$$\mathrm{Re} = \frac{\rho_b v_m D_i}{\mu_b} \tag{6}$$

Where ρ_b is the bulk air density, is the mean velocity and μ_b is the bulk air dynamic viscosity. An apparent friction factor, f can be evaluated from the following equation,

$$f = \frac{(\Delta P / L) D_i}{(1/2)\rho_b {v_m}^2} \tag{7}$$

Where L is the axial distance between two pressure taps and v_m is the mean velocity. All of the thermo-physical properties of air are determined at the overall bulk air temperature.

4. Results and discussion

Heat transfer results

Prior to the present work, Nusselt numbers for the smooth tube have been measured under a uniform heat flux condition and then compared with those obtained from the fundamental equation (8) by Dittus and Boelter in order to validate the present results.

$$Nu = 0.023\,\mathrm{Re}^{0.8}\,\mathrm{Pr}^{0.4} \tag{8}$$

The heat transfer results of the present work agree well with little discrepancies from 5% to 13%. In addition, the experimental results of the present smooth tube in term of the Nusselt number can be expressed as

$$Nu = 0.02838\,\mathrm{Re}^{0.769}\,\mathrm{Pr}^{0.33} \tag{9}$$

The relationship between Nusselt number and Reynolds number signifies that the Nusselt number increases with the Reynolds number due to the rise of mass transfer within the tube. Fig. 3 shows that the overall Nusselt number for inserted tube with single conical ring is about 27% to 200% higher than that of smooth tube over the Re range investigated. Conical-rings located at PR=7.5 inside the tube gives around 1.3 to 2.0 times higher heat transfer over the Reynolds number range investigated. The present effect of the pitch ratio (PR=0.0, 7.5 and 9.0) of the conical-ring inserts on the heat transfer enhancement are correlated in term of the Nusselt number for different Reynolds numbers as,

$$Nu = [10^{-5}.e^{0.412(PR)}].\mathrm{Re}^{[-0.021(PR)^2+0.147(PR)+1.531]}.\mathrm{Pr}^{0.33} \tag{10}$$

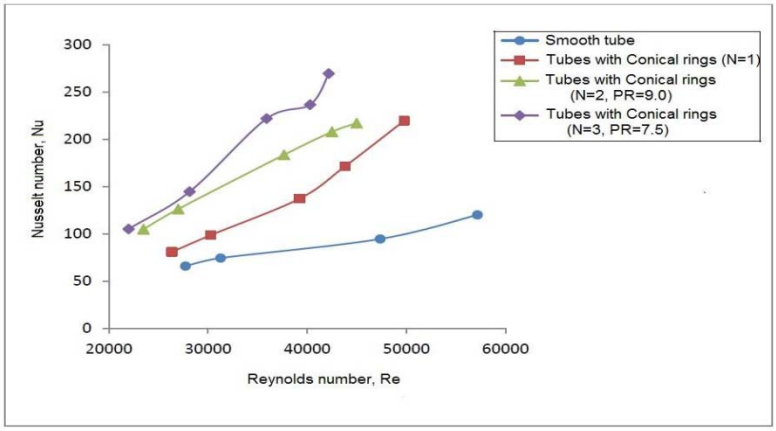

Fig. 3. Variation of overall Nusselt number with Reynolds number for both smooth tube and tubes with conical-ring inserts

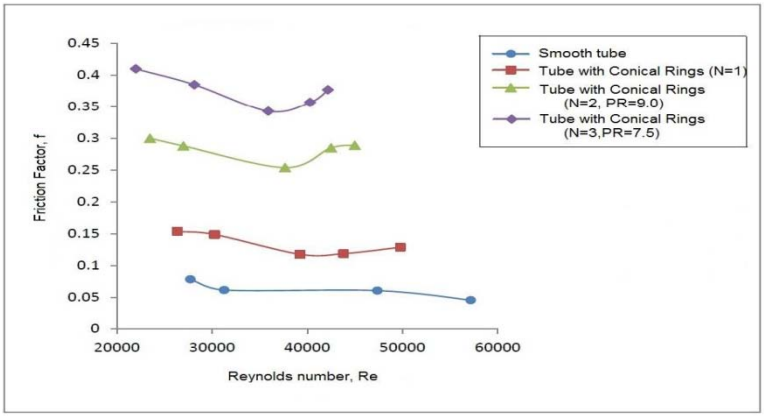

Fig. 4. Friction factor variation with Reynolds number for both smooth tube and tubes with conical-ring inserts

Friction factor results

Fig. 4 shows that the average friction factors for tubes with conical ring inserts are higher than that for the smooth tube at comparable Reynolds numbers. Evidently friction factor noticeably increases with increasing number of conical rings i.e. decreasing pitch ratio. This is due to the simple fact that the smaller distance between each pair of the conical rings, the more number of conical rings available in the tube, thus the more blockage against the flowing stream. The quantitative results show that the friction factor of the tube equipped with three conical rings (N=3) at PR=7.5 is approximately above 400% higher than that of the smooth tube.

Pumping power results

Fig. 5 exhibits that the conical-ring inserts enhances heat transfer at the cost of increased pumping power. It shows that the pumping power increases with the Reynolds number. Conical ring inserts with different pitch ratio also affects the pumping power requirement. It is observed from the Fig. 5 that the pumping power is required significantly higher, maximum in the case of maximum number of conical rings at lower pitch ratio. Extra blower power is required to overcome adversely increasing.

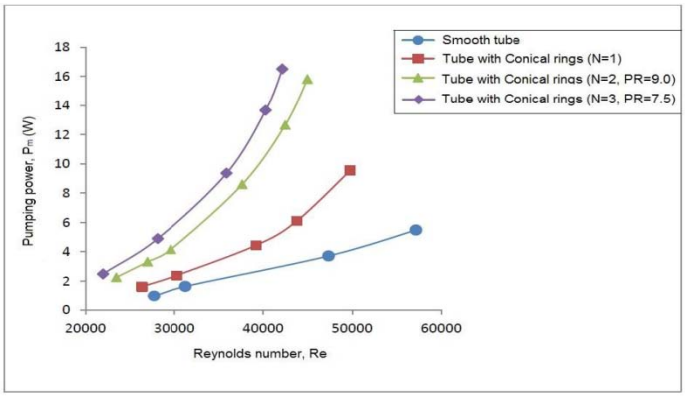

Fig. 5. Pumping power variation with Reynolds number for both smooth tube and tubes with conical-ring inserts

Thermal performance factor

According to the results shown above, the CR inserts offers heat transfer enhancement in accompany with the increase of friction factor. The increase of friction causes a rise of pumping power. Therefore, the actual effectiveness of the CR inserts depends upon the weight of the increase in heat transfer and the increase in friction which can be determined from performance evaluation. The thermal performance factor (η) at constant pumping power is the ratio of the convective heat transfer coefficient of the tube with heat transfer enhancement device (CR) to the plain tube.

$$\eta = \frac{(Nu_{CR} / Nu_s)}{(f_{CR} / f_s)^{1/3}} \tag{11}$$

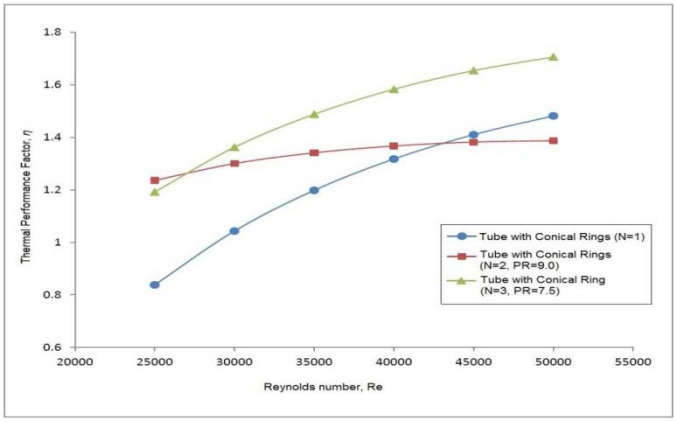

Fig. 6. Comparison of thermal performance factors among tubes with different arrangements of conical-ring inserts with respect to Reynolds number

It is observed from Fig. 6 that the thermal performance factor follows an increasing trend with the Reynolds number. For single conical ring insertion, the thermal performance factor has been found below unity signifying uneconomical enhancement at the lower Reynolds number regime, which is not the case for conical rings at PR=9.0 and 7.5. At the higher Reynolds number regime, thermal performance factor has been found maximum of above 1.6 for three conical ring inserts (N=3) located at PR=7.5. From Fig. 6 it is also seen that the thermal performance factor for two conical rings (N=2) is neither lesser than three rings (N=3) nor better than single ring (N=1) insertion in between the range of about Re=27000 to 43000, respectively.

5. Summary

Hydro-dynamically fully developed and thermally partially developed flow through circular tube has been experimentally investigated in order to test the heat transfer enhancement efficiency of conical ring inserts. Performance of the conical ring inserts has also been evaluated. The gists of the present study are given below:

1) The average heat transfer coefficient and overall Nusselt number increases with Reynolds number. The overall Nusselt number has been found to increase by about 140% to 300% revealing significant heat transfer enhancement with conical ring inserts compared to smooth tube.

2) The friction factor is found to increase with conical ring inserts by 1 to 4 times compared to the smooth tube. The pumping power is found to increase to 1.67 to 5.33 times with conical ring inserts compared to that required for smooth tube.

3) The thermal performance factor is found maximum of above 1.6 for three conical ring inserts with pitch ratio 7.5. The thermal performance is found to be better for two conical ring inserts with pitch ratio 9.0 than that of 1 conical ring insert in the Reynolds number of range of about 27000 to 43000.

The conical-rings increase fluid mixing, by increasing turbulence or by limiting the growth of fluid boundary layers close to the heat transfer surfaces. The effects of reverse flow and boundary layer disruption by the rings enhance the heat transfer coefficient and momentum transfers at the expense of pressure drops.

6. Recommendation for future work

The present study has been carried out for conical-ring inserts with converging arrangements. These investigations may also be done with diverging or converging-diverging arrangements. Conical ring inserts with different diameter ratios may be implemented to study the heat transfer enhancement as well.

11. References

[1] M.A.R. Sarkar, S.H. Khan, S. Saha, M.S. Islam, and M.A. Khair, "Review of Insert Devices as Heat Transfer Enhancement Techniques", *Proc. of the 6th Intl. Mechanical Engineering Conference*, Paper No.HT-11, pp. 1-13, 2012.

[2] S.H. Khan, S. Saha, and M.A.R. Sarkar, "Numerical Investigation of Heat Transfer Enhancement in Turbulent Flow through a Tube with Conical-ring Inserts", *Proc. of the Intl. Conference of Mechanical, Industrial and Energy Engineering*, Paper No.MIE 12-107, pp. 1-6, 2013.

[3] A.A. Jadoaa, "Experimental Investigations of Heat Transfer and Pressure Drop Characteristics of Flow through Tube Fitted with Drill-cut Conical-rings", *Journal of Eng. & Tech*, Vol.29, No.3, pp. 477-487, 2011.

[4] A.A. Mohammed, "Heat Transfer and Pressure Drop Characteristics of Turbulent Flow in a Tube Fitted with Conical Ring and Twisted Tape Inserts", *Journal of Eng. & Tech*, Vol.29, No.2, pp. 226-239, 2011.

[5] A.M. Sarkar, M.A.R. Sarkar, and M.A. Majid, "Heat Transfer and Pressure Drop in Turbulent Flow through a Tube with Longitudinal Perforated Star-shaped Inserts", *Journal of Enhanced Heat Transfer*, Vol.18, No.6, pp. 491-502, 2011.

[6] J.U. Ahmed, M.A. Wazed, S. Ahmed, Y. Nukman, T.M.Y.S. Tuan Ya, and M.A.R. Sarkar, "Enhancement and Prediction of Heat Transfer Rate in Turbulent Flow through Tube with Perforated Twisted Tape Inserts: A New Correlation", *Journal of Heat Transfer*, Vol.133, No.041903, pp. 1-9, 2011.

[7] M.A. Wazed, J.U. Ahmed, S. Ahmed, and M.A.R. Sarkar, "Enhancement of Heat Transfer in Turbulent Flow through a Tube with a Perforated Twisted Tape Insert", *Journal of Enhanced Heat Transfer*, Vol.18, No.1, pp. 1-13, 2011.

[8] V. Kongkaitpaiboon, K. Nanan, and S. Eiamsa-ard, "Experimental Investigation of Heat Transfer and Turbulent Flow Friction in a Tube Fitted with Perforated Conical Rings", *Proc. of the Intl. Communication of Heat and Mass Transfer, Paper* No.37, pp. 560-567, 2010.

[9] P. Promvonge, and S. Eiamsa-ard, "Heat Transfer and Turbulent Flow Friction in a Circular Tube Fitted with Conical-nozzle Turbulators", Proc. of the *Intl. Communication of Heat and Mass Transfer, Paper* No.34, pp. 72-82, 2007.

[10] P. Promvonge, and S. Eiamsa-ard, "Heat Transfer Enhancement in a Tube with Combined Conical-nozzle Inserts and Swirl Generator", *Proc. of the Energy Conversion and Management*, Paper No.47, pp. 2867-2882, 2006.

[11] M.A.R. Sarkar, M.Z. Islam, and M.A. Islam, "Heat Transfer in Turbulent Flow through Tube with Wire-coil Inserts", *Journal of Enhanced Heat Transfer*, Vol.12, No.4, pp. 385-394, 2005.

Paper ID: TE-09

Heat absorption and Joule heating effect along a vertical wavy surface on MHD free convection flow with viscosity dependent on temperature

N. Parveen and M. A. Alim
Department of Mathematics, Bangladesh University of Engineering and Technology
Dhaka-1000, Bangladesh
E-mail: nazma@math.buet.ac.bd

Abstract

The interaction of free convection with heat absorption and Joule heating of viscous incompressible fluid and heat transfer characteristics on MHD steady two-dimensional laminar flow along a uniformly heated vertical wavy surface with viscosity dependent on temperature has been analyzed numerically. Using the appropriate variables; the basic equations are transformed to convenient form. The resulting nonlinear systems of partial differential equations are mapped into the domain of a vertical flat plate. The governing equations are solved numerically using an implicit finite difference scheme of Keller-box type. The effect of various physical parameters such as the heat absorption parameter, Joule heating parameter and viscosity parameter on the streamline and isotherms of the fluid as well as the shearing stress and heat transfer rate in terms of the skin friction coefficient and local Nusselt number are computed and presented graphically in detail while, magnetic parameter (M) and the amplitude-to-length ratio of the wavy surface (α) are considered fixed. It is found that the numerical results are strongly dependent on the set of parameters entering into the problem.

Keywords: *Heat absorption, Joule heating, temperature dependent viscosity, MHD, free convection, Keller-box method, wavy surface.*

1. Introduction

The study of heat generation or absorption in moving fluids is important in problems dealing with chemical reactions and those concerned with dissociating fluids. The characteristics of free convection flow of electrically conducting fluid in the presence of heat absorption on magnetic field along a wavy surface is important from the technical point of view and such type of problems have received much attention of many researchers. If the surface is roughened the flow is disturbed by the surface and this alters the rate of heat transfer. For examples, flat-plate solar collectors, flat-plate condensers in refrigerators and heat exchanger. The viscosity of the fluid to be proportional to a linear function of temperature, two semi-empirical formulae which was proposed by Charraudeau [1]. Yao [2] first investigated the free convection heat transfer from an isothermal vertical wavy surface and used an extended Prantdl's transposition theorem and a finite-difference scheme. He proposed a simple transformation to study the free convection heat transfer for an isothermal vertical sinusoidal surface. These simple coordinate transformations method to change the wavy surface into a flat plate. Vajravelu and Hadjinolaou [3], studied the heat transfer characteristics in the laminar boundary layer of a viscous fluid over a stretching sheet with viscous dissipation or frictional heating and internal heat generation. In this study they considered that the volumetric rate of heat generation, q^m [W /m^3], should be $q^m = Q_0(T- T_\infty)$, for $T \geq T_\infty$ and equal to zero for $T < T_\infty$, where Q_0 is the heat generation/absorption constant. The above relation explained by Vajravelu and Hadjinolaou [3], is valid as an approximation of the state of some exothermic process and having T_∞ as the onset temperature. When the inlet temperature are not less than T_∞ they used $q^m = Q_0(T- T_\infty)$. Alam et al. [4] considered the problem of free convection from a wavy vertical surface in presence of a transverse magnetic field using Keller box method. The combined effects of thermal and mass diffusion on the natural convection flow of a viscous incompressible fluid along a vertical wavy surface investigated by Hossain and Rees [5]. Cheng [6] studied the natural convection heat and mass transfer near a vertical wavy surface with constant wall temperature and concentration in a porous medium. The problem of natural convection of fluid with temperature dependent viscosity along a heated vertical wavy surface have been studied by Hossain et al. [7]. Molla et al. [8] numerically investigated natural convection flow along a vertical wavy surface with uniform surface temperature in presence of heat generation/absorption. Molla et al. [9] also studied radiation effect on

mixed convection laminar flow along a vertical wavy surface. Very recently, Parveen and Alim [10] considered the effect of MHD free convection flow in presence of Joule heating and heat generation with viscosity dependent on temperature along a vertical wavy surface.
In all the aforementioned analysis the heat absorption and Joule heating effect on magnetic field with temperature dependent viscosity free convection flow along wavy surface have not been studied. The current study is used to deal with this problem. Using the appropriate transformations, the boundary layer equations are reduced to dimensionless partial differential forms. Numerically results have been obtained in terms of local skin friction and the rate of heat transfer in terms of local Nusselt number, the streamlines as well as the isotherms for a selection of relevant physical parameters and discussed graphically.

2. Mathematical formulation of the problem

The boundary layer analysis outlined below allows $\bar{\sigma}(X)$ being arbitrary, but our detailed numerical work assumed that the surface exhibits sinusoidal deformations. The wavy surface may be described by

$$Y_w = \bar{\sigma}(X) = \alpha \sin\left(\frac{n\pi X}{L}\right) \tag{1}$$

where L is the wave length associated with the wavy surface.
The geometry of the wavy surface and the two-dimensional cartesian coordinate system are shown in Fig. 1.

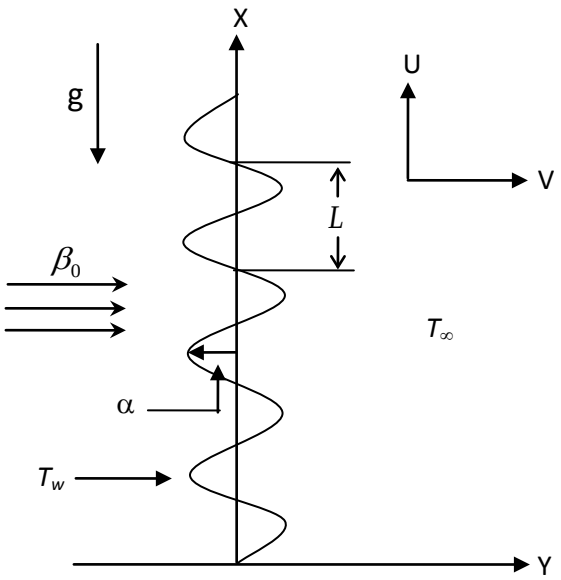

Fig. 1. Physical model and coordinate system

Under the usual Boussinesq approximation, the governing equations describing the conservation of mass, momentum and energy, respectively can be written non dimensional form as follows:

$$\frac{\partial u}{\partial x} + \frac{\partial v}{\partial y} = 0 \tag{2}$$

$$u\frac{\partial u}{\partial x} + v\frac{\partial u}{\partial y} = -\frac{\partial p}{\partial x} + Gr^{1/4}\sigma_x \frac{\partial p}{\partial y} + \left(1+\sigma_x^2\right)(1+\varepsilon\theta)\frac{\partial^2 u}{\partial y^2} + \varepsilon\left(1+\sigma_x^2\right)\frac{\partial \theta}{\partial y}\frac{\partial u}{\partial y} - Mu + \theta \tag{3}$$

$$\sigma_x\left(u\frac{\partial u}{\partial x} + v\frac{\partial u}{\partial y}\right) = -Gr^{1/4}\frac{\partial p}{\partial y} + \sigma_x\left(1+\sigma_x^2\right)(1+\varepsilon\theta)\frac{\partial^2 u}{\partial y^2} + \varepsilon\sigma_x\left(1+\sigma_x^2\right)\frac{\partial \theta}{\partial y}\frac{\partial u}{\partial y} - \sigma_{xx}u^2 \tag{4}$$

$$u\frac{\partial \theta}{\partial x} + v\frac{\partial \theta}{\partial y} = \frac{1}{\Pr}\left(1+\sigma_x^2\right)\frac{\partial^2 \theta}{\partial y^2} + Q\theta + Ju^2 \tag{5}$$

In the above equations Pr, Q, ε, J and M are respectively known as the Prandtl number, heat absorption parameter, viscosity variation parameter, Joule heating parameter and magnetic parameter, which are defined as

$$\Pr = \frac{C_p \mu_\infty}{k},\ Q = \frac{Q_0 L^2}{\mu C p G r^{1/2}},\ \varepsilon = \varepsilon^*(T_w - T_\infty),\ J = \frac{\sigma_0\ \beta_0^2\ \nu\ Gr^{1/2}}{\rho C_p (T_w - T_\infty)} \text{ and } M = \frac{\sigma_0 \beta_0^2 L^2}{\mu Gr^{1/2}}$$

The variable viscosity chosen in this study which is introduced by Charraudeau [1] and used by Hossain et al. [7] as follows:

$$\mu = \mu_\infty[1+\varepsilon^*(T-T_\infty)] \tag{6}$$

where μ_∞ is the viscosity of the ambient fluid and ε* is a constant.
Following Yao [2], here introduce the following non-dimensional variables

$$x=\frac{X}{L},\ y=\frac{Y-\overline{\sigma}}{L}Gr^{\frac{1}{4}},\ u=\frac{\rho L}{\mu_\infty}Gr^{-1/2}U,\quad v=\frac{\rho L}{\mu_\infty}Gr^{-1/4}\left(V-\sigma_x U\right)$$

$$\theta=\frac{T-T_\infty}{T_w-T_\infty},\sigma_x=\frac{d\overline{\sigma}}{dX}=\frac{d\sigma}{dx},Gr=\frac{g\beta(T_w-T_\infty)}{\nu^2}L^3\ ,\ p=\frac{L^2}{\rho\nu^2}Gr^{-1}P$$

Equation (4) indicates that the pressure gradient along the *y*-direction is $O(Gr^{-1/4})$, which implies that lowest order pressure gradient along *x*-direction can be determined from the inviscid flow solution. For the present problem this pressure gradient ($\partial p/\partial x = 0$) is zero. Equation (4) further shows that $Gr^{1/4}\partial p/\partial y$ is O(1) and is determined by the left-hand side of this equation. Thus, the elimination of $\partial p/\partial y$ from equations (3) and (4) leads to

$$u\frac{\partial u}{\partial x}+v\frac{\partial u}{\partial y}=\left(1+\sigma_x^2\right)(1+\varepsilon\theta)\frac{\partial^2 u}{\partial y^2}-\frac{\sigma_x\sigma_{xx}}{1+\sigma_x^2}u^2+\varepsilon\left(1+\sigma_x^2\right)\frac{\partial u}{\partial y}\frac{\partial\theta}{\partial y}-\frac{M}{1+\sigma_x^2}u+\frac{1}{1+\sigma_x^2}\theta \tag{7}$$

The corresponding boundary conditions for the present problem are

$$\left.\begin{aligned} &u=v=0,\quad \theta=1 \qquad at\quad y=0\\ &u=\theta=0,\quad p=0 \qquad as\quad y\to\infty \end{aligned}\right\} \tag{8}$$

Now we introduce the following transformations to reduce the governing equations to a convenient form:

$$\psi=x^{3/4}f(x,\eta),\quad \eta=yx^{-1/4},\quad \theta=\theta(x,\eta) \tag{9}$$

where η is the pseudo similarity variable and ψ is the stream function.
Introducing the transformations given in equation (9) into equations (7) and (5) the momentum and energy equations are transformed the following forms,

$$\left(1+\sigma_x^2\right)(1+\varepsilon\theta)f'''+\frac{3}{4}ff''-\left(\frac{1}{2}+\frac{x\sigma_x\sigma_{xx}}{1+\sigma_x^2}\right)f'^2+\frac{1}{1+\sigma_x^2}\theta-\frac{Mx^{1/2}}{1+\sigma_x^2}f'+\varepsilon\left(1+\sigma_x^2\right)\theta' f''=x\left(f'\frac{\partial f'}{\partial x}-f''\frac{\partial f}{\partial x}\right) \tag{10}$$

$$\frac{1}{\Pr}\left(1+\sigma_x^2\right)\theta''+\frac{3}{4}f\theta'+x^{1/2}Q\theta\ \ +J\quad x^{3/2}f'^2=x\left(f'\frac{\partial\theta}{\partial x}-\theta'\frac{\partial f}{\partial x}\right) \tag{11}$$

The boundary condition (8) now takes the following form:

$$\left.\begin{aligned} &f(x,o)=\ f'(x,o)=0,\qquad \theta(x,o)=1\\ &f'(x,\infty)=0,\qquad\ \ \theta(x,\infty)=0 \end{aligned}\right\} \tag{12}$$

The rate of heat transfer in terms of the local Nusselt number, Nu_x and the local skin friction coefficient, C_{fx} take the following forms:

$$Nu_x(Gr/x)^{-1/4}=-\sqrt{1+\sigma_x^2}\,\theta'(x,o) \tag{13}$$

$$C_{fx}(Gr/x)^{1/4}/2=(1+\varepsilon)\sqrt{1+\sigma_x^2}\ f''(x,o) \tag{14}$$

3. Method of solution

The governing equations are solved numerically with the help of implicit finite difference method together with the Keller-Box scheme [11]. The discretization of momentum and energy equations are carried out with respect to non-dimensional coordinates *x* and η to convey the equations in finite difference form by approximating the functions and their derivatives in terms of central differences in both the coordinate directions. Then the required equations are to be linearized by using the Newton's Quasi-linearization method. The linear algebraic equations can be written in a block matrix which forms a coefficient matrix. The whole procedure namely reduction to first order followed by central difference approximations, Newton's Quasi-linearization method and the block Thomas algorithm, is well known as Keller-box method.

4. Results and discussion

Here we have investigated numerically heat absorption and Joule heating effect of viscous incompressible fluid on MHD two-dimensional laminar flow along a uniformly heated vertical wavy surface with temperature dependent viscosity. In simulation, the values of heat absorption parameter are considered to be 0.0 to -4.0, Joule heating parameter ranging from 0.0 to 0.2 and viscosity parameter ranging from 0.0 (constant viscosity) to 15.0 while magnetic parameter M = 0.1, the amplitude-to-length ratio of the wavy surface α = 0.3 and Prandtl number Pr = 0.7 which corresponds to the air at 2100^0K and Pr = 0.0288 which corresponds to the mercury at 0^0C respectively. The numerical results have been obtained for the set of parameters entering into the problem and presented graphically.

The local skin friction coefficient C_{fx} and the rate of heat transfer in terms of the local Nusselt number Nu_x for the effect of heat absorption parameter Q against x are plotted in Fig. 2 while α = 0.3, M = 0.1, ε = 5.0, J = 0.05 and Pr = 0.0288. It is noted that the skin friction coefficient significant decreases along the downstream direction of the surface and the rate of heat transfer from the surface increases with the increase of the heat absorption parameter Q. Heat absorption mechanism creates a layer of cold fluid adjacent to the heated surface and finally the temperature of the fluid decreases. For this reason the temperature gradient that is heat transfer rate in terms of the local Nusselt number from the surface increases. Owing to the lessening temperature, the viscosity of the fluid decreases and the corresponding local skin friction coefficient decreases.

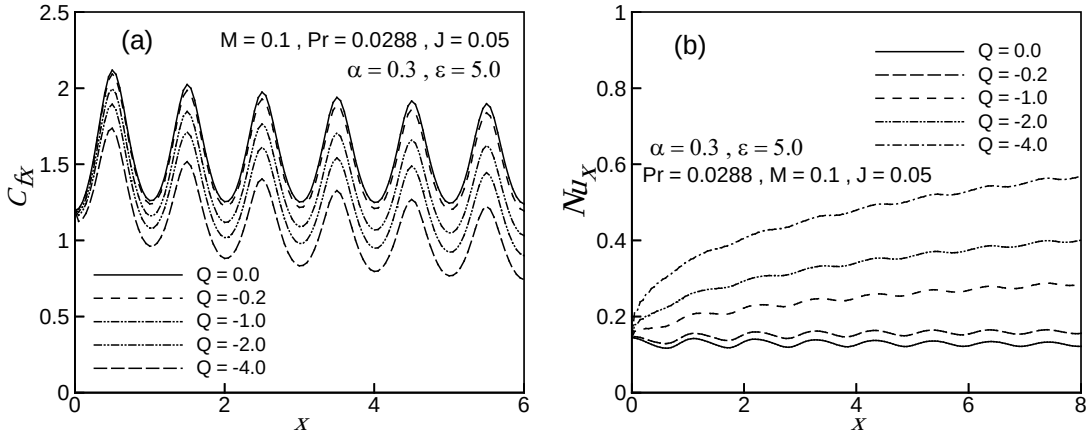

Fig. 2. Effect of Q on (a) skin friction coefficient C_{fx} and (b) rate of heat transfer $Nu_{x.}$

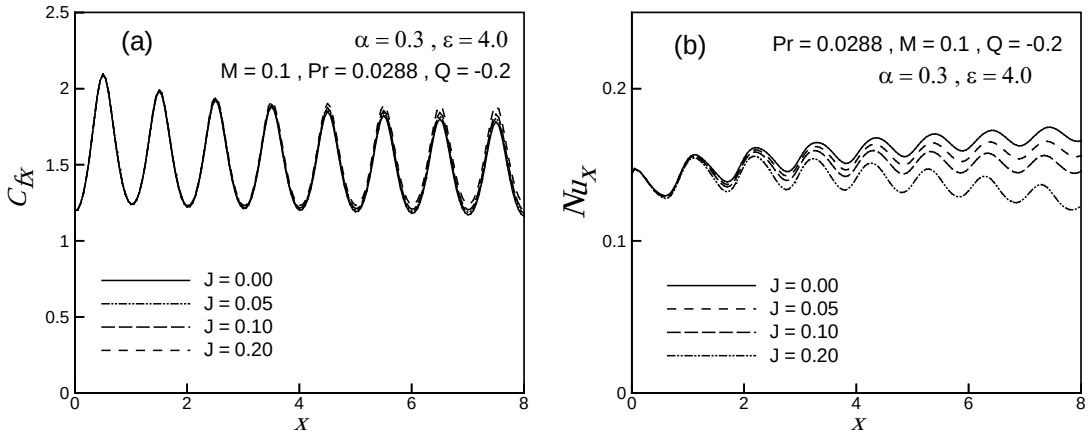

Fig. 3. Effect of J on (a) skin friction coefficient C_{fx} and (b) rate of heat transfer Nu_x.

The effect of variation of Joule heating parameter on the skin friction coefficient C_{fx} and local rate of heat transfer Nu_x are displayed in Fig. 3. The skin friction coefficient against x increases slowly along the upstream direction of the surface. On the other hand, the opposite situation observed for the rate of heat transfer. The highest values of local skin friction coefficient are recorded to be 2.09234 and 2.09576 for J = 0.0 and 0.2 respectively. The maximum values of local rate of heat transfer are 0.17824 and 0.15550 for J = 0.0 and 0.2 respectively. Finally, it is seen that the local skin friction coefficient increases by approximately 0.16% and the rate of heat transfer decreases by approximately 13% which occurs at the different position of x.

Fig. 4(a) and fig. 4(b) deal with the effect of viscosity parameter ε within the boundary layer for different values of the controlling parameters Q = - 0.01, M = 0.1, α = 0.3, J = 0.02 and Pr = 0.7. It is observed that an increase

in the value of variable viscosity parameter ε, the skin friction coefficient increases along the upstream direction of the surface and to decrease of the heat transfer rates. It is observed that the local skin friction coefficient increases by approximately 57% and the rate of heat transfer devalues by approximately 33% as ε changes from 0.0 to 15.0.

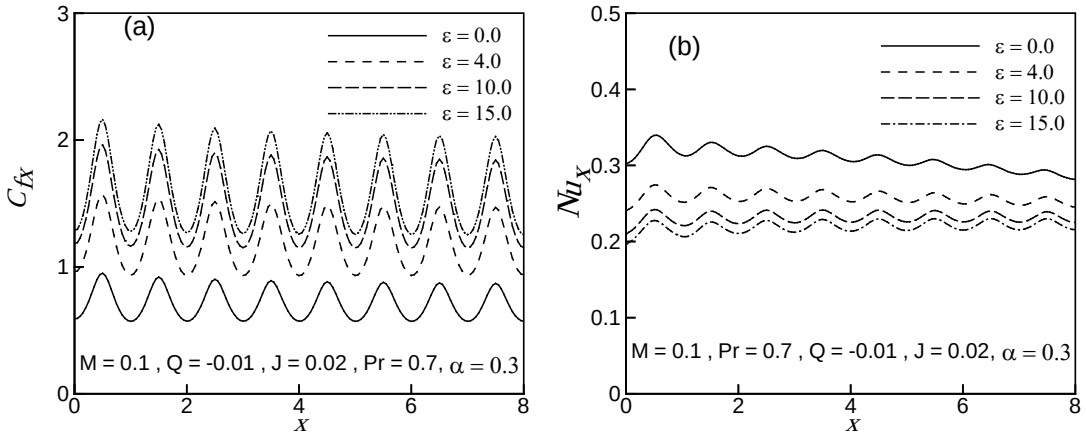

Fig. 4. Effect of ε on (a) skin friction coefficient C_{fx} and (b) rate of heat transfer Nu_x.

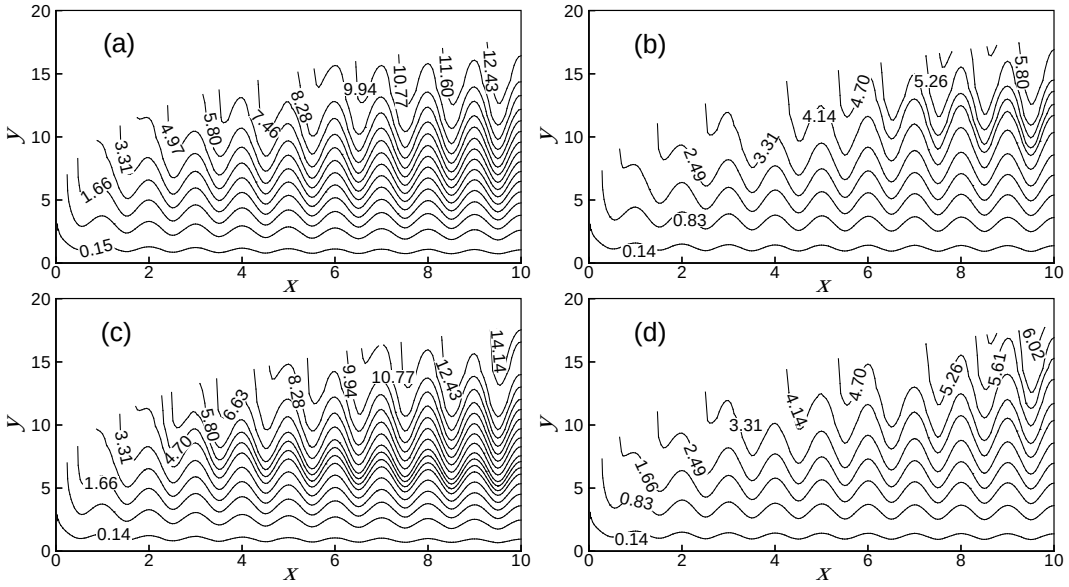

Fig. 5. Streamlines for (a) Q = 0.0, J = 0.0 (b) Q = - 4.0, J = 0.0 (c) Q = 0.0, J = 0.2 (d) Q = - 4.0, J = 0.1 while Pr = 0.0288, M = 0.1, ε = 5.0 and α = 0.3.

The effects of heat absorption parameter Q and Joule heating parameter J, on the development of streamlines which are illustrated in Fig. 5 for the amplitude-to-length ratio of the wavy surface α = 0.3, M = 0.1, ε = 5.0 and Prandtl number Pr = 0.0288. When Q = 0.0 and J = 0.0, where Joule heating effect is neglected and in absence of internal heat absorption as shown in Fig. 5(a) and found that maximum value of stream function ψ_{max} is 12.43. Fig. 5(b) indicates that the effect of heat absorption parameter strongly affect the velocity of the fluid flow and leads to thinner the velocity boundary layer. In this case the maximum value of stream function ψ_{max} is 5.80. From Fig. 5(c), it is observed that when the effect of Joule heating (J = 0.2) is considered the boundary layer becomes thicker. This is because Joule heating is the heating effect of conductors carrying currents. So velocity of the fluid flow increases and the maximum value of stream function ψ_{max} is 14.14 that is shown in Fig. 5(c). The combined effect of Q and J, are shown in Fig. 5(d). Here the maximum value of ψ_{max} is 6.02. From these figures it is observed that the value of stream function ψ becomes higher for the effect of Joule heating parameter J and ψ becomes smaller in presence of heat absorption parameter Q as well.

The variation of isotherms with heat absorption parameter Q and Joule heating parameter J for α = 0.3, M = 0.1, ε = 5.0 and Pr = 0.0288 are shown in Fig. 6. We can say after observing the isotherms of this figure that

temperature enhances within the boundary layer due to the higher values of *J*. On the other hand, an opposite situation is observed on the temperature field within the boundary layer in the case of heat absorption.

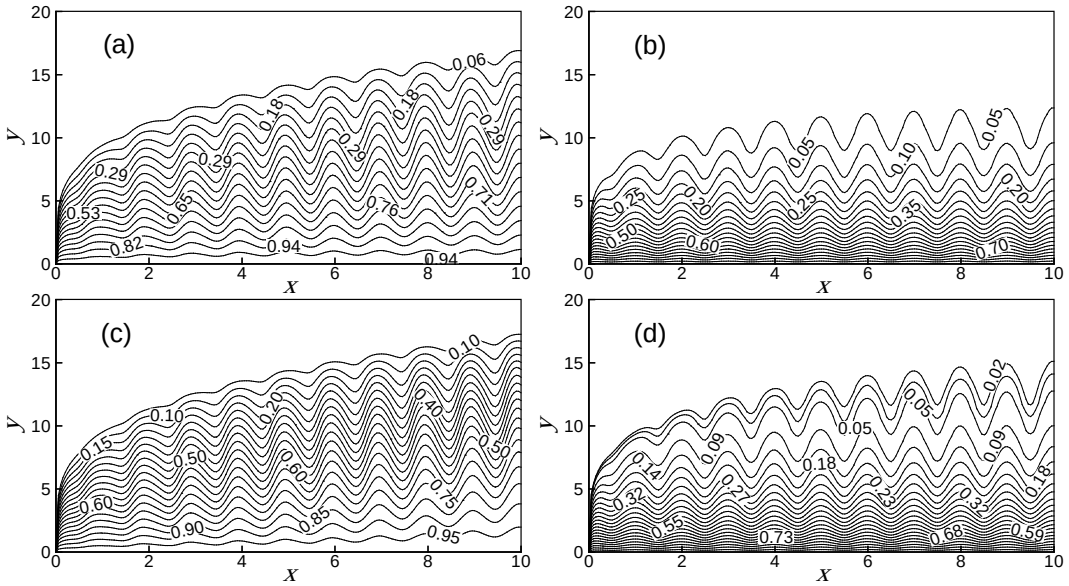

Fig. 6. Isotherms for (a) Q = 0.0, J = 0.0 (b) Q = - 4.0, J = 0.0 (c) Q = 0.0, J = 0.2 (d) Q = - 4.0, J = 0.1 while Pr = 0.0288, M = 0.1, ε = 5.0 and α = 0.3.

5. Conclusion

The problem of free convection heat transfer of viscous incompressible fluid with heat absorption and Joule heating on MHD two-dimensional laminar flow along a uniformly heated vertical wavy surface including viscosity dependent on temperature has been analyzed numerically. The effects of heat absorption, Joule heating and variable viscosity on momentum and heat transfer have been studied in detail. The conclusions of this study are as follows:

- The skin friction coefficient decreases that is the frictional force at the wall reduces over the whole boundary layer but the rate of heat transfer enhances in presence of heat absorption.
- The skin friction coefficient enhances and the rate of heat transfer reduces for higher values of the Joule heating parameter and temperature dependent viscosity parameter.
- In presence of heat absorption, the velocity of the fluid flow and the temperature distribution of the fluid decrease within the boundary layer. But the opposite results obtained for the effect of *J*.

6. References

[1] J. Charraudeau, "Influence De Gradients De Properties Physiques En Convection Force Application Au Cas Du Tube", *Int. J. Heat Mass Transfer*, Vol. 18, pp. 87-95, 1975.

[2] L. S. Yao, "Natural Convection along a Vertical Wavy Surface", *ASME J. Heat Transfer*, Vol. 105, pp. 465–468, 1983.

[3] K. Vejravelu and A. Hadjinicolaou, "Heat Transfer in a Viscous Fluid over a Stretching Sheet with Viscous Dissipation and Internal Heat Generation", *Int. comm. Heat Transfer*, Vol. 20, pp. 417-430, 1993.

[4] K. A. Alam, M. A. Hossain and D. A. S. Rees, "Magnetohydrodynamic Free Convection along a Vertical Wavy Surface", *Int. J. Appl. Mech. Engrg*, Vol. 1, pp. 555–566, 1997.

[5] M. A. Hossain and D. A. S. Rees, "Combined Heat and Mass Transfer in Natural Convection Flow from a Vertical Wavy Surface", *Acta Mechanica*, Vol. 136, pp. 133–141, 1999.

[6] C. Y. Cheng, "Natural Convection Heat and Mass Transfer near a Vertical Wavy Surface with Constant Wall Temperature and Concentration in a Porous Medium", *Int. Comm. Heat Mass Transfer*, Vol. 27, pp. 1143–1154, 2000.

[7] M. A. Hossain, S. Kabir and D. A. S. Rees, "Natural Convection of Fluid with Temperature Dependent Viscosity from Heated Vertical Wavy Surface", *Z. Angew. Math. Phys.*, Vol. 53, pp. 48–52, 2002.

[8] M. M. Molla, M. A. Hossain and L. S. Yao, "Natural Convection Flow along a Vertical Wavy Surface with Uniform Surface Temperature in Presence of Heat Generation/Absorption", *Int. J. Therm. Sci.*, Vol. 43, pp. 157-163, 2004.

[9] M. M. Molla and M. A. Hossain, "Radiation effect on mixed convection laminar flow along a vertical wavy surface", *Int. J. Therm. Sci*., Vol. 46, pp. 926–935, 2007.

[10] N. Parveen and M. A. Alim, "MHD free convection flow in presence of Joule heating and heat generation with viscosity dependent on temperature along a vertical wavy surface", *Int. J. Energy Tech.*, Vol. 4, No. 21, pp. 1-10, 2012.

[11] H. B. Keller, "Numerical Methods in Boundary Layer Theory", *Ann. Rev. Fluid Mech.*, Vol. 10, pp. 417-433, 1978.

Paper ID: TE-11

Design, Construction and Testing of a Port Fuel Injection (PFI) System for a Four Cylinder SI Engine

Md. Syed Ali Molla [1], Mohd. Sapuan Salit [2], G.M. Sutan Mahmud Rana [3]
[1]Professor, Dept. of Mechanical Engineering, Khulna University of Engineering (KUET)
[2]Professor , Faculty of Engineering, UPM, Malaysia
[3] Under Graduate Student of Mechanical Engineering, Khulna University of Engineering (KUET)
E-mail: mmsali03@yahoo.com [1],*sapuan@eng.upm.edu.my* [2], *gsmrana@gmail.com*[3]

Abstract

The Port Fuel Injection system have the advantages over throttle body manifold fuel injection system for providing uniform fuel air mixture in each cylinder and it can control fuel injection quantity more precisely. Thus it can provide fuel economy and minimize environmental pollution. The present research work can help the automotive engineers to understand the design and operation principle of Port Fuel Injection technologies in operation , maintenance and research fields.

Keywords: *Port fuel injection, Fuel economy, Pollution control*

1. Introduction

The construction of the carburetor is relatively simple and it has been used almost exclusively on gasoline engines in the past. However, in response to recent demands for cleaner exhaust emissions, more economical fuel consumption, and improved drivability, the carburetor now must be equipped with various compensating devices and it makes carburetor more complex. In place of carburetor, therefore, Electronic Fuel Injection (EFI) System got advantages, which can assures the proper air-fuel ratio to the cylinder by controlling electronic devices in accordance with various driving conditions. In the port fuel injection system, the fuel is supplied directly into the intake port in suction stroke where the injection period varies with speed and load [1]. In the port fuel injection system fuel is injected in the intake port which provides desired homogeneous mixture in each cylinder (1-5] which can reduce emissions and increased engine efficiency.

Engines generate their worst emissions-just after cold-start. During warm-up of an engine, a small shot of fuel is injected just before the exhaust valve opens. There is still enough heat and oxygen in the chamber for this charge to ignite, and the heat from t Unlike throttle body fuel injection (TBI), hat after burn gets the catalyst warm-up to operating temperature just seconds after cold-start. In port fuel injection system, injectors are either open or closed and pulsed unlike throttle body fuel injection (TBI) system.

2. Layout and Components of Port Fuel Injection System

The fuel delivery system incorporates the following components:

(i) Fuel tank, (ii) Fuel pump (iii) Fuel pipe and filter in line (iv) Fuel delivery pipe (rail) (v) Pulsation damper (in many engines) (vi) Fuel injectors (vii) Cold start injectors (most engines) (viii) Fuel pressure regulator and (ix) Fuel return pipe

There are two types of electric fuel pump used in the EFI systems. The early conventional EFI system used an externally mounted in-line pump. These roller cells pumps incorporate an integral pressure pulse damper or silencer designed to smooth out pressure pulses and provide quiet operation

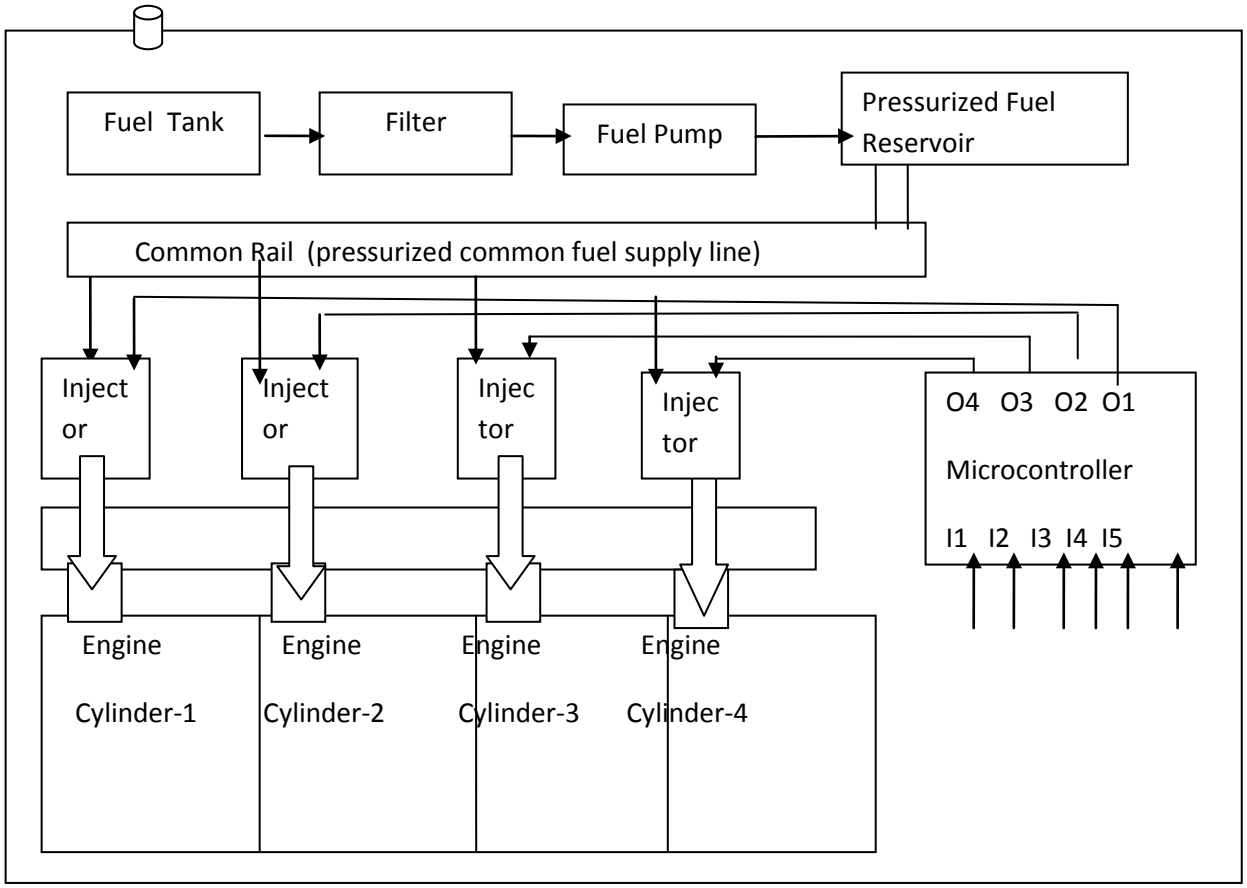

Fig. 1: Schematic Diagram of Fuel Supply System

Later model engines utilize an in-tank pump integrated with the fuel sender unit. These turbine pumps operate with less discharge pulsation and run quieter than the in-line variety [2-5] . In-tank pumps can be serviced by removing the fuel sender unit from the tank. Make sure that the pump coupling hose is in good condition prior to replacing the pump.In a port fuel injection engine, the fuel must be injected in a short period of time and with maximum injector pressures of 35 psig [2-5]. The electric fuel pump supplies the fuel to the injectors under pressure. As soon as the injector opens, fuel sprays out. An electric solenoid in the injector opens and closes the valve. The solenoid has a small coil that becomes magnetized when a voltage is supplied.

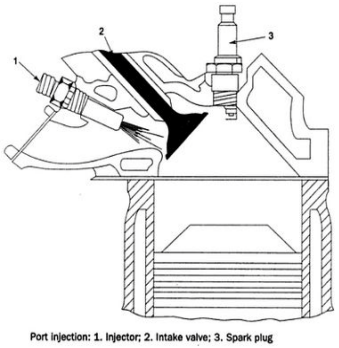

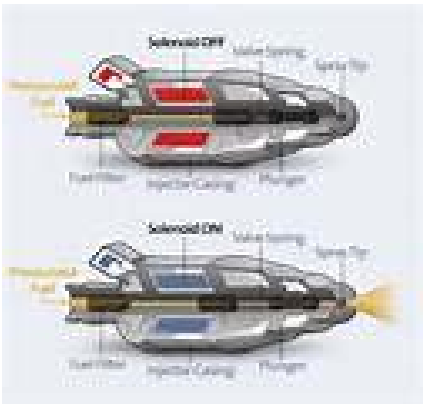

Fig. 2(a) Fuel injection in the intake port **Fig. 2(a) Fuel injector Cross- section**

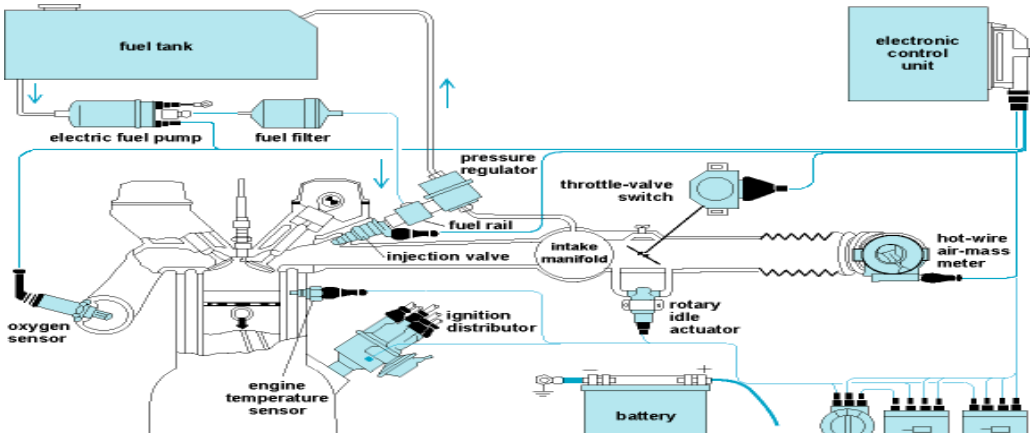

Fig. 2: Diagram of Fuel Injector and Fuel Injection System in US Vehicles

3. Design Consideration for the Program in Microcontroller

A microcontroller has following key features:

- Central Processing Unit –usually small and simple
- Output and input interface such as serial ports.
- RAM for data storage.
- Peripherals such as timers and watchdog circuits.
- ROM for program storage.
- Clock generator- an oscillator for a quartz timing crystal, resonator or RC circuit.

This integration minimizes the number of chips and the amount of wiring and PCB space that would be needed to produce equivalent systems using separate chips. Now a day's microcontroller is used in traffic signals, electrical devices, washing machines, microwave ovens, telephones, vehicles etc.

The engine management system usually continually chooses among three combustion modes: ultra lean burn, stoichiometric, and full power output. Each mode is characterized by the air-fuel ratio. The stoichiometric air-fuel ratio for petrol (gasoline) is 14.7 to 1 by weight, but ultra lean mode can involve ratios as high as 25:1. These leaner mixtures of PFI system is much leaner than in a conventional engine, reduce fuel consumption [6].

PFI system was designed for variable speed and variable load and other operating conditions of a real engine. In this design instead of three modes, six modes of engine operation like starting (choke circuit) idle circuit, slow speed circuit, medium speed circuit, high-speed circuit, acceleration circuit are considered. In each running condition there is provision of extra fuel supply for high load and low load operation so that wide varying of fuel air ratio can be supplied keeping in conformity of engine operation conditions.

Various types of sensors, ICs and transistors are used to sense the speed and suction pressure and engine operating conditions. An engine demand various quantity of air depending on load and speed. The intake air flow and air pressure represents the variation of load. The distributor of EFI, PFI and DGI systems have built in signaling system for engine rpm and crank angle postion. Ne – signal and Ge-signal give engine rpm and crank angle position. Oxygen signal fitted in catalytic converter give presence of excess or low oxygen in exhaust gas which in term give information to the engine that it is running with lean or rich or with optimum fuel air ratio.

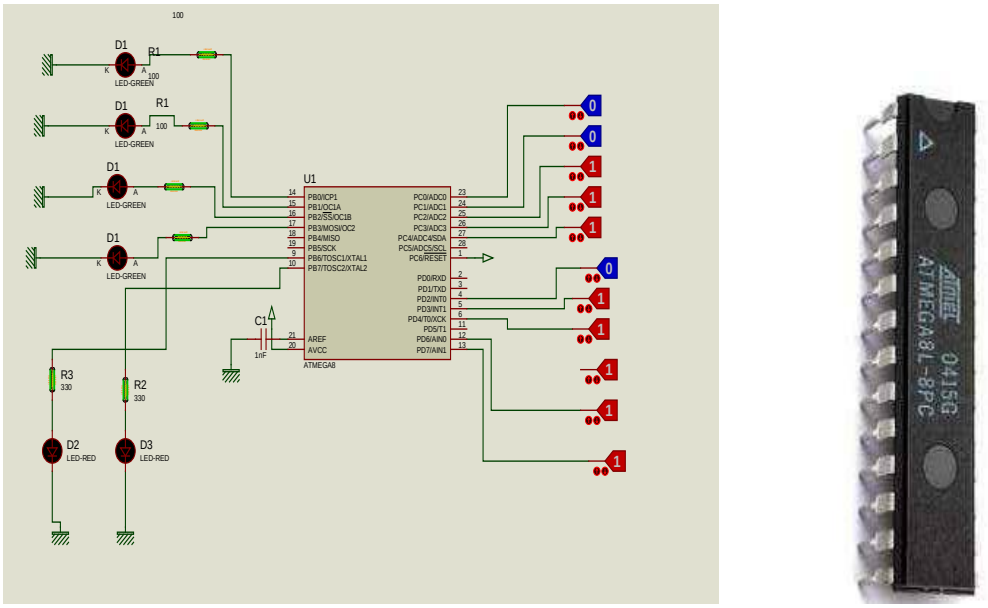

Fig. 3: Microcontroller Input Output diagram and IC

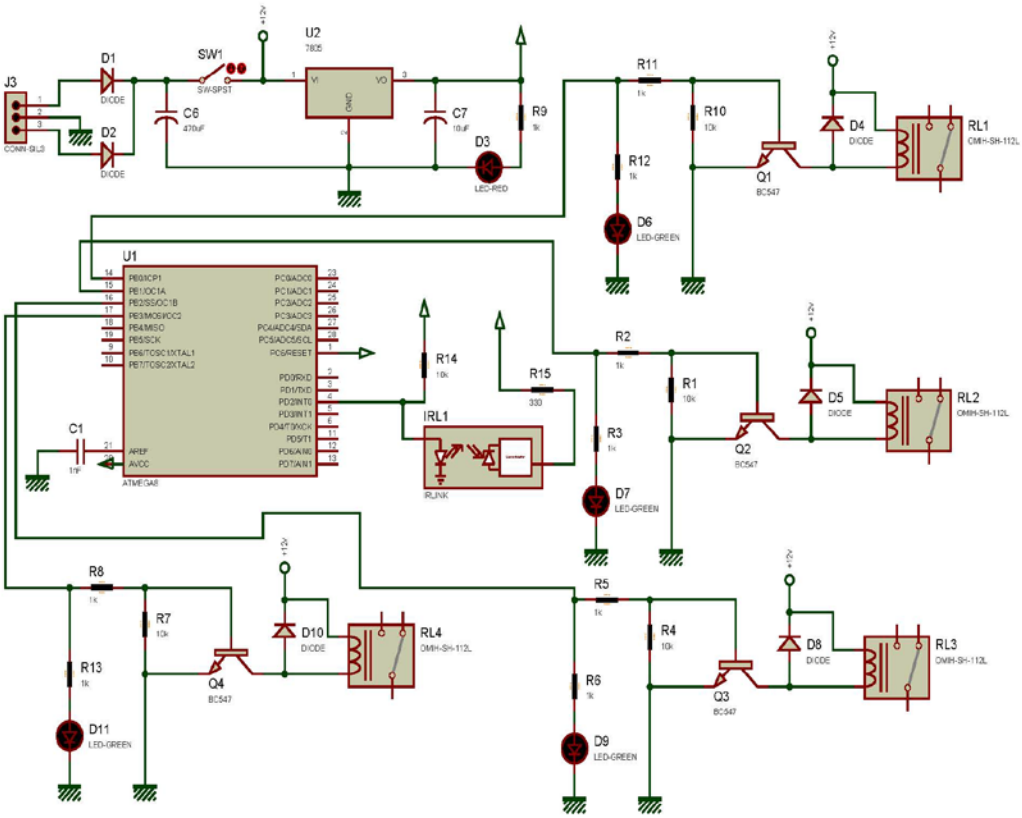

Fig. 4: Schematic Diagram of Main Circuit

The program was made on the logics required for operating conditions of the engine [7]. Input signals are taken for Starting position (I1), Idle Position (I2) Slow running position (I3), Medium Speed Position (I4)

High-speed (I5) and Acceleration (I6). The air velocity and pressure determine the loading position in each mode. The Oxygen sensor gives the level of fuel air ratio. All these parameter are set to the programe to get required output signal for Injector nozzle opening.

Before programming on a microcontroller based PFI system, the fuel air ratio required in all engine operating conditions like starting system (choke system), idle system, slow speed, medium speed, high speed system, acceleration system with variable engine load are considered and accordingly the required input are set to microcontroller. The output of microcontroller to injectors, controls injector valve opening times on which fuel injection quantity varies depending on engine operating conditions. The controlling parameters especially valve opening time can be changes during engine test on test bed or on road running conditions if desired. Thus engine can run with required fuel air ratio if designed parameters are changed and set to the required value in road test.

4. Experimental setup

A common fuel rail for fuel supply from fuel tank is constructed from local workshop. A fuel pump and four injectors are procured from local market and these are installed with fuel supply common rail in the experimental set up. An artificial fly wheel is coupled to a Dc motor having various to generate signal of engine rotation and sensing crank angle position. The module of fuel supply is replaced by the microcontroller .Necessary power supply for fuel pump, injectors and microcontroller board is completed.

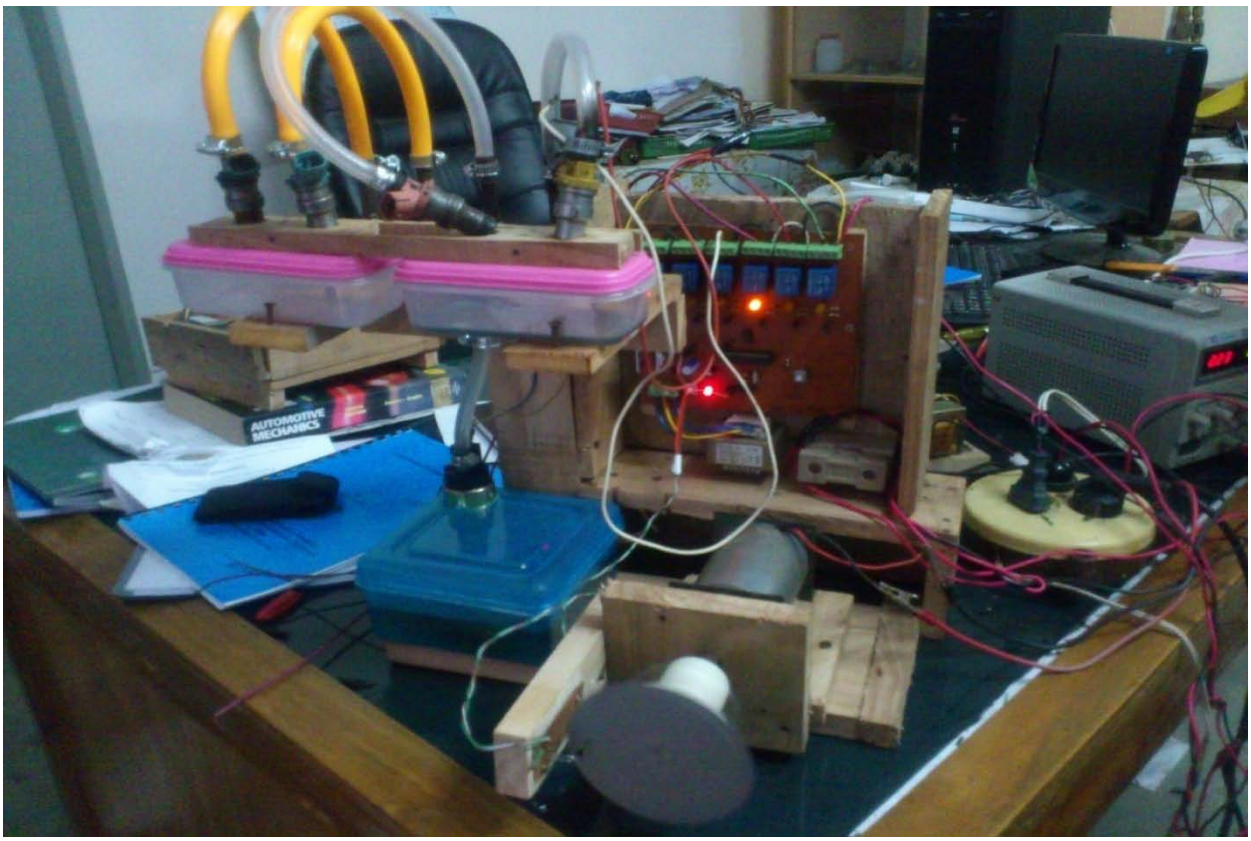

Fig. 5 Experimental Setup for the Model of a PFI

5. Results and Discussion

After completion of the experimental set-up the performance of the fuel supply module was tested this showed that fuel injection quantity can be varied to any required value.

This module can be set Port Fuel Injection system vehicle without or with small modification. Carburetor mounted vehicle with electronic distributor has the facility to give engine speed (rpm) and crank angle sensing device and oxygen sensor. In other word it can be used to controls the amount of fuel to be supplied from injector to engine cylinder in all engine operation modes.

6. Conclusion

At the end**,** it may be concluded that-

(i) The program for controlling the Port fuel injection is found to work properly.
(ii) The model test result showed variable fuel injection quantity at different speed and load can be maintained.
(iii) The emission reduction potential is very high as fuel injection can be controlled depending upon Engine running condition.
(iv) Fuel delivery module cost 1500-2000 USD in US market but locally made module costs nearly 20-25 USD or BD TK 1500- 2000 .

References:

[1] W. H, Crouse and D, L. Anglin, "Automotive Mechanics", 10th revision/McGraw-Hill Book Company, USA
[2] Fuel Systems at Sears® | Sears.com
[3] www.StreetSideAuto.com/Edelbrock
[4] www.Sears.com/Fuel-System-Services
[5] JEGS.com/Electric
[6] M.L. Mathur, and R.P. Sharma, "Internal Combustion Engines", 7th Edition, Dhanapat Publications,1997.
[7] M.M. Mano, "Digital Logic and Computer Design", U.S. Edition, Prentice-Hall of India, Private

Paper ID: TE-12

Performance Test of a Diesel Engine with Different Esters of Alternative Fuel

S.M. Najmul Hoque[*1], Mohd. Rafiqul Alam Beg[1], Barun Kumar Das[1] and S.M. Rasid[1]
[1]Department of Mechanical Enginerring, Rajshshi University of Engineering and Technology, Rajshahi-6204, Bangladesh
[*]Corresponding author: Shumon99234@gmail.com, Phone: +8801716591872

Abstract

Vegetable oil as a biomass energy can be considered as possible alternative fuel. At present the world is highly dependent on petroleum fuels for generating power, vehicle movement, agriculture and domestic useable machinery operations and for running different industries. Thus the demand of the petroleum fuel increases simultaneously. However the reserve of the petroleum fuel is limited. As a result, attention has gone to the search of renewable source of fuel which can meet the demand. The present experimental study reports the performance characteristics of a diesel engine by using methyl esters of neem oil and methyl esters of sunflower oil in comparison to 100% diesel operation. The properties of esterified vegetable oil are almost similar with the diesel fuel. The thermal efficiency curves for both diesel and esterified oils are comparable as well. However, the maximum value of thermal efficiency of esterified oils is slightly less than diesel fuel. Both oils perform as fuels for diesel engine with acceptable BSFC. Volumetric efficiency is continuously decreased with increasing RPM for both diesel and biodiesel. Cylinder wall temperature is a considerable factor for this case. Exhaust gas temperature of vegetable oil is lower than diesel fuel because of incomplete combustion. These two promising options of alternative fuel can be investigated further as potential substitute of diesel.

1. Introduction

The use of vegetable oil as fuel for diesel engine is not new Dr. Rudolph Diesel used peanut oil to fuel one of his engines at Paris exposition of 1900 [1,2]. After the second world war the limited resource of conventional fuels high price and energy crisis have sent the scientists worldwide scrambling on a search of alternative fuels [3]. After the 1973 oil embargo, it was very important to study the alternative sources of fuel diesel engines because of the concern over the availability and price of petroleum based fuels the present source of fuels used in IC engine and diesel will deplete within about 30 years if consumed at the same rate what is currently going on. For this reason researchers are undertaking research pertinent to several renewable sources of energy including biodiesel. There are several possible alternative source of fuels, for example, vegetable oils, alchohols such as methanol & ethanol; hydrocarbon gases such as CNG LPG hydrogen producer gas etc. [4] Among them, vegetable oils present a very promising alternative to diesel oil since they are renewable and one produced easily in rural areas where there is an acute need for modern forms of energy . In Bangladesh diesel is primarily used for transportation agriculture and electric power generation. Diesel is becoming scarce and costlier and hence there is a need to preserve diesel for only automotive and agriculture uses. Sustaining this demand country has to face a big amount of import bill for crude oil in this case alternative fuels provide a new dimension in the fuel technology.

This choice of the vegetable oil for diesel engine fuel naturally depends upon the local conditions. And the production of vegetable oil is very simple and in mainly agricultural country as ours it can be made quite economically [4]. The auto ignition properties of vegetable oils are almost the same as those of diesel fuels and hence can be used in diesel engines with little or no engine with little or no engine modification [5]. However some problems are associated with we use vegetable oil as alternative fuels in diesel engine. These problems can be minimizes by various ways and the process of esterification is best among those as it is more suitable than other process. Methyl alcohol and NaOH is used for the esterification process. Srinivasa and Krisna (1991)

reported that vegetable oil present a very promising alternating to diesel oil since they are renewable and are produced easily in rural areas where there is an acute need for modern forms of energy. A number of oils are being considered worldwide for using engine. The vegetable oil tested were Karanji oil (Pongamia Glabra), pithraj, rice bran oil and plam oil on a single cylinder diesel engine. The inherent properties of vegetable oils make them suitable for use in Cl engine. Nabi et al (2009) prepared biodiesel from non-edible renewable karanja (Pongamia Pinnata) oil, determined properties and investigated influence of biodiesel on engine performance and emissions. Engine experiment result showed that all biodiesel blends reduced engine emissions including carbon monoxide (CO), smoke and engine noise, but increased oxides of nitrogen (NOx) [6]. They also extended their work by using Pitraj *(*Aphanamixis polystachya*)* in diesel engine successfully in 2010 [7].

However for longer use Methyl esters are preferable because of their lower viscosity and lower smoking tendency. The smoke emission with methyl esters is a little higher than with diesel oil but here again optimized injection timing could reduce the smoke emission foresters. Bari & Roy [8] explained that the properties of rice barn oil as a fuel are determined experimentally and it is observed that the properties of rice bran oil acceptable to use in diesel engine except viscosity. Because of high viscosity rice bran oil cannot be directly used in the engine at normal temperature (20^0 to30^0 C) However it is established here that rice bran oil can be used in the engine even at normal temperature if kerosene is blended with it. Alternatively preheating of the oil overcomes the difficulty of high viscosity and can be used directly in the engine. In this work rice bran oil was blended with kerosene and the mixture was used to test the performance of a four stroke diesel engine. The test result leads to the conclusion that rice bran oil can be a very prospective substitute of diesel fuel. Ludwig Elsbett and workers:[9]: shows in their paper Economic and environmental aspects of different liquid fuels are discussed with particular emphasis on vegetable oil as a future form of solar fuel. A presentation is given of a DI diesel engine running on vegetable oil and the advantages of vegetable oil in combination with this engine compared to engines running on diesel fuels. Vegetable oil does not require additional energy for processing nevertheless a costly proposal was made to esterize vegetable oils with methanol using sodium as a catalyzer producing glycerin as methyl ester is a poisonous substance very aggressive to many materials such a proposal does not offer any advantages as there is no need for important qualities of glycerin anyhow and methanol can only be produced with considerable energy inputs.

In the present investigation Methyl ester of neem & Methyl ester of sunflower is used as both of them can be grow as domestic field in Bangladesh. Test was conducted with Methyl esters of both fuels in a DI diesel engine to compare the performance with diesel fuel.

2. Methodology

In this work, laboratory quantities of vegetable oils were sampled from local areas nearby Rajshahi, Bangladesh and processed to methyl esters. Sunflower oil is chosen as edible oil while Neem is chosen as in edible to compare with diesel fuel. Basic reaction for transterification process is shown in figure 1. Firstly, NaOH is mixed with methanol to produce sodium methoxide, then this sodium methoxide is poured and vigorously mixed with vegetable oil. The temperature of the mixture is kept constant (500^0C) until the reaction is completed. Now biodiesel is separated from the mixture and washed by water. Waste oil is treated before conversion into biodiesel to remove impurities.

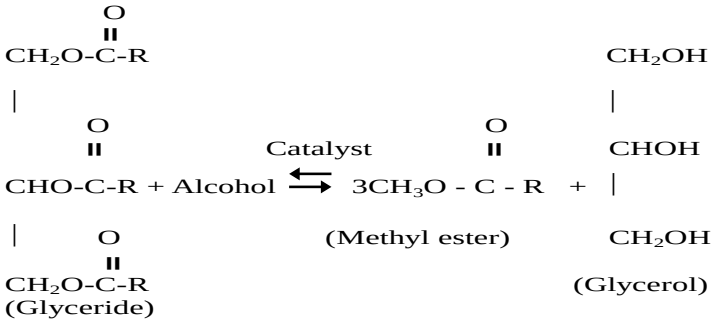

Figure 1: Transesterification reaction

A four-stroke single cylinder (specification shown in table-1) naturally aspirated stationary DI diesel engine is used. All experimental data are taken after 30 minutes of engine start after which the exhaust line temperature is no further increased i.e. constant and there is almost no fluctuation of emissions. This condition of the engine is chosen because of the consistent data at this condition. Tests are carried out at the warmed up condition of the engine at different engine loadings and at 700-1200 rpm. Loads are measured by electric dynamometer. The diesel fuel used in this study is No. 2 diesel fuel with a lower calorific value of 43000 kJ/kg and cetane number of 50.

Table 1: Engine specifications

Engine type	4-stroke DI diesel engine
Number of cylinders	One
Bore × Stroke	80 × 110 mm
Swept volume	553 cc
Compression ratio	16.5:1
Rated power	4.476 kW @ 1800 r/min
Fuel injection pressure	14 MPa (900-1099 r/min) 20 MPa (1100-2000 r/min)
Fuel injection timing	24° BTDC

3. Results and discussion:

The physical characteristics of vegetable oil esters are closer to those of diesel oil the comparison of this characteristic with of diesel and vegetable oil was shown below:

Table 2: Comparison of esterified vegetables oil with diesel

Esterified Oil	Calorific value (Kcal/kg)	Viscosity (Centipoise)	Specific gravity (gm/ml)
Methyl ester of neem	8450	42.5	0.865
Methyl ester of Sunflower	8600	29.25	0.887
Diesel oil	10200	5.5	0.84

As shown in the table, calorific value of both sunflower and neem were very close to diesel. Normally vegetable oils show higher density and viscosity than diesel and higher in this case density values were found near the diesel but viscosity was considerable amount higher than the base diesel. A very positive gain by esterification process is the high cetane number of esters is in the range of 50 and above indicated their superiority.

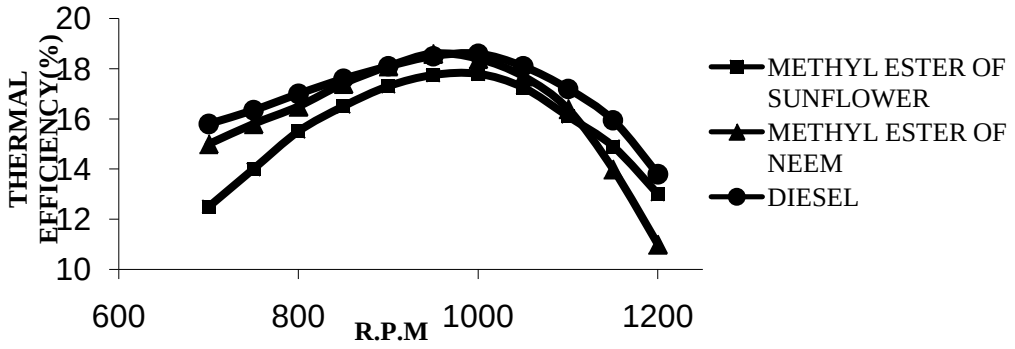

Figure 1: RPM VS Thermal efficiency

The experimental results, in all the cases the performances of the engine with esterified vegetable oils were compared with the diesel oil operation. The variations of thermal efficiency of the selected diesel engine with diesel fuel and methyl esters are shown in figure 1 for comparison. The thermal efficiency with all the three fuels was found very close to one another. The esterification improves cetane number, reduced viscosity and changes chemical structure of the vegetable oil which is desirable for diesel engine [10] hence, the thermal efficiency of the esterified oil is improved. Thermal efficiency for esterified vegetable oil is lower than diesel oil must be attributed to lower calorific value and poor velocity.

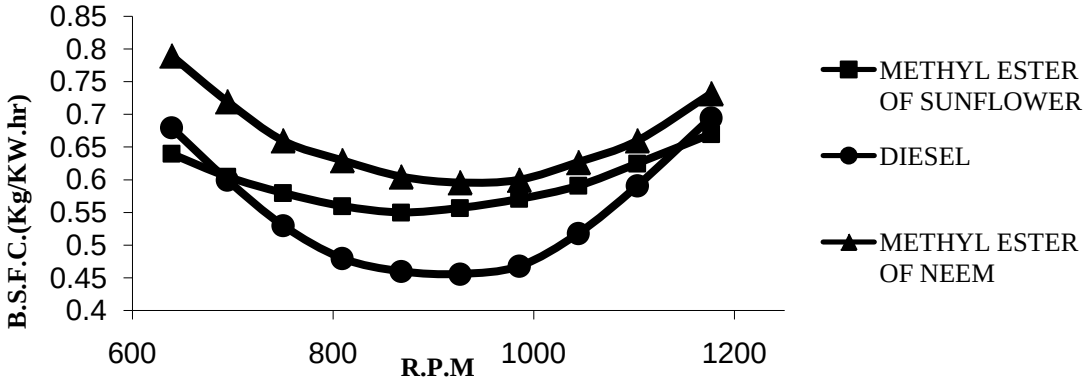

Figure 2: RPM VS B.S.F.C

Figure 2 flaunts the BSFC comparison of diesel oil with esterified sunflower and neem oil in respect to RPM. BSFC was found to reduce with respect to increasing thermal efficiency or vice versa with the increasing of rpm but increased after 1000 RPM. BSFC for esterified vegetable oil was slightly higher than diesel oil.

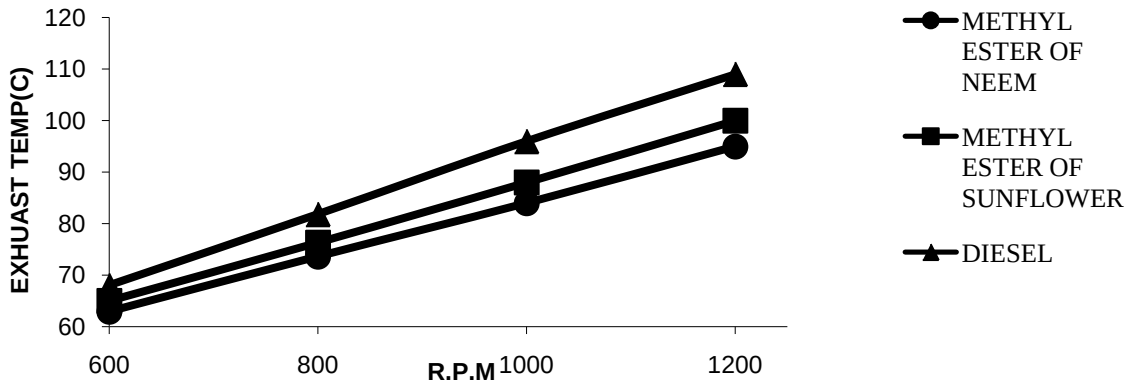

Figure 3: RPM VS Exhaust gas temperature

Variation of the exhaust gas temperature with respect to rpm (Fig. 3) indicates that vegetables oil produce lower exhaust temperature compare to reference diesel. BSFC for the esterified vegetable oil was higher than diesel oil but thermal efficiency was not as high as diesel oil. So this condition indicates the incomplete combustion when esterified vegetable oil is used. For this reason exhaust gas temperature of esterified vegetable oil is low.

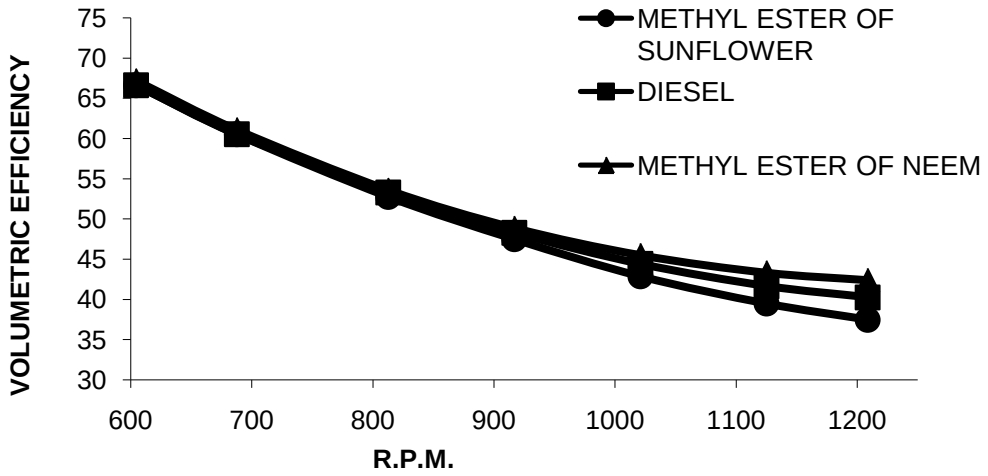

Figure 4: RPM Vs Volumetric efficiency

The variations of volumetric efficiency with rpm are illustrated by figure 4. Volumetric efficiency for esterified vegetable oil was slightly lower than diesel oil. Volumetric efficiency intermittently decreased with respect to increasing rpm. Cylinder wall temperature was ascending when rpm and for this reason less density of air induced in the cylinder consequently volumetric efficiency diminished.

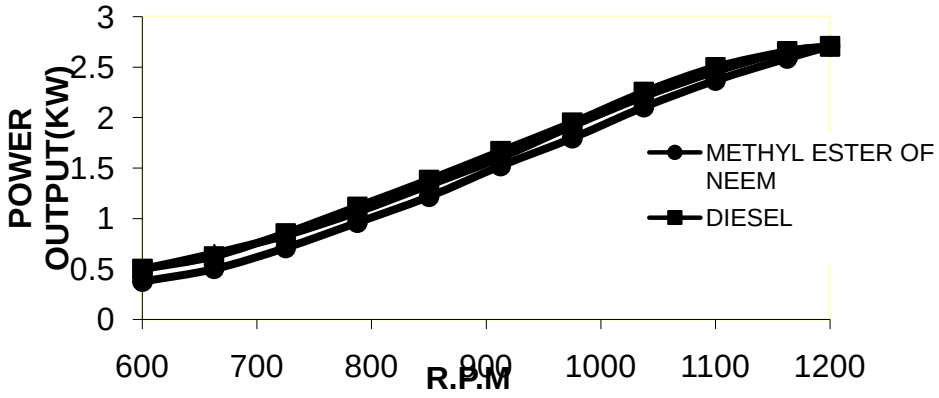

Figure 5: RPM Vs Power output

Figure 5 shows the variation of power output with rpm. Power increases with respect to increasing rpm. Higher rpm consume higher amount of fuel at the same time energy release rate is high which causes increases power output.

4. Conclusions

The following conclusions can be drawn from the study:

i) The properties of esterified vegetable oil are comparable with the diesel fuel
ii) The thermal efficiency curves for both diesel and esterified oils are comparable though the maximum value of thermal efficiency of esterified oils are slightly less than diesel fuel at 950RPM

iii) Both esterified sunflower and esterified neem oil perform as fuels for diesel engine with acceptable BSFC, the BSFC of esterified vegetable oils are slightly higher than diesel fuel
iv) Volumetric efficiency of both diesel and esterified vegetable oils are continuously decrease with increasing RPM Cylinder wall temperature is a considerable factor for this case
v) Exhaust gas temperature of vegetable oil is lower than diesel fuel because of incomplete combustion

5. Reference

1. Goering, C.E., Schwab, A. W., Daughterty, Pryde, E.H. & Heakin, A.J. – "Fuel properties of Eleven Vegetable Oils", American Society of Agricultural Engineers, 0001-2351/82/2506-1472,1982.
2. Srinivas P. R. and Gopal krishnan- "Vegetable Oils and Their Methyl Esters as Fuels for Diesel Engines",Indian Journal of Technology Volume 29, PP 292-297, 1991.

3. Beg, R. A – "Effect of Mixing on the Performance of a Single Cylinder Dual Fuel Diesel Engine"- M. Sc. Thesis Mechanical Engineering Department BUET, Dhaka, Bangladesh1987.
4. Hoque SMN, Uddin MS, Nabi MN and Rahman MM "Biodiesel from Non-Edible Renewable Karanja Seed Oil and its Effect on DI Diesel Engine Combustion" 4th BSME-ASME International Conference on Thermal Engineering, 27-29, December, 2008, Dhaka, Bangladesh.
5. A.S. Huzayyin, A.H. Bawady, M.A. Rady, A. Dawood, Experimental evaluation of diesel engine performance and emission using blends of jojoba oil and DF, Energy Conversion and Management 45, pp 20–93–12, 2004.
6. Nabi MN, Hoque SMN and Akhter MS; "Karanja (Pongamia Pinnata) Biodiesel Production in Bangladesh, characterization of karanja biodiesel and its effect on diesel emissions" **Fuel Processing Technology.** Volume 90, Issue 9,, pp: 1080-1086, 2009.
7. Nabi MN, Hoque SMN and Uddin MS "Biodiesel Production from Non-Edible Renewable Pitraj (Aphanamixis Polystachya) Oil in Bangladesh And Its Effect on DI Diesel Engine Combustion", **International Energy Journal, RERIC**, Volume 11, Issue 2, pp: 73-80**,** 2010.
8. Bari, Saiful and Roy, M.M. – Prospect of Rice Bran Oil as an Alternative to Diesel Fuel", published in 5th International Conference, The University of Reading, UK. 5-7 April, 1995
9. Elsbett, Ludwing, Elsbett, Gunter, Elsbett Klaus & Kaiser, Thomas – " The Development of Engines to Run on Vegetable Oil", ISES Solar World Congress 1987 Hamburg.
10 . Beg, R. A., Datta, K. Research Scholars and Dr Bose, P.K., Reader ME. Department jadavpur University- " Performance and Emissions Characteristics of A Naturally Asprirated Diesel Engine With Esterfied Vegetable Oil", published in All India Seminar on Renewable Energy Resource for Rural Development Present Status & Future Prospects 1st and 2nd December 1995.

Paper ID: TE-14

Design, Operation and Maintain Of A Potato Cold Storage in Bangladesh

Md. M. Islam[1], Md. M. M. Hasan[2]M A R Sarkar[3]
[1,2]Department of Mechanical Engineering, BUET, Bangladesh
[2]Professor, Department of Mechanical Engineering, BUET, Bangladesh
Email: malekdurlov@yahoo.com[1], nmrshd1207@yahoo.com[2], rashid@me.buet.ac.bd[3]

Abstract

Potato is the third largest crop in Bangladesh. Its cultivation has been getting popular in Bangladesh over the last several years. For supplying potato in all the seasons' storage of potato is necessary. Many agricultural commodities, potato in particular, are being kept in commercial cold storages. For this reason many potato cold storages were built in Bangladesh. There are about 383 cold storages in Bangladesh. Since the design parameters are not well defined and the problems associated with these cold storages are also not properly addressed. Till now most of the cold storage are using so called old and traditional technologies. This paper deals with different aspects of cooling load estimation and its design. This paper also deals with operation & maintenance of a potato cold storage. This paper presents some ideas about possible efficiency improvement of existing cold storages.

Keywords: *Cold Storage, Heat Transfer, Cooling Load.*

1. Introduction

A cold Storage is a building or a group of buildings with thermal insulation and a refrigerating system in which perishable food products can be stored for various lengths of times in set conditions of temperature and humidity. Such storage under controlled conditions slows the deterioration and spoilage that would naturally occur in an uncontrolled natural environment. In addition to providing control of temperature and humidity, cold Storages can also be designed to deliver controlled atmospheres by maintaining the requisite concentration of various gases that aid in the preservation of food products.
The cultivation of potato increased considerably over the past years because of its various uses as food. For large scale commercial preservation of potatoes cold storages are used in Bangladesh. But the total number of cold storages in the country is much lower than that actually needed. There are altogether 383 cold storages of which some are out of operation due to various reasons. Average capacities of these cold storages are 2500 metric tons. To preserve the produced potatoes in Bangladesh, the number of cold storages should be increased by about 5 times the present number. Potatoes have to be stored after harvest for a shorter or longer period in order to maintain even supply to the market throughout the year for direct human consumption as well as for the processing industry. Seed potatoes have to be stored after harvest till the next planting time. In Bangladesh were found to be operated within the temperature range of 1.67 to 2.8^0C and relative humidity was maintained within the range of 80 to 95 percent. Operating hours of the cold storage unit range from 10 to 18 hrs. The control system was either manual or automatic. Average capacity utilization ranged from 74.42 to 100 percent. The weight losses due to evaporation of moisture from potatoes in different cold storages range from 1.2 to 2.38 percent.

2. Cooling Load Calculation

To simplify the cooling load calculations, the total cooling load is divided into the number of individual loads according to the sources of heat supplying the load. The summation of these loads is the total cooling load on the equipment. The cooling load is consists of

a. The transmission load(q1),
b. Infiltration load(q2),
c. Products load(q3),

d. Respiration load(q4),
e. Other load sources (q5) and
f. Unknown and unexpected load(q6)

a. Transmission heat load (q_1):

The calculation of the transmission heat created by walls, floor and ceiling requires information on thickness and type of isolation material used in construction of cold room, construction of building, physical specifications of the cold storage volume, inside and outside environment temperatures and the effect of sunshine. The wall gain load is a measure of heat flow rate by conduction through the walls of the refrigerated space from the outside.

$q_1 = U \times A \times (T_o - T_i) \times h$
$= 1.1 \times 736.76 \times (40-2) \times 24$
$= 739117.63$ KJ

When a wall is constructed for several layers of different layers of different materials, the total thermal resistance of the wall is the sum of the resistances of the individual materials in the wall construction.

$1/U = \sum x_i / k_i$
$U = 1.1$ W/m^2 K

b. Infiltration load (q_2):

The infiltration heat load is defined as the value obtained through the entrance of the air with a higher enthalpy to the cold storage. When the door of a refrigerated space is opened, warm outside air enters the space to replace the more dense cold air that is lost from the refrigerated space through the open door. The heat, which must be removed from this warm outside air to reduce its temperature and moisture content to the space design conditions, becomes a part of the total cooling load on the equipment.

$q_2 = c_p \times z \times V \times (T_o - T_i)$
$= 1300 \times 8 \times 1225.7 \times (40-2)$
$= 484396.64$ KJ

c. Product load (q_3):

Product load is made up of the heat that must be removed from the refrigerated product in order to reduce the temperature of the product to the desired level. The term product used here is taken to mean any material whose temperature is reduced by the refrigerating equipment. In some instances, the product is frozen, in which case, the latent heat removed is also a part of the product load.

$q_3 = G \times C_1 \times (T_{out} - T_{in})$
$= 100000 * 3.43 * (40-2)$
$= 13034000$ KJ

d. Respiration Heat (q_4):

Fruits and vegetables are still alive after harvesting and continue to undergo changes while in storage. The more important of these changes are produced by respiration, a process during which oxygen from the air combines with the carbohydrates of the plant tissue and results in the release of carbon dioxide and heat. The heat released is called respiration heat and must be considered as a part of the product load where considerable quantities of fruit and /or vegetables are held in storage at a temperature above the freezing temperature.

$q_4 = G * C_2$
$= 100 * 122400$
$= 12240000$ KJ

e. Other heat loads (q_5):

The miscellaneous load sometimes referred to as the supplementary load, takes into account all miscellaneous sources of heat. Chief among these are people working in or otherwise occupying the refrigerating space, along with the lights or other electrical equipment operating inside the space.

$q_5 = q_{51} + q_{52}$
$= 32000 + 69120$ KJ
$= 101120$ KJ

$q_{51} = n \times c_i \times t_1$
$= 4 * 1000 * 8$
$= 32000$ KJ

$q_{52} = N_{ay} \times t_2$
$= 8640 * 8$
$= 69120$ KJ

f. Unknown and unforeseen heat loads (q_6):

It is common practice to add 5% to 10 % to the total cooling load as a safety factor. The percentage used depends on the reliability of the information used in the calculation of the total cooling load. As a general way, 10 % is used.

$q_6=0.1(q_1+q_2+q_3+q_4+q_5)$
$=0.1*26598633.6$
$=2659863.3$ KJ

Total Cooling Load:

Total cooling load of the potato cold storage will be-

$q=q_1+q_2+q_3+q_4+q_5+q_6$
= 29258496.3 KJ/24h
= 1219104.01 KJ/h
= 96.3 Ton

3. Cold Storage Design Criteria

Some of the more important of these features are:

Space:
a. For routine handling of scheduled deliveries to the plant relative to scheduled shipments from the plant
b. For heavier than usual demands
c. To allow for future expansion

Platforms:
a. Convenient for the approach of trucks and/or railroad reefers
b. Receiving platform above shipping dock to exploit gravity handling
c. Large enough to avoid congestion and to facilitate rapid loading and unloading

Interior transportation facilities:
a. Gravity conveyors for loading, unloading
b. Incline conveyors (powered)
c. Elevators, where more than one story

Construction details:
a. Firm footings and foundation to prevent floor and wall cracking.
b. Adequate and properly applied insulation throughout.
c. Curtained walls to eliminate exposure of cold room walls to outside temperature.
d. Maximum temperature rooms located next to walls exposed to outside temperature.
e. Waterproof weather-exposed surfaces, especially roof.

Extra equipment's:
a. Provide adequate standby equipment for emergencies.
b. Install humidifiers such as spray heads in chill compartments for moisture control.
c. Install temperature alarms (maximum or minimum in critical rooms).

Utilities:
a. Ensure adequate and cheap supply of condenser cooling water or install appropriate cooling towers.
b. Ensure adequate source of power to operate compressor, fans, pumps, etc.
c. Provide good lighting in all parts of the plant and the warehouse.
d. Provide weighing scales.

Control:
a. Ample office space for carrying on the normal business transactions of warehouse and the refrigerant plant.
b. Checking points established at appropriate locations to control and record deliveries and shipments.
c. Fire extinguishers strategically located and ready for use.

4. Design

The design is for 100 Ton of potato storage capacity. Potato capacity per bag is 80kg. So, total 1250 bags of potato should be stored. The standard dimensions of bag is length 0.4572 meter, width 0.4572 meter and height

0.762 meter. For structure and other spaces another 0.4572 meter is necessary in both width and height. So, each bag will need 0.762×0.762×1.0668 =0.619 cubic meter. For, total 1250 bags the volume required is 774.3 cubic meter. For evaporator, other accessories, ducts, chillers, freezers, docking station another 450 cubic meter is required.
After visiting different cold storage in Dhaka city and from the above calculation the design criteria of a 100 ton potato cold storage are given below.

Storage Capacity	100,000 kg
Storage Size	18.3×9.15×7.32 m
Total Surface Area	736.76 m^2
Volume	1225.7 m^3
Insulation	3.5 cm of Styrofoam
Outside Temperature	40 ^oC
Inside Temperature	2 ^oC
Humidity	90%
Specific heat of potato	3.43 kJ/Kg-K
Miscellaneous heat loads	4 workers, 1000 kJ per h for each person
	Lighting load 8640 kJ

5. Construction Feature of Cold Storage

The design of cold storage includes the drawing up of specifications, sketching of a site plan and a general plan, the setting of the dimensions of the cold rooms (which depends on stacking arrangement), the calculation of heat balances and refrigeration capacity and the insulation thickness, selection of refrigeration system components, their installation and testing and finally performance evaluation. Any deviation from this procedure results in defective cold storage construction, increasing in cost of storage of the product due to increased operational and maintenance cost.

Storage building:

The building ideally should have a floor perimeter in the shape of a square. A rectangular configuration has more wall area per unit volume of the cold storage, resulting in higher construction cost and higher heat in-leak compared to square shape. The orientation of walls should be such that they receive minimum solar radiation. A dark, flat roof can be 42 ^oC warmer than that of the outside air temperature. Painting a south facing wall with a light color can reduce the effective wall temperature by 11 ^oC compared with a dark colored wall.

Insulation material:

Thermal insulation of a cold storage is necessary for proper control of storage conditions. A lower capital investment with an inferior quality and thinner insulation leads to a larger heat in-leak. A larger compressor with more power consumption is required to make good for the additional cooling load. Therefore, quality and quantity of insulation material has a direct relation with the power consumption. The optimum insulation quality and its thickness, of course, is a function of the energy cost and hence a function of the instant of time. It is however not so in practice and reality.In Bangladesh usually Styrofoam or rice husk is used for insulation.

Vapor barrier:

It plays a big role in determining the insulation quality with passage of time that ultimately affects the electrical energy consumption in cold storage. In the absence of vapor barrier, the insulation material may absorb the water vapor and after condensation therein, the energy consumption increases dramatically as the thermal conductivity of wet insulation increases by about 32 times.

6. Selection of Components of Cold Storage

Generally methods of refrigeration can be classified as non-cyclic and cyclic. Other methods are Gas Cycle, Thermoelectric refrigeration, Magnetic refrigeration, Air cycle, Vortex tube, Thermo acoustic refrigeration etc.

Compressors

At the heart of the vapor compression cycle is the mechanical compressor. There are generally three types of compressors that are used in vapor compression systems. These are: Reciprocating, Rotary, and Centrifugal. There are also scroll and screw compressors but not widely used. But in the cold storages mostly reciprocating compressor are used.

Evaporator

Evaporators are heat exchangers in which a refrigerant is evaporated at low temperature and pressure for the purpose of removing heat from the refrigerated space or material. There are different type of evaporator like dry expansion evaporator, air-cooling evaporator, flooded type evaporator, liquid cooling evaporator etc. In Bangladesh mainly air-cooling evaporator is used in most of the cases.

Condenser

The condenser is the component in the refrigeration cycle where heat is removed and rejected. There are mainly three type of condenser air cooled, water cooled and evaporative condenser. For cold storage water cooled condenser is used.

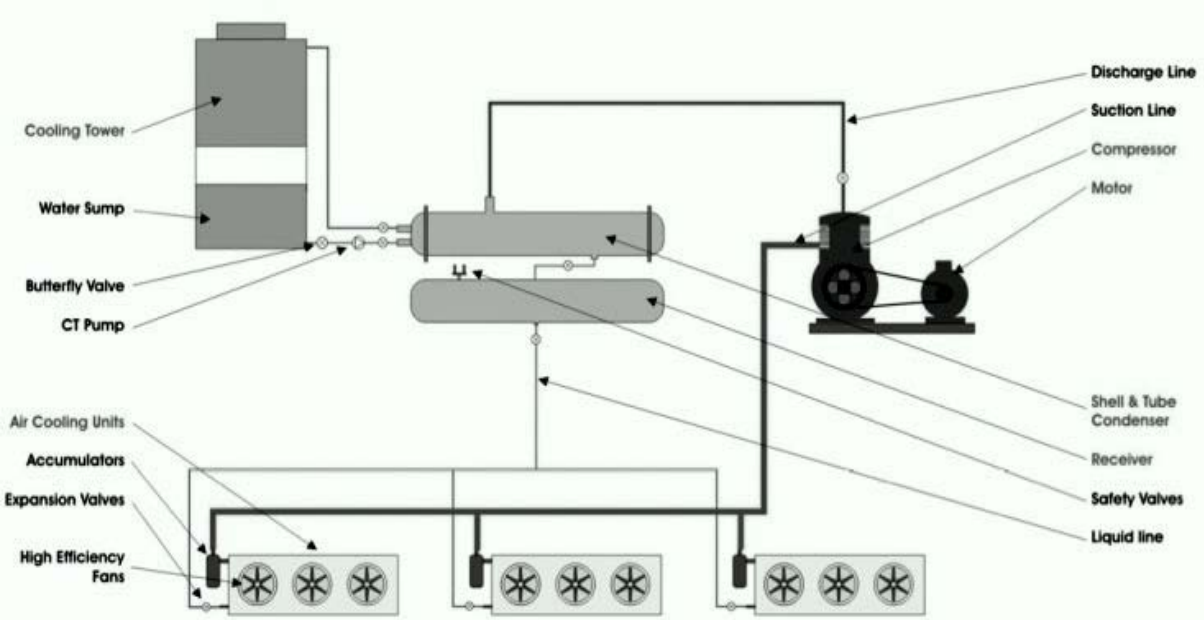

Fig: Schematic of Ammonia Cycle Cold Storage

Expansion devices

The expansion device is just opposite of compressor. The expansion devices are different types. They are thermostatic expansion valve, automatic expansion valve, and capillary tube etc. Dx type expansion valve is mainly used in cold storage.

Control System

Controls are necessary to maintain optimum operating conditions commensurate with varying load situations. Automatic control makes the plant independent of skilled supervision. It also achieves a higher degree of accuracy in maintaining the required temperature, pressure and humidity. Though cold storage load does not fluctuate as frequently as it does in air conditioning systems every cold Storage is equipped with automatic control mechanisms that ensures smooth running. In most of the cold storages self-actuated control system is used.

7. Conclusion

In order to reduce the post-harvest deterioration, potatoes are kept in cold Storage for long-term storage. The stored potatoes are subjected to heat and mass transfer during the extensive storage period of about 8 months.
Uniform cooling in bulk of potatoes within commercial cold Storage is difficult to attain, owing to existence of an uneven distribution of the airflow, which results in considerable temperature and humidity difference within the stored product. The variability of the cooling rate and resultant spatial variation in temperature of the product inside a cold Storage causes the product quality to deteriorate through either increased respiration at

higher temperature or by chilling injury at lower temperature. The poor airflow distribution through stacks of bagged potatoes could also result in non-uniform humidity, which might lead to condensation of moisture wherein relative humidity reaches at saturation or excessive dehydration wherein the relative humidity remains very low. The prevailing situations in the potato cold Storage lead to storage losses even up to 10 % against the prescribed maximum limit of 5% during the storage period of 8 months. Therefore, one of the main aims in designing storage system is to ensure a uniform targeted temperature and humidity in the bulk of stored product. In Bangladesh, the storage losses in potato cold stores account for 5–10% of the stored product in the form of rotting, cold injury, weight loss, sprouting, nutritive value degradation, etc. However, the potato losses may increase up to 40 – 45 % due to poor storage management and operations.

Possible causes behind higher energy consumption beyond permissible limit:

There are many factors affecting the energy consumption and storage losses in a potato cold Storage. Some important of them are listed below-

- Irregular loading pattern.
- Overloading of the storage chamber.
- Defect in the design and operation of the refrigeration system of cold storage.
- Poor airflow distribution in the storage chamber and within the stack mass.
- Prevalent stack size and stacking arrangement.
- Overlooking or completely elimination of curing process before loading the potatoes in cold storage chamber.

Scientific approaches to reduce the problems:

The problems of higher energy consumption and storage losses in the potato cold storage industry have been known since decades and efforts were also made by the cold storage owners, operators and other concerned personals to overcome these defects.

- **Data collection on airflow, temperature in the cold storage chamber**:

To get an insight view of the problems of energy consumption and storage losses, a thorough knowledge of airflow, temperature and relative humidity distribution in the cold storage chamber is necessary. The required knowledge can be obtained either through experimentation or mathematical simulation. Due to the availability of faster computers at reasonable prices, the detailed information on airflow, temperature distribution and moisture loss in the cold storage chamber could be obtained economically in short time thorough mathematical analysis.

- **Analysis of collected data to identify the defects in the existing cold storage**:

Once an insight view of cold storage in terms of temperature, relative humidity and airflow distribution is available, the probable zones such as hot and cold spots, dead area, moisture condensation, etc. could easily be located. The product in the stack would suffer severe moisture loss, if the relative humidity in the stack dropped below 80% and moisture might also condensed on cold surfaces of the potatoes when the relative humidity in the surrounding air approaches near 100%.

8. Recommendation

There are unlimited capabilities of this technique in the processing industries. The following are some of the areas wherein this technique could be used for the improvement of performance of the cold storage.

- To investigate the effect of air velocity, storage air temperature and relative humidity and hence optimization of storage air conditions.
- To check the initial quality of potatoes, like maturity, variety, size, shape, etc.
- To study the effect of stacking arrangement and gaps between the stacks.
- To Determine the gaseous composition of storage environment and hence, the required frequency for charging the fresh air into the cold storage chamber.
- To modify the arrangement of cooling coils and ceiling fans to improve the air circulation.
- To regulate the reducing sugar in the potato during the long-term storage as required for potato processing industries.

REFERENCES

[1] Magoo Nitin "*High-Temperature Refrigerated Warehouse Operation under Real-Time Pricing of Electricity*" M.Sc Thesis paper, 2003.

[2] Tridib Kumar Goswami "*Efficient Design, Operation, Maintenance And Management Of Cold Storage*"

[3] Keith O. Fuglie "*Economics of Potato Storage*"

[4] M.M. Islam, M.H. Kabir, M.A.Sattar And M.S. Kabir "*Management Practices In Selected Cold Storage In Bangladesh*"
[5] Schoenemann J.A. 1977. Grading, Packaging And Marketing Potatoes, In: Potatoes Production, Storing. Processing,Ora Smith, Ed., 2nd Edition. The Avi Publishing Company Inc., West Port, Pp. 470-505
[6] ASHRAE Handbook- Fundamentals (2010)
[7] ASHRAE Refrigeration Handbook (1998)
[8] F. Stoecker Wilbert / Jerold W. Jones, "*Refrigeration & Air Conditioning*" 2nd edition. McGraw-Hill International Edition.

Paper ID: TE-16

Performance evaluation of PV Module using Water Filters and Infrared Reflective Glass Covers

Y. Baradey, M.N.A.Hawlader*, M. Idresand S. I.Ihsan

Department of Mechanical Engineering, Faculty of Engineering,
International Islamic University Malaysia, Jalan Gombak, 53100 Kuala Lumpur, Malaysia
e-mail:mehawlader@iium.edu.my

Abstract

The Photovoltaic (PV) system converts only a selected band (0.35µm to 0.82 µm) of solar radiation to electricity. The absorption of radiation outside this band leads to a temperature raise of PV module which affects its performance. Experiments were performed to prevent radiation outside the selected to reach the PV panel using water filtersand different types of infrared reflective pigments. The results of the experiments showed that the optimum water filter panel was the one with thickness of 10 mm. It led to about 4% improvement in the open circuit voltage of the module, and a significant reduction in the module's average operating temperature up to 21^{o}C. The optimum coated cover glass was 10 micron IRR glass cover which led to about 50% reduction in solar radiation, 22^{o}C reduction in the average temperature of the module, and 5.3% improvement in its open circuit voltage.

Keywords: *PV, water filters, infrared reflective pigments, infrared reflective glass cover.*

1.0 Introduction

Photovoltaic (PV) system is a device that converts solar radiation directly to electricity [1]. When solar cells receive the incident solar radiation, a complex interaction between the absorbed photons and the solar cell's structure occurs.This interaction is considered the main process of transformation of solar energy into electricity because it leads to generate so called electron-holes pairs[2]. However, the most effective semiconductors that can be used in manufacturing solar cells have band energies in the range of 1.0 – 1.8 eV. For crystalline silicon solar cells, which is used in this research, the band gap energy equal to 1.12 ev [3]. Photons that have energy equal or greater than the band gap energy of the crystalline solar cells are in the range of 0.35 to 0.82 µm. The rest of the solar radiation (below 0.35 and above 0.82 µm) will not be converted to electricity but converted to heat [2].An increase oftemperature of the solar cells above the desired value leads to a decrease the output power, efficiency, and the lifetime of the photovoltaic module[4].Maintaining the operating temperature of the photovoltaic system at low value was the main objective of many researches devoted by different research centers during the last decade. According to Teo et al. [5]water is considered one of the most significant way to extract heat from PV, because it has high heat capacity and thermal conductivity, so that PV/T system which is the combination between photovoltaic module or panel and thermal system (usually flat plate thermal collector) have been largely used and investigated during the last two years in order to cool down the photovoltaic systems and make them more efficient and competitive. The second common technique that was also largely tested and investigated using different types of coated glass covers in order to reflect the undesired parts of solar radiation and preventing them to reach the photovoltaic module.

In 1994, Beauchamp [6] used blue-red reflecting cover glasses to reduce the absorptance of infrared radiation in GaAs and amorphous solar cells. He found out that three percent of output power increased due to lowering the temperature of solar cells by using blue-red coated cover glasses. Sopian et al. [7] improved the thermal and the electrical efficiency of the thermal photovoltaic system by designing and testing a double pass air PV/T collector.Tripanagnostopoulos et al.[8] added thin flat metallic sheet (TFMS) in the middle of the air channel in the PV/T-air collector but its effect on the operating temperature of the photovoltaic cells was not significant.Russell et al.[9] conducted experiments on triple junction solar cell using Ultra violet reflective (UVR) and infrared reflective (IRR) coatings on glasses in order to reflect the ultraviolet and infrared radiation

that are outside of the cell's response range but the efficiency gained was only about 0.5%. Rahman et al. [10] used two type of infrared reflective pigments and he found out that the efficiency of coated solar cells increased by 7.6% when compared to an uncoated cell.

In this study, three thicknesses (5mm, 10mm, and 20mm) of water filters were used to eliminate components of the radiation not contributing to electricity generation. Three types of infrared reflective pigments were also considered to study effects on PV module. Tests were conducted under different meteorological conditions and important parameters were measured to evaluate performance.

2.0 TheExperiment

Poly–crystalline photovoltaic module is used in order to study its performance with and without water filter panels and infrared reflective glass covers under Malaysian meteorological conditions.This type of photovoltaic module was chosen as it, nowadays, comprises about 90% of the photovoltaic market. In this study, efforts were devoted to find suitable means and ways to improve its output power, efficiency, and performance. However, it is tested in different times during different days to get the average of its performance under different meteorological conditions. Its open circuit voltage, short circuit current, top and bottom temperature and incident solar radiation were measured, monitored and recorded.However, in all experiments, there was about 10 cm distance between cover glass and / or water filter panel and the top surface of the photovoltaic module in order to measure and record the transmitted radiation from them (the radiation that penetrates through the cover glass or water filter panel and reach the module) ,as shown in the Figure 1.A Pyranometer was used to measure the incident solar radiation on the top surface of the cover glass or water filter panel (I Top) as well as the transmitted one (I Bottom). One of its limitations is that it does not measure the wavelength of the solar radiation. Digital Multi-meter was used to measure the open circuit voltage and short circuit current of the module. Thermocouples were used to measure the temperature of the top and bottom surface of the photovoltaic module (T Top and T Bottom), as shown in Figure 1.

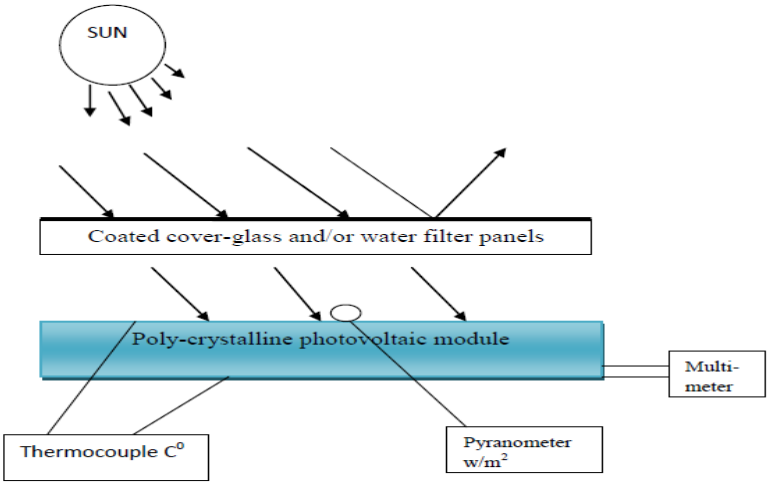

Figure 1: Schematic diagram of the experimental set-up

3.0 Resultsand Discussion

Photovoltaic only

The results of all experiments conducted on the PVM only showed that its top and bottom temperatures were increasing with time and irradiation until it reaches a high value (sometimes it reached more than 70 C^0), which clearly affected the open circuit voltage and , hence, the power output of the PV Module . Figures 2, 3 and 4

represent average temperature (Ttop + T bottom)/2) vs time, voltage vs time, incident radiation and current vs time, respectively.

Water Filters

The experimental results show asignificant reduction in the solar radiation due to 5mm water filter panels whichreached about 200 W/m^2 at an average incident radiation of 646 W/m^2, leading to about 20^{o}C reduction in the average temperature of its structure, as shown in Figure 2. Open circuit voltage of the module decreased with time, and it was improved by 2.3%, as shown in Figure 3. However, the reduction in radiation due to 10 mm water filter panel reached 270 W/m^2 at 852 W/m^2 average incident radiations, led to 21^{o}C reduction in the module's average temperature, and about 4% increment in its open circuit voltage, as shown in Figure 2 and 3. The results of the experiment also showed that 20 mm water filter panel absorbed and/or reflected about 300 W/m^2 of the incident solar radiation at about 1000 W/m^2. The reduction in radiation maintained the average temperature of the module around 44^{o}C, which equal to about 25^{o}C reductions in temperature. Therefore, about 3% improvement in the open circuit voltage was achieved, as shown in Figure 3.Short circuit current and radiation vs time for the optimum water filter is shown in Figure 4.

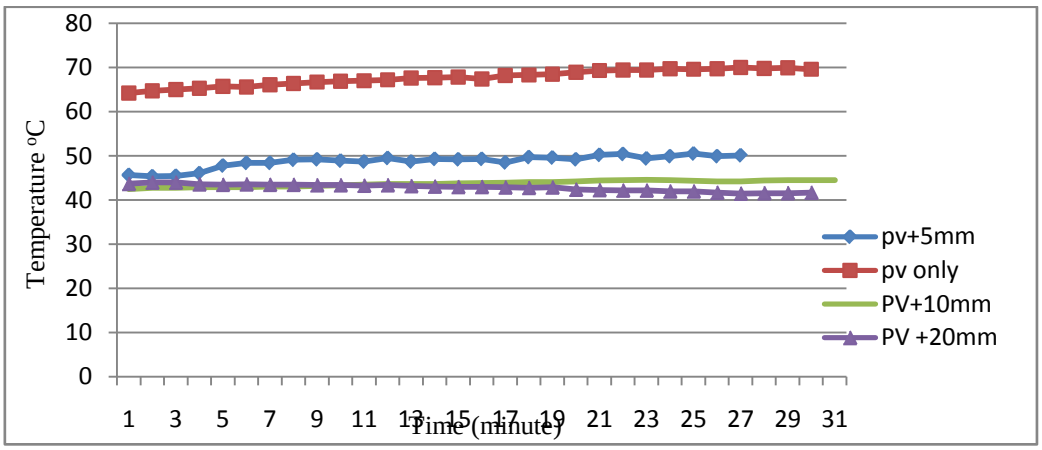

Figure 2: Comparison between Average Temperature for PVM Only and PVM with Different Thickness of Water Filter Panels

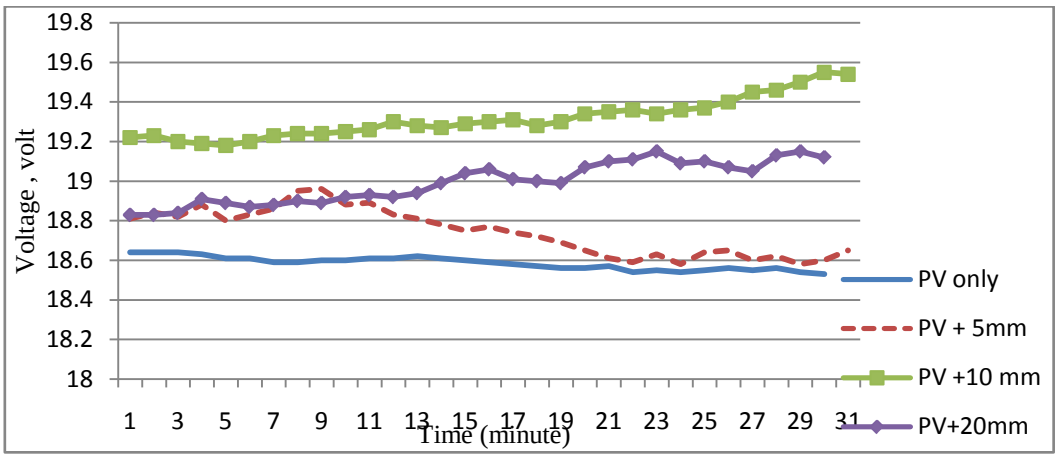

Figure 3: Comparison between Open Circuit Voltage for PVM Only and PVM with Different Thickness of Water Filter Panels

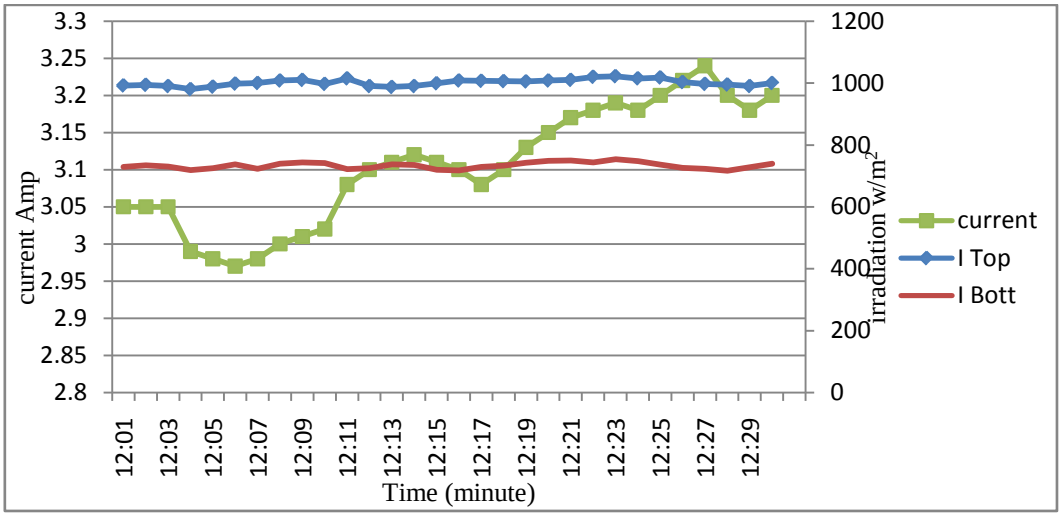

Figure 4: Top and Bottom Radiation and Current VS Time for 10 mm Water Filter Panel

Different Glass Covers

The performance of the photovoltaic module was investigated using a 3mm- transparent glass. The average enhancement obtained in the open circuit voltage was about 2.75 %, while the average enhancement in the short circuit current was about 9.6%, as shown in Figures5 and 6,respectively. The enhancement in both short circuit current and open circuit voltage led to about 26.4% increase in the output power, and 3% improvement in the efficiency of the PVM. The average reduction in the temperature sometime reached more than 12^{o}C due to the same uncoated glass cover, as shown in Figure 7.

The optimum coated cover glass was 10 micron IRR glass cover which led to 5.3% improvement in its open circuit voltage, and about 22^{o}C reduction in the average operating temperature of the module, as shown in Figure 5 and 7, respectively. The reduction in radiation due to10 micron IRR cover glass was very high (in some experiments was about 50%), because the proposed function of it (depending on the claim of the company and the reflectance curve vs wavelength of the pigment) is to eliminate all infrared radiation, which represent about 49% of the solar radiation, and preventing it to reach the photovoltaic module, so that this reduction in radiation was expected. Moreover, the experimental results for 20micron IRR glass cover showed that about 20^{o}C reduction in the average temperature of the module leading to about 2% improvement in the open circuit voltage, as shown in the same Figures. However, the reduction of radiation due to 30 and 40 micron IRR glass covers was too high; it sometimes reached 60% of the incident solar radiation, and about 20^{o}C reduction in the module's average temperature was achieved, but it caused no improvement in its open circuit voltage because it is expected that the interaction between the radiation and the pigment layer was very high.

Short circuit current of the module was negatively influenced by the significant reduction of the radiation due to the pigmented glass covers. It is strongly believed that the negative effect occurred due to the reflectance of the near infrared component of irradiation, so that the reflected and/or absorbed radiation due to IRR glass covers includes some amount of radiation that belongs to the spectral response range of the module. Furthermore, it is also believed that there was a thermal interaction between the incident photons and the pigment's particles making the photons that penetrate the pigment layer lose some of their energy which affects their ability to create electron-holes pairs. The thickness of the coating layer played an important role in influencing the amount of the transmitted radiation. The results related to the thickness of the infrared coating layer showed that the thickness should be less than 5 micron to avoid any possible interaction between the incident photons and the pigment layer.

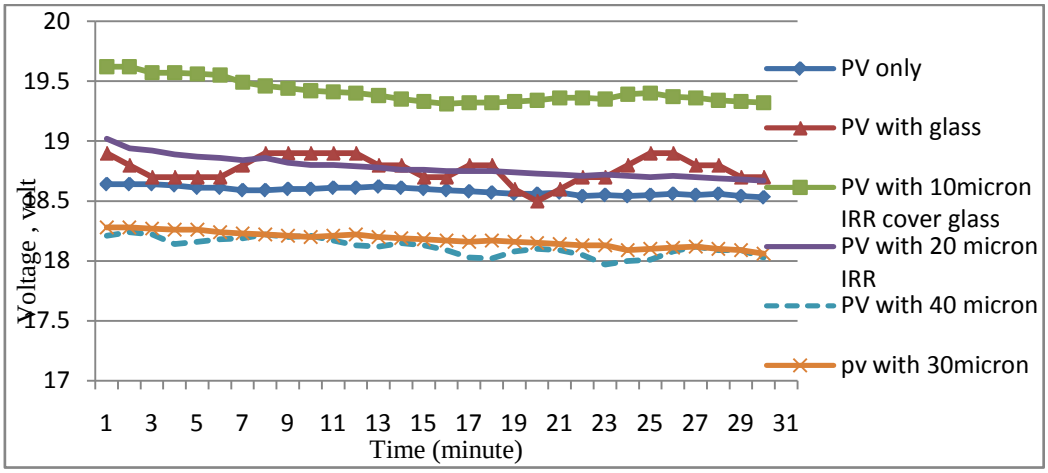

Figure 5: Comparison between Open Circuit Voltage for PV Only and PV with Different Cover Glass Used VS Time

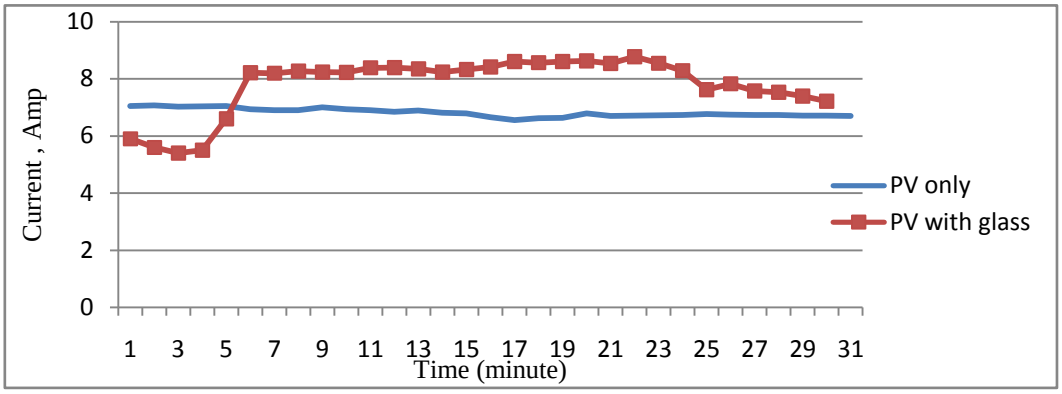

Figure 6: Comparison between Short Circuit Current for PV Only and PV with Uncoated Glass VS Time at Same Amount of Incident Radiation

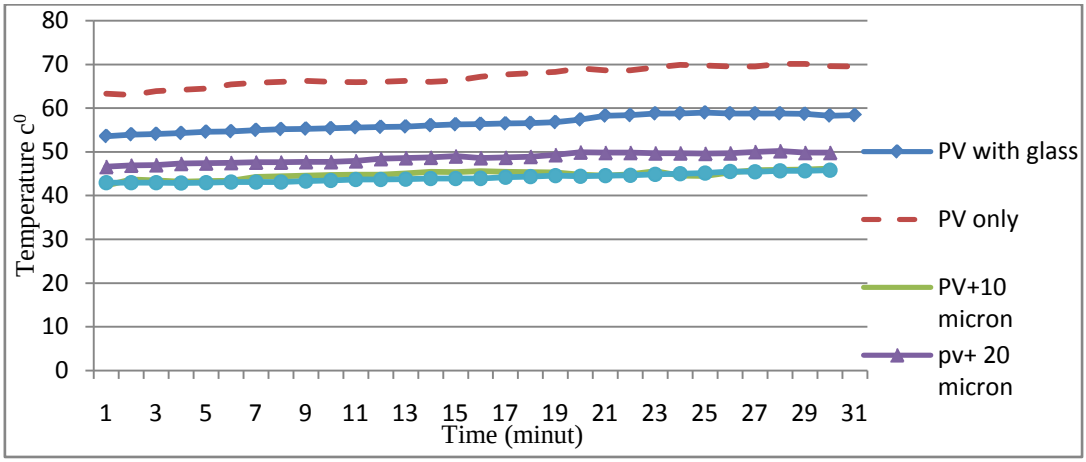

Figure 7: Average Temperature for PVM Only and PVM with different glass covers VS Time at Same Radiation

4.0 Conclusions

In this paper, the performance of a poly-crystalline photovoltaic modulewas evaluated with two different techniques: water filters and reflecting pigments. The results of the experiments revealed that the optimum water filter panel was 10 mm filter panel. It led to about 4% improvement in the open circuit voltage of the module, and about 21^{o}C reduction in the module's average temperature. The results also showed that 3mm uncoated glass cover led to about 12^{o}C reduction in the average temperature of the module, 2.75% improvement in its open circuit voltage, 9.6% enhancement in its short circuit current, and 3% in the efficiency. For other infrared reflective glass covers, the thickness of the pigment layer played a significant role in influencing the performance of the photovoltaic module as well as the reduction in the solar incident radiation, higher thickness led to higher reduction and vice versa. The optimum coated cover glass was 10 micron IRR glass cover which led to about 50% reduction in solar radiation, 22^{o}C reduction in the average temperature of the module, and 5.3% improvement in its open circuit voltage.

References

[1] International Renewable Energy Agency, (2012),"Renewable energy technologies: cost analysis series". *Solar Photovoltaic* 1, (4/5) 2012.

[2] P. Hersch and K. Zweibel, "Basic Photovoltaic Principles and Methods", Technical Information Office, SoIar Energy Research Institute, 1617 Cole Boulevard, Golden, Colorado 80401: United State of America,1982.

[3]B. K. Hodge, "Alternative Energy Systems and Applications", United States of America. John Wiley & Sons, 2010.

[4] G.L. Jin, H.Ruslan, S. Mat, M. Y. Othman, A. Zaharim and K.Sopian, "Experimental studyon single-pass Photovoltaic-Thermal (PV/T) air collector withabsorber", *Paper presented at 9th WSEAS international conference on system science and simulation in engineering,*Pages 435-438, 2010**.**

[5] H. G. Teo, P.S. Lee and M. N. A.Hawlader,"An active cooling system for photovoltaic modules", *Applied Energy*,90,309-315,2012.

[6]W. T. Beauchamp, W. T.,"Qualification test results for blue-red reflecting solar cell covers",*Paper presented at Photovoltaic Energy Conversion,* 5-9 December 1994,Waikoloa, Hawaii, 1994.

[7]K. Sopian, H. T.Liub, S.Kakacb, and T. N. Veziroglu, "Performance of a Double PassPhotovoltaic Thermal Solar Collector Suitable for Solar Drying Systems",*Energy Conservation & Management,41,* 353-365, 2000.

[8] Y. Tripanagnostopoulos, M.Bazilian, I.Zoulia, and R.Battisti, *"Hybrid PV/T System with Improved Air Heat Extraction Modification"*,(2002),http://www.ecn.nl/fileadmin/ecn/units/egon/pvt/pdf/patras04.pdf , retrieved 4 April 2013from

[9] J. Russell, G. Jones, and J. Hal, *"A New Uvr/IrrCoverglass for Triple Junction Cells", 2005,* http://ieeexplore.ieee.org/iel5/4059527/4059868/04060036.pdf , retrieved 26December 2012.

[10] Rahman et al.,"Interference pigment coated solar cells for use in high radiant flux environments", *Jordan Journal of Mechanical and Industrial Engineering,* 4(1),129-134, 2010.

Paper ID: TE-17

Investigation of Condensation Heat Transfer Characteristics for R1234ze(E), R32, R410A and Zeotropic Mixture of R1234ze(E) and R32 inside Smooth Tube

Md. Anowar Hossain[*1], Akio Miyara[2], Md. Zahidul Sarkar[1], Md. Jahangir Alam[1]
[1]Department of Mechanical Engineering, Dhaka University of Engineering &Technology, Gazipur 1700, Bangladesh
[2]Department of Mechanical Engineering, Saga University, 1 Honjomachi, Saga-shi 840-8502, Japan
E-mail: anowar96me@gmail.com

Abstract

This research work presents experimental results of two-phase flow condensation heat transfer characteristics of the refrigerants R1234ze(E),R32, R410A and zeotropic mixtures of R1234ze(E)/R32 (55/45 and 70/30 mass%) inside smooth horizontal tube. The test section is a horizontally installed smooth tube with effective length of 3.6 m and inner tube inner diameter of 4.35 mm. The experiment has been carried out under the conditions of mass flux varying from 150 to 445 kgm^{-2}s^{-1}, at condensation saturation temperatures 35, 40 and 45°C over the vapor quality range of 0.0 to 1.0. The effect of vapor quality, mass flux and saturation temperature on HTCs have been conducted and analyzed. The experimental results show that the heat transfer coefficient decreases as the condensation progresses for both pure and mixture refrigerants. The refrigerants exhibit high heat transfer coefficient at the high mass flux. There is not so significant effect of saturation temperature on the heat transfer coefficient. The mixtures show lower heat transfer coefficient than pure. Among the mixtures, 70% R1234ze(E) shows lower heat transfer coefficient than 55% R1234ze(E) mixture. It is seen from the results that the heat transfer coefficient of R1234ze(E)/R32 (55/45 mass %) is almost similar to R410A. So, Zeotropic mixture of R1234ze(E)/R32 (55/45 mass %) could be a good alternate of R410A.

Keywords: *Zeotropic mixture, Refrigerant, Heat transfer coefficient.*

1. Introduction

Chlorofluorocarbons (CFCs) and hydrochlorofluorocarbons (HCFCs) have been phased out under the Montreal and Kyoto protocol, respectively. HFOs (hydrofluoroolefins) such as R1234yf and R1234ze(E) have much more awareness in recent era because of their low global warming potential (GWP). Pure R1234ze(E) is inferior in the fields of room and packaged air conditioning and heat pump systems because of low operating pressure. HFC refrigerant, especially R32 (difluoromethane) is a high pressure and superior as a refrigerant. R32 has also relatively lower GWP among HFCs. So, mixture of R1234ze (E) and R32 can be effectively used in the field of air conditioning due to their mild impact on environment. Two special attributes of zeotropic mixture are identified as temperature glide and composition shift during phase change can possibly be utilized to improve the energy efficiency or the coefficient of performance of a system for cooling/heating application. Some property measurement works had done such as Akasaka, Brown et al., Grebenkov et al., Higashi, Miyara et al., Motta et al., Srinivasan et al., Tanaka et al., Yamaya et al. [1-9] are listed in the reference. Hossain et al. [10] experimentally studied on condensation heat transfer and pressure drop in horizontal smooth tube for R1234ze (E), R32 and found that for mass flux of around 300 kg m^{-2} s^{-1}, HTC of R1234ze(E) is about 30% lower than R32 and about 28% higher than R410A. Koyama et al. [11] recommended that pure R1234ze (E) is not suitable for an alternative of R410A, but mixtures of R1234ze(E) and R32 are promising candidates for replacing R410A in domestic heat pump systems. The present work deals with the comparative study of heat transfer coefficient of R1234ze(E), R32, R410A and zeotropic mixtures R1234ze(E)/R32 (55/45, 70/30 mass%) during horizontal in-tube condensation.

.

2. Experimental Method

Fig. 1 shows the schematic diagram of the experimental apparatus which is a vapor compression heat pump cycle comprising a inverter controlled compressor, an oil separator, a condenser, a subcooler, an expansion valve and a test condenser. Cold water kept at a constant temperature is supplied to the test condenser from the source unit. The refrigerant flow rate is regulated by varying the rotating speed of the compressor and opening the expansion valve and is measured by a coriolis type mass flow meter. Fig. 2 shows the test section. The test section is a horizontally installed double tube heat exchanger. The total length of the test section is 6.59 m where the effective heat transfer length is 3.6 m which is split into two parts for space accommodation and connected the two parts by a U-bend. Refrigerant flows inside an inner tube and cooling water flows through the annular space in a counter current. In order to measure quasi-local heat transfer, the annular channel is divided into 12 subsections with each 2 subsection length 300 mm. The inner tube is the smooth test tube made of copper and of

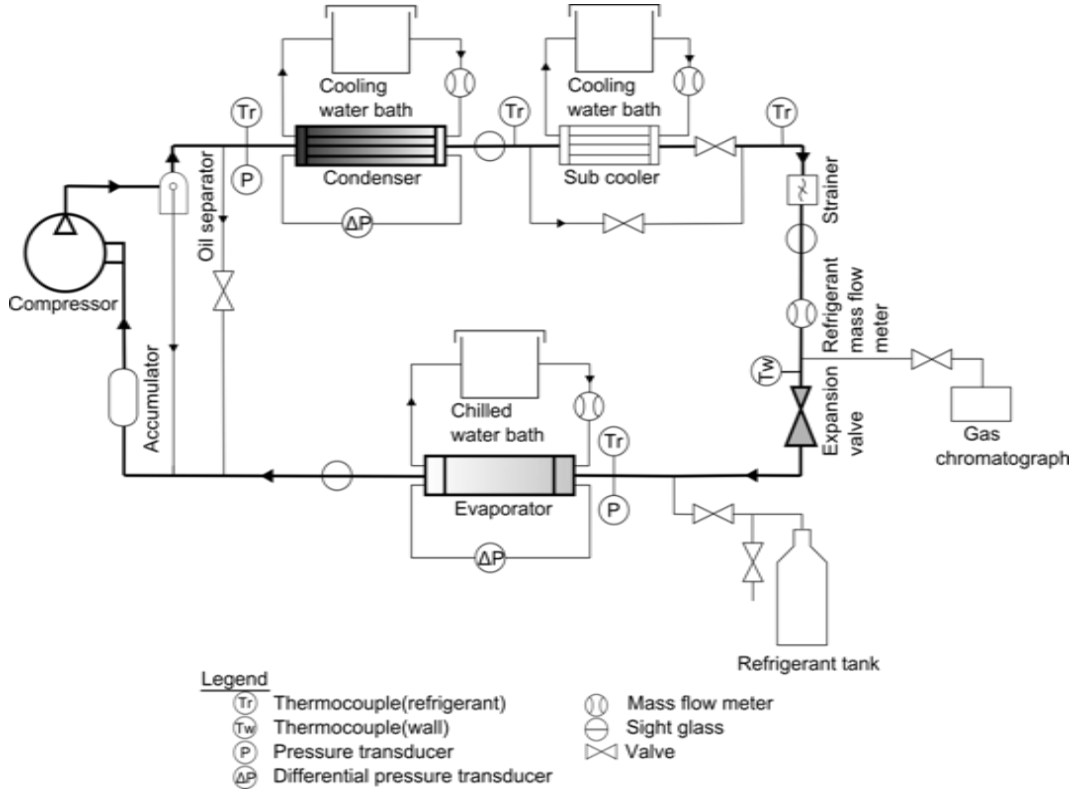

Fig. 1. Schematic diagram of experimental apparatus

4.35 mm inner diameter and 6.35 mm outer diameter. The outer tube is made of poly-carbonated resin and of 9 mm inner diameter and 13 mm outer diameter. Details of the experimental measurement and uncertainties has discussed in Hossain et al. (2012) [16].

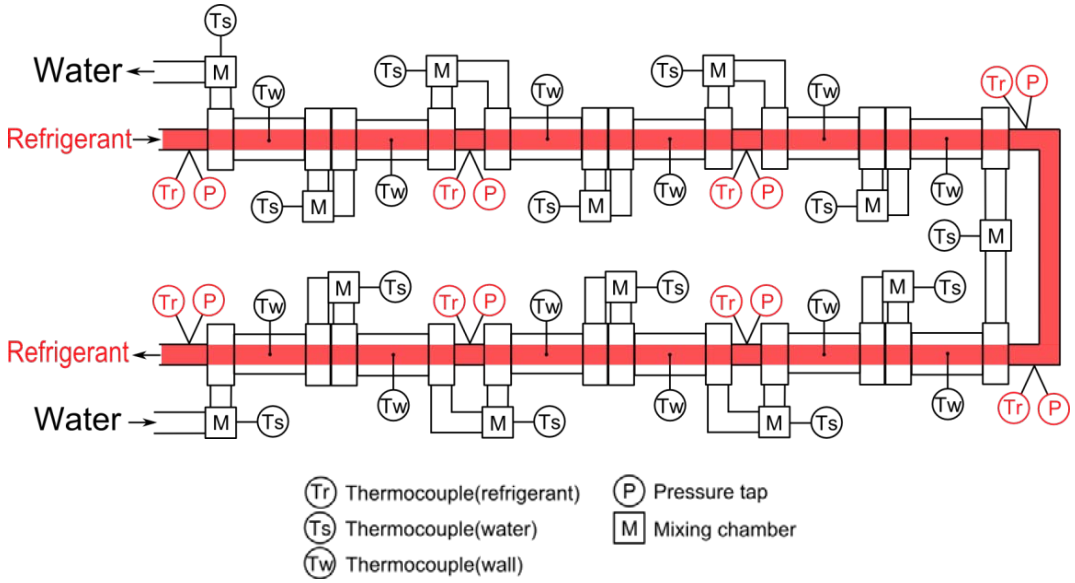

Fig. 2. Test section

The quasi-local condensation heat transfer coefficient of each subsection is defined as follows-

$$\alpha_{\exp} = \frac{q_R^{"}}{T_s - T_{wi}} \qquad (1)$$

where, $\alpha_{\exp}$ is local heat transfer coefficient, T_s is the saturation temperature of the refrigerant, $q_R^{"}$ is refrigerant heat flux and T_{wi} is the inner tube wall temperature . The representative inner wall temperature at middle length of each subsection of the test tube is obtained by

$$T_{\mathrm{wi}} = T_{\mathrm{wo}} - \frac{q_s \eta_{HB} \ln(d_{\mathrm{o}} / d_{\mathrm{i}})}{2\pi\lambda_c \Delta z} \qquad (2)$$

Here, T_{wo} is average outer wall temperature calculated from measurement point of Top, right, bottom and left, q_s is heat transfer rate for the subsection, η_{HB} is heat balance factor, $d_{\mathrm{o}}, d_{\mathrm{i}}$ are outer and inner diameter of the tube, λ_c is coolant thermal conductivity, and Δz is the pressure drop length. Table 1 shows the experimental conditions.

Table 1 Test range for the condensation experiment

Refrigerant	R1234ze (E)	R32	R410A	R1234ze(E)/R32
G (kg m^{-2} s^{-1})	147-403	220-400	215-400	169-395
T_{sat} (°C)	35, 40, 45	40	40	35, 40, 45
x (-)	0.02-0.99	0.007-0.99	0.007-0.99	0.01-0.98
P (kPa)	650-900	2505-2641	2339-2440	1462-1987

3. Results and Discussion

Fig.3 shows the flow pattern map plotted by using El Hajal et al equations. Fig. 3(a) is for pure refrigerants and Fig. 3(b) is for R1234ze(E)/R32(55/45 mass%) zeotropic mixture at the saturation temperatures of 35, 40 and 45°C for condensation inside a horizontal smooth tube. It is seen from the figures that most of the data points are in the intermittent and annular flow and a very few are in the stratified wavy flow regime.

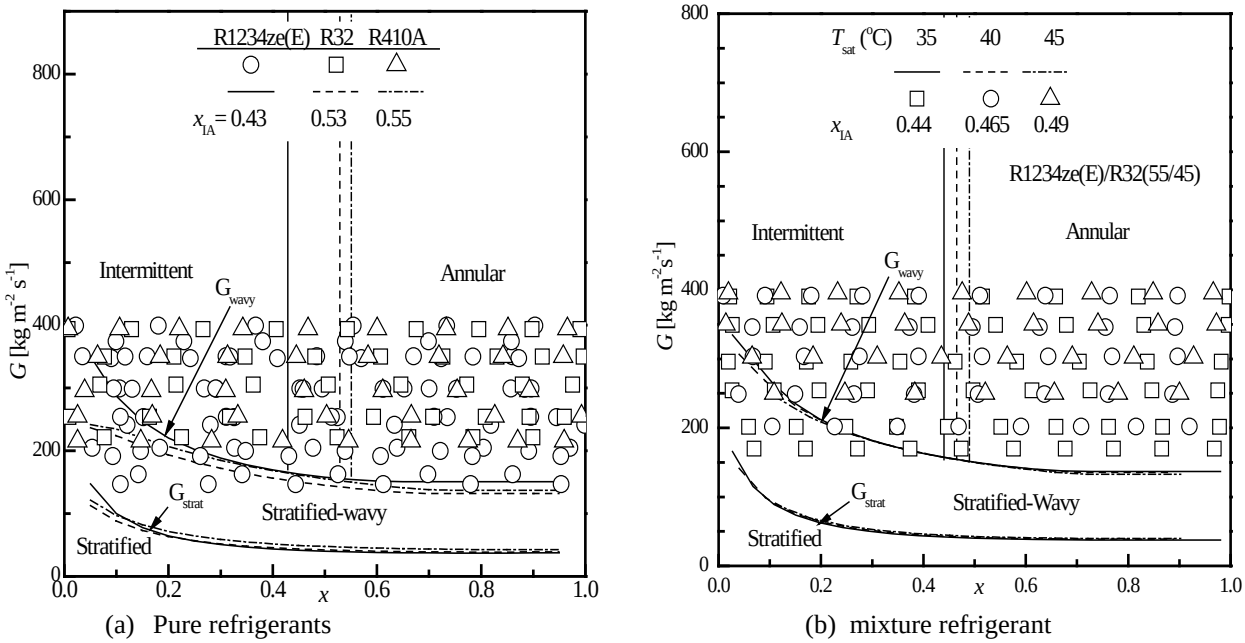

Fig. 3. Flow pattern map plotted by using El Hajal et al. (2003)

It is seen from the flow pattern map that there is noticeable variation among the transitional vapor quality (x_{IA}) between intermittent flow and annular flow among the pure refrigerants R1234ze(E), R32, R410A and mixture refrigerant at saturation temperatures of 35,40 and 45°C because (x_{IA}) is a function of density and viscosity ratio. As the ratio of density and viscosity is high the value of (x_{IA}) will be low Hajal et al (2003). For pure refrigerants, x_{IA} is higher for R410A and R32 from R1234ze(E) because of density ratio. For mixture, x_{IA} increased with increasing saturation temperature due to the increased of density and viscosity ratio. Fig.4 shows the effect of saturation temperature on experimental heat transfer coefficient for R1234ze(E)/R32 (55/45 mass%). It is seen from this figure that there is not so significant effect of saturation temperature on the heat transfer coefficient because with saturation temperature change the system pressure also change as well as the thermal and transport properties of the refrigerants.

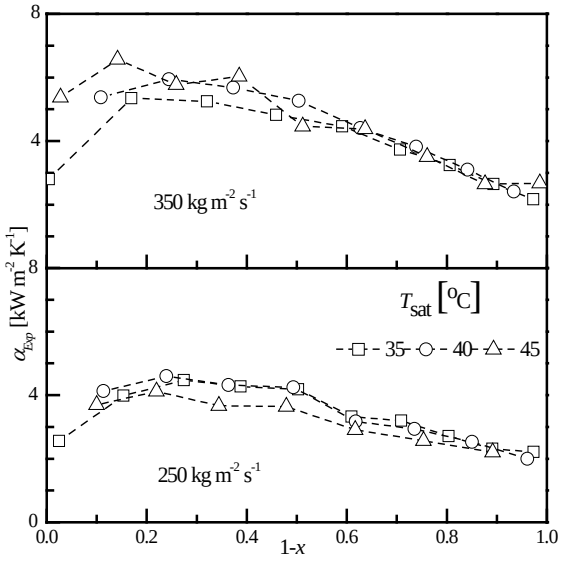

Fig. 4. Effect of saturation temperatures on experimental heat transfer coefficient for R1234ze (E)/R32 (55/45 mass %).

Fig.5 shows the local heat transfer coefficient variation along the tube with respect to (1-*x*) at 40 °C saturation temperature and at 300 and 400 kg m^{-2} s^{-1} mass flux of refrigerants R1234ze (E), R32, R410A and mixtures of R1234ze (E) and R32. Experimental results show that the heat transfer coefficient decreases as the condensation progresses for both pure and mixture refrigerants. The mixtures show lower heat transfer coefficient than the pure R1234ze (E) and R32 and among the mixtures, 70% R1234ze (E) shows lower heat transfer coefficient than 55% R1234ze (E) mixture.

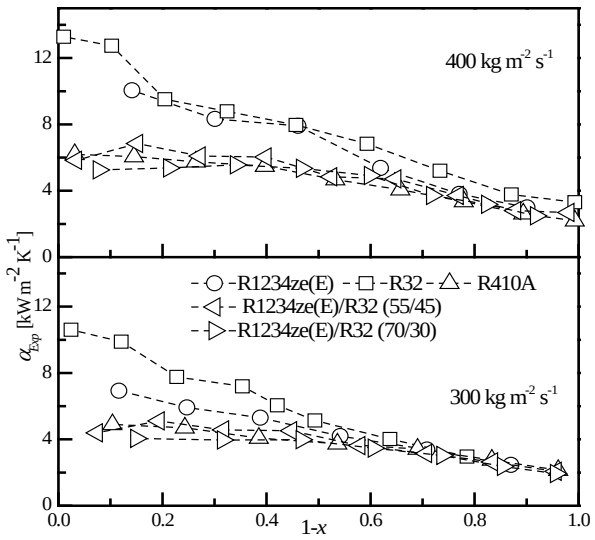

Fig. 5. Comparison of experimental local heat transfer coefficient.

The variation of temperatures of the refrigerants and tube wall are shown in Fig.6 and the variation of the heat flux is shown in Fig.7. When condensation occurs at the vapor-liquid interface of the mixture the temperature at the interface is always less than the temperature of the axial vapor flow, so that the mass fraction of more volatile component (R32) at the interfacial vapor is always greater than the mass fraction of the bulk axial vapor flow.

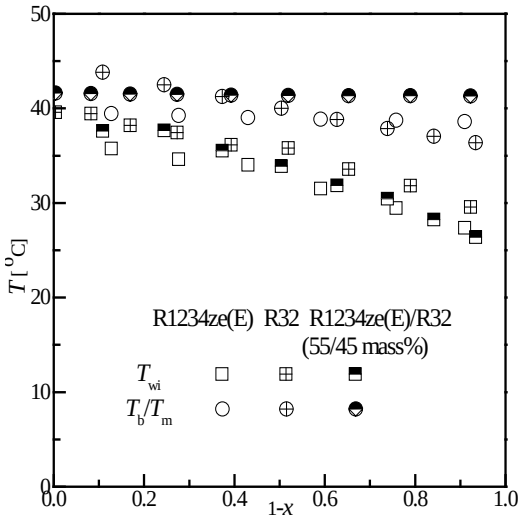

Fig.6. Temperature variation with vapor quality at mass flux 350 kg m^{-2} s^{-1} and T_{sat}=40 °C.

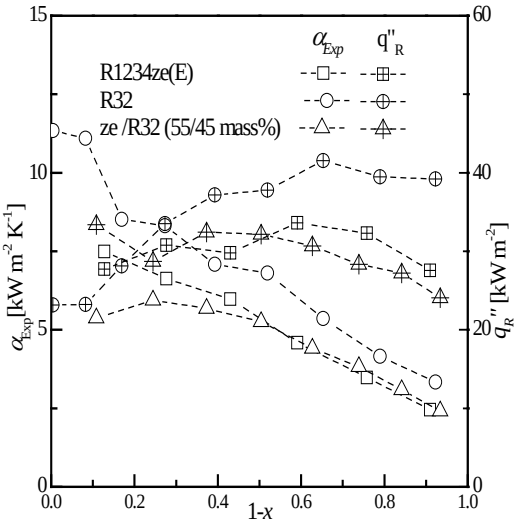

Fig.7. Effect of vapor quality on heat flux and heat transfer coefficient at mass flux 350 kg m^{-2} s^{-1} and T_{sat}=40 °C.

A counter diffusion of more volatile component (R32) from the interface to the bulk vapor flows occurs, which retards the mass diffusion from the vapor core to the interface and results in a reduction of the condensation and thus the heat transfer rate. This mass transfer resistance also causes decrease of vapor-liquid interface temperature and heat transfer is degraded. Moreover, the higher liquid thermal conductivity of pure R32 is

responsible for its higher heat transfer coefficient than the mixture. Among the mixtures, 45% R32 mixture has higher liquid thermal conductivity than the 30% R32 mixture at same saturation temperature [5] so the later shows higher HTC than the former. In comparison with R410A, 45% R32 mixture shows higher heat transfer coefficients than that of the R410A while for 30% R32 mixture it is closer to the R410A. Fig.5 also shows that the refrigerants R1234ze(E), R32, R410A and the mixtures exhibit high heat transfer coefficient at the high mass flux. This is due to the thin liquid film on the tube surface at high mass flux. For the mixture, the effect of the mass transfer resistance due to the composition and temperature shift of the vapor phase decreases as the vapor velocity increases. R1234ze(E) is more dominant by mass flux because the force convection is more effective for R1234ze(E).

4. Conclusion

The condensation heat transfer coefficient of R1234ze (E), R32, R410A and zeotropic mixture R1234ze (E)/R32 has been measured experimentally. The local heat transfer coefficient of pure R1234ze (E), R32 and R410A is higher than the mixtures and as the mass fraction of R32 increases in the mixture the heat transfer coefficient increases. The effect of saturation temperature on heat transfer coefficient is not so significant during condensation of R1234ze (E)/R32 mixture inside smooth tube. It can be concluded that pure R1234ze (E) is not suitable for an alternative of R410A, but mixtures of R1234ze(E) and R32(55/45 mass %) are promising candidates for replacing R410A in domestic heat pump systems.

5. References

[1] Akasaka, R. (2010). "An application of the extended corresponding states model to thermodynamic property calculations for trans-1,3,3,3-tetrafluoropropene (HFO-1234ze(E)", *Int. J. Refrigeration*, Vol. 33, pp. 907-914.

[2] Brown, J.S., Zilio, C., Cavallini, A. (2010). "Thermodynamic properties of eight fluorinated olefins", *Int. J. Refrigeration*, Vol.33, pp. 235-241.

[3] Grebenkov, A.J., Holes, R., Pham, H., Singh R. (2009). "Physical properties and equation of state for Trans-1,3,3,3-tetrafluoropropene", *3rd IIR conference on thermo physical properties and transfer processes of refrigerants*, Boulder, CO, Paper no. 191.

[4] Higashi, Y. (2010). "Thermophysical properties of HFO-1234yf and HFO-1234ze (E)", *Int. Symp. Next-generation Air Conditioning and Refrigeration Technology, Tokyo, Japan.*

[5] Miyara, A., Tsubaki, K., Sato, N. (2010). "Thermal conductivity of HFO-1234ze(E)+HFC-32 mixture", *Int. Symp. Next-generation Air Conditioning and Refrigeration Technology, Tokyo, Japan.*

[6] Motta, S.F.Y., Becerra, E.D.V., Spatz, M.W. (2010). "Low global warming alternative refrigerants for stationary AC&R applications", *Int. Refrigeration and Air Conditioning Conference*, Purdue, July 12-15.

[7] Srinivasan, K., Ng, K.C., Velasco, S., White, J.A. (2012). "A corresponding states treatment of the liquid-vapor saturation line", *J. Chem. Thermodynamics*, Vol. 44, pp. 97-101.

[8] Tanaka, K., Kobayashi, K., Higashi, Y. (2010). "Pressure-Volume-Temperature relationship for HFO-1234ze(E)+HFC- 32 mixture", *Int. Symp. Next-generation Air Conditioning and Refrigeration Technology*, Tokyo, Japan.

[9] Yamaya, K., Matsuguchi, A., Kagawa, N. (2011). "Study on specific heat capacity of HFC-32+HFO1234ze(E) mixture in the liquid phase", *10th IEA Heat Pump Conference*, Japan.

[10] Hossain, M.A., Osaka, Y., Miyara, A. (2012). "Experimental study on condensation heat transfer and pressure drop in horizontal smooth tube for R1234ze(E), R32 and R410A", *Int. J. Refrigeration*, doi:10.1016/ j.ijrefrig.2012.01.002 (in press).

[11] Yu, J., Momoki, S., Koyamata, S. (1999). "Experimental study of surface effect on flow boiling heat transfer in horizontal smooth tubes", *Int. J. Heat Mass Transfer*, Vol. 42, pp. 1909-1918.

[12] Hossain, M.A., Onaka, Y., Miyara, A., 2012. "Experimental study on condensation heat transfer and pressure drop in horizontal smooth tube for R1234ze(E), R32 and R410A", *Int. J. Refrigeration* 35, 927-938.